FACULDADE DE ENGENHARIA DA UNIVERSIDADE DO PORTO

U. PORTO

FEUP FACULDADE DE ENGENHARIA
UNIVERSIDADE DO PORTO

Sensors fusion and movement analysis for sports performance optimization

Bárbara França Domingues Cardoso

DISSERTATION

INTEGRATED MASTER IN BIOENGINEERING

Supervisor at FEUP: Miguel Velhote Correia, PhD

Supervisor at Kinematix: Jorge Pinto, CDO

15th September 2017

Sensors fusion and movement analysis for sports performance optimization

Bárbara França Domingues Cardoso

INTEGRATED MASTER IN BIOENGINEERING

15th September 2017

Abstract

Nowadays, smart wearables for sports and fitness have a huge market due to the growing concern of people in their health condition and improving their performance. Health and fitness trackers, such as smartwatches, have been developed to record activity and monitor vital signs, while being comfortable and not causing constraint in body movement. Heart rate is strongly related with energy expenditure, maximal oxygen uptake and physical activity. The benefits of using wearable sensors in human activity recognition and estimation of energy expenditure had been widely studied, achieving solutions with high accuracy and low computational cost.

This work aims to gather information from feet and arms in order to make running and other sports more efficient. TUNE is a wearable device that monitors both feet to track technique and feet symmetry when running, which is an important measure in evaluation of injury occurrence and sports performance. However, a smartphone is needed to record data and to access to the information provided by TUNE. A smartwatch worn on the wrist is a great way to overcome the need of a smartphone during a run. In addiction, it can provide valuable information from the arms movement and heart rate.

A wearable system, composed of TUNE and the smartwatch Moto 360, was used to measure relevant movements of upper and lower limbs and physiological signals in sports context. The acceleration and heart rate signals provided by the smartwatch were pre-processed, and acceleration signals were used to perform activity recognition. Energy expenditure was then estimated based on the activity being performed, the heart rate measures, the personal information of the subject and the GPS data from TUNE. Heart rate signal was used to determine HR zones of exercise and training intensity, and the movement of the arm was analysed through step counting and the measurement of the amplitude of the arm in terms of acceleration, which were compared with TUNE data, such as step counting and ground contact time.

To validate the developed system, 4 subjects performed 2 cycles of activities. One was performed 3 times including walk very slow, normal walk, run, cycle and rope jump, and the other cycle consisted of running at a free speed. The developed system was validated against COSMED K4b2 including a Polar heart rate chest strap.

The results obtained demonstrated that heart rate measurements from Moto 360 differ from the Polar chest strap ones with an error of 9% and a correlation coefficient of 0.78. Comparing the relation between speed and heart rate intensity with the physical/health information of the test subjects, there is a linear relationship between their BMI and this relation. All activities were classified with a precision above 90%, expect the walking ones. Walking very slow was most classified as normal walk, leading to low accuracies and precisions. In what regards running activity, it was classified with 90% of accuracy. Energy expenditure results showed that there are significant differences between the developed system and COSMED K4b2, with a correlation coefficient of 0.55. Walking and running presented the best results in terms of total energy expenditure value, being the overall error of the developed system of 14%. Energy expenditure estimation achieved a NRMSE of 18% for running activity, increasing to 37% when testing all activities. The observed

errors are mainly due to the propagation of errors of hear rate measurements and activity recognition. From acceleration signals of the smartwatch, steps were counted with an error of 2% and acceleration amplitude proved to vary in indirect proportion with ground contact time.

Even though the results obtained showed that Moto 360 does not have the best accuracy and reliability measuring heart rate, mainly for medical purposes or to monitor cardiac patients, its reliability value is acceptable for heart rate monitoring of sportspeople who aim to improve their performance and follow an active and healthy lifestyle. The combined HR-activity model had shown promising results estimating energy expenditure. The model used in this work still needs some improvements, as well as the wearable devices themselves. However, it introduced a convenient way to monitor physical health with enough reliability. Furthermore, movement analysis of the arm proved to be closely related to movement analysis of the feet, so combining a smartwatch with TUNE demonstrated to make running even more efficient.

Although the results were promising, further work is required to potentially improve sports experience with regard to user-interface, fatigue detection, analysis of the movement of the arm and wearable technology evolution.

Keywords: Activity Monitoring; Energy Expenditure; Inertial Sensors; Heart Rate Monitoring; Running Symmetry; Sensor Fusion; Smartwatch; Sports; Upper Limb; Wearables.

Acknowledgements

Contents

List of Figures

List of Tables

x

List of Abbreviations

ACC   Accelerometer
AF   Average Filter
ALR   Additive Logistic Regression
ANN   Artificial Neural Networks
ANS   Autonomic Nervous System
AR   Autoregressive
AUC   Area Under Curve
BIC   Bayesian Information Criterion
BMI   Body Mass Index
BPF   Band Pass Filter
BPM   Beats Per Minute
CFS   Correlation-based Feature Selection
CO   Cardiac Output
CRF   Cardiorespiratory Fitness
CSI   Cubic Spline Interpolation
DCT   Discrete Cosine Transform
DFT   Discrete Fourier Transform
DLW   Doubly Labeled Water Method
DOF   Degrees Of Freedom
DT   Decision Tree
ECG   Electrocardiogram
EE   Energy Expenditure
ETC   Extra Trees Classier
FEUP   Faculty of Engineering of the University of Porto
FBF   Fuzzy Basis Function
FFT   Fast Fourier Transform
FHR   Fetal Heart Rate
FSR   Force Sensitive Resistor
FSS   Feature Subset Selection
GMM   Gaussian Mixture Model
GPS   Global Positioning System
HAR   Human Activity Recognition
HF   High Frequency
HM   Hybrid Model
HMM   Hidden Markov Model
HR   Heart Rate
HRM   Heart Rate Monitor
HPF   High Pass Filter
ICA   Independent Component Analysis

IMU	Inertial Measurement Unit
IQR	Interquartile Range
kNN	K-Nearest Neighbours
LDA	Local Discriminant Analysis
LF	Low Frequency
LOSO	Leave-One-Subject-Out Validation
LPF	Low Pass Filter
LR	Linear Regression
MAD	Median Absolute Deviation
MAF	Moving Average Filter
MCR	Mean Crossing Rate
MDA	Mean Distance Between Axes
MDL	Minimum Description Length
METs	Metabolic Equivalents
MLR	Multiclass Logistic Regression
MLP	Multilayer Perceptron
MRMR	Minimum Redundancy and Maximum Relevance
NB	Naive Bayes
NFC	Neuro Fuzzy Classifier
PA	Physical Activity
PCA	Principal Component Analysis
PNS	Parasympathetic Nervous System
PPG	Photoplethysmography
PSD	Power Spectral Density
RFE	Recursive Feature Elimination
RMS	Root Mean Square
ROC	Receiver Operating Characteristic
SD	Standard Deviation
SE	Spectral Entropy
SMA	Signal Magnitude Area
SNS	Sympathetic Nervous System
SPEC	User Specific
SV	Stroke Volume
SVM	Support Vector Machine
SW	Sliding Window
TAP	Total Average Power
TP	Total Power
ZCR	Zero-crossing Rate

Chapter 1

Introduction

Smartphones and mobile applications are revolutionizing peoples' lifestyles. Since the introduction of Apple's Iphone in 2007 and the first smartphone running Android in late 2008, the smartphone industry has been steadily developing and growing, both in market size and in models and suppliers (eMarketer, AP, 2015). The development of mobile applications has become a huge market worldwide, particularly with regard to applications that can improve healthcare and sports performance. The ever increasing availability of wearable devices and fitness trackers has pushed mobile fitness apps into the limelight. Sportspeople are increasingly concerned to improve their performance, that is why mobile applications for sports are engaging more and more supporters. Moreover, the emerge of wearable solutions made it more convenient and interesting for users (Dufau et al., 2011).

The aim of this work is to improve sport wearable solutions, allowing users to improve performance, reduce potential for injuries, increase motivation and improve their experience, as well as to promote a more effective, healthier and better performing sports practice.

1.1 Context

Concerning the huge interest and need for sportspeople to improve their performance, Kinematix[1] is focused in making devices that can extract detailed information from human movement. Running is becoming very popular with a huge number of people participating in long distance competitions for recreational purposes. However, most of these runners are not well prepared, since they don't know how to run properly. This leads to a lot of physical injuries, which is not what sports should be about.

TUNE is the latest fitness monitor of the company that is able to provide real time statistics based on the body movement and position of the runner. Data is collected in real time by extracting information directly from the feet through insoles containing electronic sensors. The information is collected before, during and after a workout and is synced to a small device located on the outside of the shoe. TUNE monitors both feet to track technique and feet symmetry when running.

---

[1] http://www.kinematix.pt

It creates a personalized training plan based on the particular information of each runner. This helps runners improve their technique, leading to a better performance and to a reduced risk of injuries. Also, this information can be used by coaches to analyze the needs of their runners, aiming to improve their efficiency.

Kinematix is focused on creating a new generation of wearables, which do not only quantify movement information, but that qualify it meaningfully. In order to take advantage of wearable solutions and provide more powerful information to runners, Kinematix aims to extend its market to a smartwatch application which, together with TUNE, can improve movement information.

In association with the Faculty of Engineering of the University of Porto (FEUP), namely the course of Biomedical Engineering, it was propose the integration of a smartwatch, taking advantage of its sensors to improve the information given to runners. Moreover, it can be used to monitor other sports where arms are used, such as tennis, golf, among others.

1.2 Motivation and Objectives

As depicted in Figure 1.1, the total wearable market is forecast to grow from 22 million units in 2014 to 175 million units by 2020. Smartwatches will be dominant category starting in 2016, followed by smart bands/bracelets (O'Donnell, 2015). Many of these wearables include health and fitness trackers (Gfk, 2015a,b). The smart wearables for the sports & fitness industry is expected to have a market worth of $44.2 billion in 2021 (Moores, 2016), which exhibits the huge interest of people in this type of wearables.

In 2004, Hreljac (2004) reviewed the current state of knowledge related to overuse running injuries and they reported that between 37% and 70% of recreational runners sustain an overuse injury every year due to high impact forces and accelerations, produced when the foot strikes the
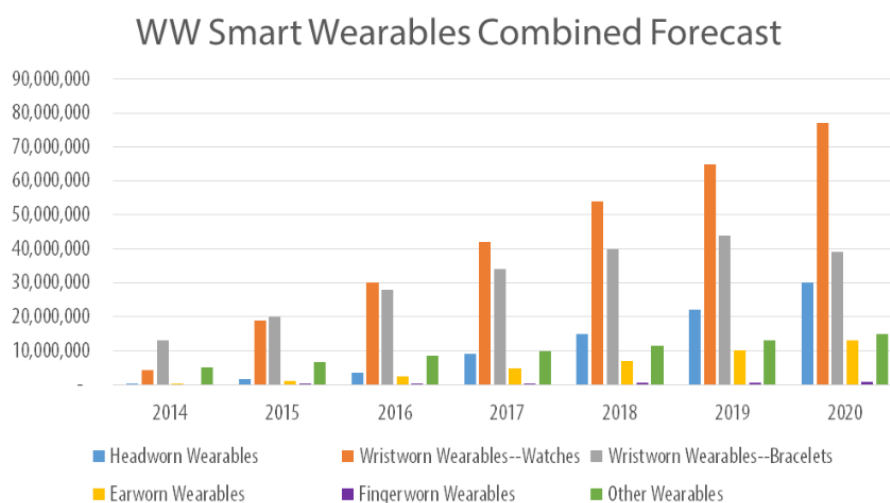
Figure 1.1: Worldwide Wearable Unit Shipments by category from 2014 to 2020 (O'Donnell, 2015).

ground. Concerning the nature of many injuries, asymmetrical running may be a primary cause of injury or, at least, an early indicator of an underlying injury (Moran et al., 2015). Either way, identifying running asymmetry may facilitate more effective injury detection and/or management. TUNE fits this need since it tracks technique and feet symmetry when running.

To improve runners' experience, the latest smartwatches come equipped with on-board storage and even music streaming access, so users can leave their smartphones behind and run without any constraint in body movement. But, more than this, these devices can be utilized to give important information to the runner in real time, as well as to acquire movement and physiological signals. Besides runners, other athletes, such as tennis and golf players, have shown interest in smartwatches in order to achieve a better technique and improve their performance. Smartwatches have built-in sensors, for instance, accelerometer, ambient light sensor, gyroscope, GPS and heart rate sensor, which allow to monitory body movements and activities.

The main objective of this dissertation was to apply in wearables advanced methods of sensor fusion information, such as inertial sensors, GPS and heart rate to recognize patterns of movement and activity, and to obtain measures of physical activity and energy expenditure. A wearable system, composed of TUNE and a smartwatch Moto 360, was used to measure relevant movements and physiological signals in sport context, namely in running.

The system was implemented in the smartwatch to track the upper limb and to obtain physiological signals in order to integrate both information in an energy expenditure estimation module. Energy expenditure (EE) was estimated using both physical activity (metabolic equivalents) and heart rate (physiologic information) measures, which proved to be the most accurate method to estimate EE in previous works, when compared with both methods alone. Moreover, EE computation was activity-specific, using activity recognition methods to distinguish between a set of physical activities including walking, running, cycling and rope jumping.

Furthermore, heart rate zones of exercise and training intensity were analysed regarding personal information of each user in order to present relevant information related to the cardiac functions. Such information is helpful with respect to how human body responds to physical activities and it is essential to improve performance. With regards to the movement of the arm, acceleration signals were used to count steps and to calculate the amplitude of the arm in terms of acceleration. These measurements were linked with TUNE data, such as step counting and ground contact time, to evaluate the possibility of integration of the movement analysis with the smartwatch during a run.

1.3 Structure

Besides this introduction, which explains the motivation and the main objectives of the proposed work, this dissertation includes 5 more chapters.

Chapter 2 includes the background, where the fundamental topics regarding the upper limb movements and heart rate analysis are explained. Moreover, the concepts for the fusion of inertial

and heart rate sensors to access energy expenditure are described, as well as the methodologies used in human activity recognition.

Chapter 3 includes the literature review, where the existing studies in human activity recognition and estimation of energy expenditure are revised. Current wrist-worn devices and mobile applications which use inertial and heart rate sensors for sports are pointed out, and some public datasets that were created to evaluate human activity recognition techniques and to monitor physical and aerobic activities are described.

Chapter 4 presents the work developed in this dissertation, including the research methodology and the development of a system which fuses inertial and heart rate sensors implemented in wearables. The technologies and methodologies used are explained in detail.

In Chapter 5, the experimental work is described including the setup, the protocol and the datasets used and developed to validate the developed system. The results obtained are present and discussed.

Finally, Chapter 6 summarizes the main achievements and conclusions of this dissertation and presents suggestions for future work and improvements.

Chapter 2

Background

This Chapter provides an explanation of fundamental topics regarding the upper limb movements and heart rate analysis. For both topics, it is described the most used sensors and techniques to quantify relevant information in activity monitoring, mainly in sport context. Furthermore, it includes the background concepts for the fusion of inertial and heart rate sensors to access energy expenditure, used to quantity physical activity. Moreover, methodologies for pattern recognition are described concerning human movement and activity recognition.

2.1 Upper Limb Movement Analysis

The upper limb is characterized by its high number of degrees of freedom (DOF), therefore it is important to be aware of the kinematics of the upper limb to understand its movements.

There is a wide range of sensors that can be used to quantify and qualify movements of the upper limb. Modern smartphones and related devices contain some of these sensors and their addition into everyday devices has paved the way towards enhanced contextual awareness and ubiquitous monitoring for healthcare applications (Guiry et al., 2014).

2.1.1 Kinematics

The upper limb is connected to the pectoral gridle and consists of the bones of the arm, forearm, wrist and hand. It is connected to the body by muscles, which act as fixators to hold the scapula firmly in position when the muscles of the arm contract. The scapular muscles move the scapula into different positions, thereby increasing the range of movement of the upper limb (Putte et al., 2016).

Besides muscles, joints also play an important role in the movement. Regarding the upper limb, it can be considered the shoulder joint, elbow joint and wrist joint. Each joint structure relates to the movements that occur at that joint. In the upper limb, the two main types of movements are angular and circular movements (Hamill and Knutzen, 2006).

Angular movements occur when one bone moves relative to another and the angle between these two structures changes as a consequence. The most common angular movements are flexion, extension, abduction and adduction (Figures 2.1a and 2.1b). On the other hand, circular movements occur when a structure rotates around an axis. The most common circular movements are pronation, supination, rotation and circumduction (Figures 2.1c, 2.1d and 2.1e). Circumduction only happens in very mobile joints like the shoulder joint, corresponding to a combination of flexion, extension, abduction and adduction.

In Figure 2.1 there is a representation of these movements. Together, shoulder, elbow and wrist joints, and their surrounding muscles allow the upper limbs to perform a large set of movements (Seeley et al., 1998; Putte et al., 2016). Shoulder joint allows the arm to perform movements like flexion, extension, abduction, adduction, medial and lateral rotations and circunduction; elbow joint allows the forearm to perform movements like flexion, extension, supination and pronation; and wrist joint allows the hand to perform movements like flexion, extension, abduction and adduction.

The muscles involved in the mentioned movements are described in Table 2.1. A complex combination of muscles is involved in the movements permitted by the wrist together with hand and fingers, however movements of the fingers were left out of the table since they are not relevant in this work.

(a) Flexion/Extension   (b) Abduction/Adduction   (c) Pronation/Supination

(d) Medial/Lateral rotation   (e) Circunduction
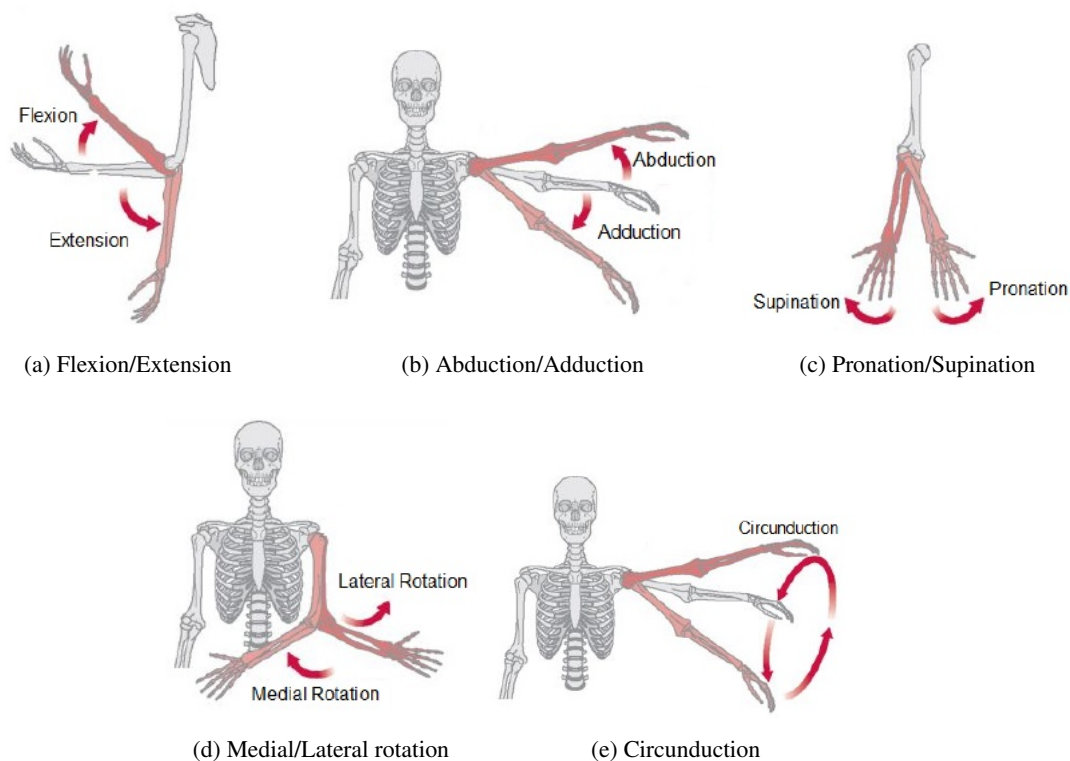
Figure 2.1: Representation of the different types of movements performed by upper limbs: *(a)*-pair flexion/extension, *(b)*-pair abduction/adduction, *(c)*-pair pronation/supination, *(d)*-pair medial rotation/lateral rotation and *(e)*-circunduction. Adapted from (Freixo, 2015).

Table 2.1: Muscles acting on the movement of the shoulder, upper arm, forearm and hand (Seeley et al., 1998; Putte et al., 2016).

Body part	Movement	Muscles	Movement	Muscles
Shoulder and Upper Arm	Flexion	Coracobrachialis Pectoralis major Deltoid	Extension	Deltoid Teres major Latissimus dorsi Pectoralis major Tríceps brachii
	Abduction	Deltoid Supraspinatus	Adduction	Pectoralis major Latissimus dorsi Teres major Teres minor Tríceps brachii Coracobrachialis
	Medial Rotation	Pectoralis Major Teres major Latissimus dorsi Deltoid Subscapularis	Lateral Rotation	Deltoid Infraspinatus Teres minor
Forearm	Flexion	Bíceps brachii Brachialis Brachioradialis	Extension	Tríceps brachii Anconeus
	Supination	Bíceps brachii Supinator	Pronation	Pronator quadratus Pronator teres
Hand	Flexion	Flexor carpi radialis Flexor carpi ulnaris Flexor digitorum profundus Flexor digitorum superficialis Palmaris longus	Extension	Extensor carpi radialis brevis Extensor carpi radialis longus Extensor carpi ulnaris Extensor digiti minimi Extensor digitorum Extensor indicis
	Abduction	Flexor carpi radialis Abductor pollicis longus Extensor carpi radialis brevis Extensor carpi radialis longus Extensor pollicis longus	Adduction	Flexor carpi ulnaris Extensor carpi ulnaris

2.1.2   Inertial Sensors

Inertial sensors are often used to detect human movement. Applying these sensors, for instances, in a wearable device attached to the arm, the information can be both used to identify the whole body position and movement, or the upper limb position and movement to recognize patterns of its activity.

These type of sensors are cost effective and widely available. Moreover, they have a high sampling rate and can work in total darkness and in unconfined environments. However, measurements from inertial sensors are sensitive to sensor location on the body, and sensor drift might occur during long operation times. Also, to recognize human motion, these sensors must be worn by subjects during acquisition and provide enough power battery supply (Chen et al., 2015). The mostly used sensors in human movement analysis are accelerometers, gyroscopes, magnetometers and barometers.

Accelerometers measure linear acceleration and tilt angle. Acceleration is measured in meters per second squared (m/s^2) or in G-forces[1] (g). They can be single or multi-axis and detect the combined magnitude and direction of linear, rotational and gravitational acceleration. Accelerometers can be divided in the following three most common types: piezoresistive, piezoelectric and differential capacitive (Yang and Hsu, 2010). Accelerometers have been used in detection of the human body movements and postures (Veltink et al., 1993; Machek et al., 2012; Lugade et al., 2014). If mounted on a segment of a human body, they measure a component of the actual acceleration of the segment at the site of the sensor, and a component of the equivalent gravitational acceleration. Signals acquired from accelerometers should be processed in order to be used in the automatic detection of movements. Machek et al. (2012) describes two algorithms for movement detection in the accelerometer data which include second differentiation, points of the inflection, cumulative sum algorithm and peak detection. Usually, high frequency noise in acceleration data needs to be removed. Thus, non-linear, low-pass median, Laplacian and Gaussian filters can be used. Moreover, FFT can extract primary information of data and reduce its dimension, and wavelet transforms are a good tool to eliminate noise during activities such as walking and running (Avci et al., 2010).

Gyroscopes measure the angular rate of rotational movement about one or more axes, in radians per second (rad/sec). They can measure complex motion accurately in multiple dimensions and track the orientation and rotation of a moving object. Further, unlike accelerometers and compasses, gyroscopes are not affected by errors related to external environmental factors such as gravitational and magnetic fields (Sunny et al., 2015). However, sensor drift can not be avoided.

Magnetic sensors, commonly referred to as compasses, detect magnetic fields and measure their absolute position relative to Earth's magnetic north and nearby magnetic materials, usually in micro Tesla (mT). The main source of measurement errors are magnetic interference in the surrounding environment and in the device (Sunny et al., 2015). Compass reading can be used to

---

[1] $g = 9.80665 m/s^2$

detect the direction change in the user's motion, such as walking, and to correct errors from other sensors, like accelerometers.

Pressure sensors, also known as barometers, measure relative and absolute altitude through the analysis of changing atmospheric pressure (*hPa*). These sensors can be used in consumer devices for sports and fitness, or location-based applications where information on elevation can be valuable (Lee and Cho, 2011). Air pressure varies with different altitude or even with places of the same altitude, but having different structures inside a building. So, barometer reading can be used to indicate the user's position change in activity recognition related to localization (Sunny et al., 2015). Integrated with a tri-axial accelerometer, the added information of altitude changes can be used to determine movement with vertical displacement, such as taking elevator or walking upstairs and downstairs (Yang and Hsu, 2010).

Systems that employ sensor fusion methods are expected to provide better information than would be possible when its sources are used individually, i.e., more accurate, more complete, or more dependable. A physical sensor measurement generally suffers from problems like sensor deprivation, limited spatial and temporal coverage, imprecision and uncertainty (Elmenreich, 2002). On the other hand, the fusion of sensor data from a set of heterogeneous or homogeneous sensors provides robustness and reliability, extended spatial and temporal coverage, increased confidence, reduced ambiguity and uncertainty, robustness against interference and improved resolution (Bosse et al., 1996).

Applying sensor fusion algorithms, it is possible to get a better information about the orientation of the upper limb relative to the geographic coordinates (Luinge et al., 2007). However, it must be borne in mind that data fusion based on samples from differing modality sensors requires accurate time synchronization, which sometimes is hard to achieve (Chen et al., 2015). In addition, a signal filtering pre-processing component is often used. Combining data from multiple inertial sensors corrects for the deficiencies of the individual sensors to calculate accurate position and orientation information. Figure 2.2 shows the combination of the four inertial sensors mentioned before to get a better estimation of position and orientation [2].
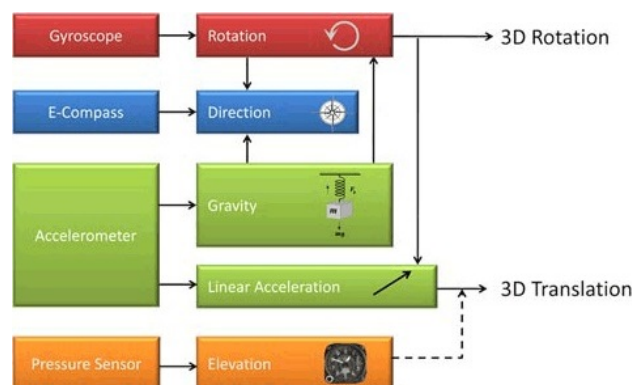
Figure 2.2: Fusion of different sensor data in order to calculate accurate position and orientation.

---

[2]http://www.kionix.com/sensor-fusion

2.2 Heart Rate Analysis

The heart rate is the reflex of each person's health status, and their lifestyle has a huge impact on their own health and well-being. Several methods can be used to measure heart rate in real time. Some of these methods are implemented in modern monitor devices and wearables, making self monitoring more efficient and practical. Moreover, the analysis of heart rate variability can be used to perform activity measurements, which might be crucial to detect possible abnormalities and/or to improve users performance in sports context. In the following, physiologic concepts of cardiovascular system which influence heart rate variability are described, as well as some methods used to measure it.

The cardiac cycle refers to the repetitive pumping process that starts with the beginning of the cardiac muscle contraction and ends with the beginning of the next contraction, i.e., a complete heartbeat. The normal cardiac cycle (0.7 to 0.8 seconds) is dependent on the contractile capability of the cardiac muscle and the functional integrity of the conduction system (Seeley et al., 1998). The sinoatrial (SA) node, located in the superior wall of the right atrium, spontaneously initiates the contraction of the heart, acting as its pacemaker. The electrical impulses generated spread all through the heart and cause rhythmic contraction and relaxation of heart muscles. Throughout the cardiac cycle, blood pressure increases and decreases, allowing the blood to flow in the right direction. Pressure increases in the ventricles during their diastole (contraction) and, when ventricular diastole (relaxation) begins, pressure in the ventricles decreases (Putte et al., 2016).

When blood enters into the arteries, it causes their walls to stretch and the pressure to increase to about 120 mmHg, the systolic pressure. At the end of systole, the pressure in the aorta decreases slowly throughout diastole and, before the ventricle contracts again, the aortic pressure usually has fallen to about 80 mmHg. This value corresponds to the diastolic pressure, which is two thirds the maximal pressure of the systolic pressure. The pressure in the right ventricle and pulmonary artery are similar to those in the aorta, but they are only about one sixth as great (Guyton and Hall, 2006).

To assess the function of the heart, it is important to measure the Cardiac Output (CO), which is the volume of blood pumped by both ventricles each minute, the Stroke Volume (SV), that refers to the volume of blood pumped per ventricle each time the heart contracts, and the Heart Rate (HR), that describes the frequency of the cardiac cycle and is typically expressed as beats per minute (BPM). These measurements are related as follows:

$$CO_{mL/min} = SV_{mL/beat} \times HR_{beats/min} \tag{2.1}$$

and they vary considerably from one person to another. For instance, the size of the heart is bigger in athletes due to the exercise, so they tend to have a higher SV and lower HR at rest. Therefore, an HR between 60 and 100 BPM is considered normal for a resting adult (Magalhães, 2016). Considering the HR of non-athletes to be approximately 72 BPM under resting conditions, it can increase to 190 BPM during exercise; also, SV can increase from 10 mL/beat to 115 mL/beat; thus, CO can go from 5 L/min to 22 L/min (Putte et al., 2016).
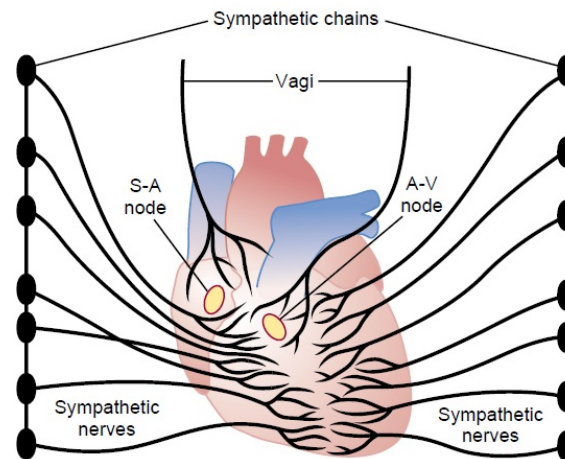
Figure 2.3: Cardiac sympathetic and parasympathetic nerves. The vagus nerves to the heart are parasympathetic nerves. Adapted from (Guyton and Hall, 2006).

Cardiac Output and Heart Rate are controlled by intrinsic and extrinsic mechanisms, i.e., by the heart itself, in response to changes in volume of blood flowing into the heart, or by nervous and chemical regulation, respectively. Concerning nervous regulation, it is achieved by means of the cardioregulatory center, which controls the action potential frequency in the nerve fibers of the autonomic nervous system (ANS). These nerves abundantly supply the heart and constitute the sympathetic (SNS) and the parasympathetic nervous systems (PNS), as shown in Figure 2.3 (Guyton and Hall, 2006). Nervous regulation also includes baroreceptors which monitor blood pressure in the aorta and in the wall of the arteries that carry blood to brain. Cardiovascular variability mainly allows to access to the activity of the nerves and baroreceptors (Aubert et al., 2003).

In a normal HR, time between two beats (R-R) can differ substantially. The heart rate variability (HRV) corresponds to the variation in time between beats (Achten and Jeukendrup, 2003). The equilibrium between SNS and PNS is implicit in the HRV and corresponds to the ability of the heart to adapt to changing circumstances. The greater the HRV, the better the heart is capable of keeping up with changes (Magalhães, 2016).

A sympathetic stimulation increases SV and HR. When the activity of the SNS is depressed below normal, both HR and strength of ventricular muscle contraction are decreased, thereby decreasing the level of cardiac pumping. On the other hand, a parasympathetic stimulation decreases HR, but doesn't have much effect decreasing the strength of heart contraction, since the vagal fibers are distributed mainly to the atria and not much to the ventricles, as shown in Figure 2.3 (Guyton and Hall, 2006). Since the R-R interval has a nonlinear inverse mathematical relation with the heart rate value, the higher the HR, the shorter the inter-beat interval. Shorter intervals usually present less variation (Nieminen et al., 2007). Thus, low HRV can be interpreted as a consequence of the SNS activity and high HRV can be indicative of dominance by the PNS. Furthermore, high HRV is associated with high maximal oxygen uptake (VO_{2max}) values. The relation between HR

and VO_2 is often used to estimate energy expenditure (Achten and Jeukendrup, 2003).

Many factors can influence heart function by increasing sympathetic or parasympathetic stimulation. It is known that emotions can increase sympathetic stimulation of the heart in response to exercise, excitement, anxiety, or anger, and increase parasympathetic stimulation in response to depression (Putte et al., 2016). Moreover, stress, overtraining and inflammation can increase SNS activity, while PNS activity promotes relaxation, sleep and recovery. Olufsen et al. (2008) showed that even posture influences HR. During a sit-to-stand movement, the HR increases due to the decrease in the blood pressure, which stimulates the sympathetic nerve (Magalhães, 2016).

2.2.1   Measurement Methods

The auscultatory method has been the mainstay of clinical blood pressure measurement. However, it is gradually being replaced by other techniques that are more suited to automated measurement. Many techniques have emerged to determinate the heart pulse and heart rate. These are integrated into monitoring devices used in clinical context and, more recently, in self-monitoring. In spite of the several techniques, this work is focused in measurement methods suitable for wearable monitoring systems which can be used in sports field.

Electrocardiography captures electrical activity of the heart through biopotencial electrodes placed on the skin. Plethysmography consists of measuring changes in the volume of blood in the capillaries. These changes can be detected by photoplethysmography (changes in light absorption) and impedance plethysmography (changes in electrical resistance). Nowadays, the majority of smartwatches capable of measuring heart rate rely on plethysmography mechanisms.

Photoplethysmography (PPG) is a mean of determining the timing of cardiac cycles via continuous monitoring of changes in blood volume in a portion of the peripheral microvasculature. These type of sensors can be based on the light transmission principle, usually applied on the finger or earlobe, or based on principle of reflection, for wrist application (Magalhães, 2016). When light radiation such as infrared is passed through a blood vessel, the received light signals are periodic and vary due to the rhythmic flow and absorption properties of blood (Kumar, 2011). This optical variation is employed to make PPG, taking into account the existing relation between the vessels volume, blood pressure and volume (Tamura et al., 2014). PPG allows to determine the heart rate, through the period of the blood flow (Zhang et al., 2016). Concerning the HR monitoring through the wrist using bracelets or watches, it must be used a PPG based on the reflection principle, where both the emission module (infrared LEDs) and the detector (photodiode) are placed on the same site.

A band-pass filter is often used to remove the DC component and the high frequency noise of the signal. The variation of the optical signal (AC component), is due to changes in blood flux. During the systole, the optical path is bigger and, consequently, the light absorption is higher. The instant heart rate can be calculated from the inverse of the time between cardiac cycles. The PPG signal is the recorded infrared waveform at the detector side. Figure 2.4 is a representation of a PPG signal, consisting of a large DC component, which is attributed to the total blood volume of the examined tissue (including bones, skin, tissues, venous blood and non-pulsatile blood), and a
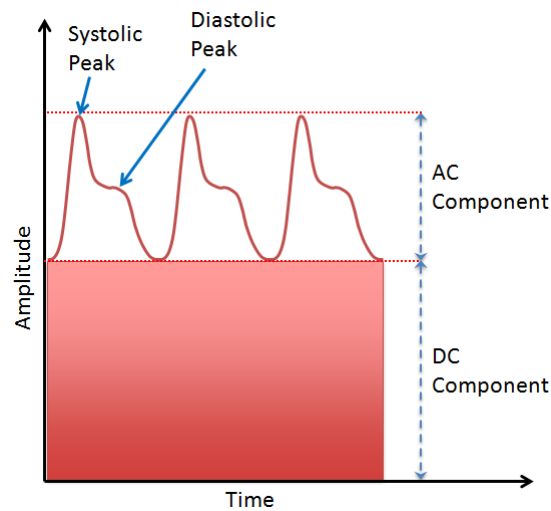
Figure 2.4: Representation of a typical PPG waveform (not to scale). From (Embedded-Lab, 2013).

pulsatile AC component, which is synchronous to the pumping action of the heart and carries vital information including the heart rate (Magalhães, 2016; Embedded-Lab, 2013).

Light propagation might be affected by different factors, such as movement artefacts, temperature control mechanism, measurement area and ambient light, making difficult to obtain a reliable optical heart rate monitoring (Delgado-Gonzalo et al., 2015).

2.2.2 Effects of Exercise Training

During exercise, heart rate increases due to both a parasympathetic withdrawal and an augmented sympathetic activity. Once SNS is not capable of controlling HR as swiftly and accurately as the PNS, it is physiologically meaningful that high frequency HRV is more obscure during exercise than at rest (Aubert et al., 2003). The decreased influence of PNS is suggested by a decrease in the values of SDNN, TP, HF and LF in the transition from rest to exercise (Achten and Jeukendrup, 2003). Therefore, there is a decrease in HRV.

The cardiovascular responses to physical activity (PA) depend on the type and intensity of exercise. For example, during endurance exercise, there is an increased volume load, in contrast to pressure load during strength exercise. During endurance training, the ability of the heart to pump blood is increased, by increasing its stroke volume (Aubert et al., 2003). Moreover, endurance exercise ensue a more efficient pressure-time relationship, since it also decreases the metabolic load on the heart at rest and at any submaximal exercise intensity, by increasing SV and decreasing HR (Guyton and Hall, 2006). Differences in HRV between trained and sedentary individuals are evident: trained individuals present higher values of R-R interval times, SDNN, pNN50, rMSSD, TP and HF, indicating their higher HRV (Achten and Jeukendrup, 2003).

The HR regulation by ANS during exercise varies substantially within an individual, depending on age, gender, heredity, fitness level, exercise mode and skill (economy of exercise). Also,

body posture, temperature, humidity, altitude, state of mood and hormonal status affect HR responses, as well as, drugs, stimulants, smoking and eating habits (Aubert et al., 2003; Achten and Jeukendrup, 2003; Acharya et al., 2006).

Aging causes changes in the heart function that are more obvious during exercise. Older people tend to fell out of breath when they exercise strenuously, due to the hypertrophy of the left ventricle which reduce its ability to pump blood, leading to increased pulmonary edema. However, physical exercise has many beneficial effects on the heart by improving its functional capacity (Putte et al., 2016). In 1970, Dr. William Haskell and Dr. Samuel Fox formulated a relation between HR and age, which suggests that the highest heart rate a human can achieve without severe sequelae (HR_{max}) is given by Simon (2002):

$$HR_{max} = FHR - age \tag{2.2}$$

Where FHR is the fetal heart rate defined as 220. Other authors suggested that, for women, a FHR of 226 provides a better estimate of the maximum heart rate than $220 - age$, being more appropriate for exercise prescriptions (Warburton et al., 2006; Froelicher et al., 2000). Although recent studies proved that this traditional equation overestimates HR_{max} in young adults (Tanaka et al., 2001), presenting a more realistic equation ($HR_{max} = 208 - 0.7 \times age$), the one proposed by Haskell and Fox stills the most widely cited formula and it is used by most of the fitness devices to track heart rate.

This relation is helpful to control the effort done during physical activities, taking into account the age and the intensity of the physical exercise. For example, if a 20 years old person, who has a maximum heart rate of 200 BPM, performs a 50-70% intensity physical workout, he/she should present a HR between 100 and 140 BPM (Tanaka et al., 2001; Magalhães, 2016).

2.3 Physical Activity and Energy Expenditure

Energy expenditure (EE) can be estimated by measuring physical activities, through accelerometers data. Accelerometers provide basic step counting and activity counts (intensity) that can be used to estimate the EE due to PA (Yang and Hsu, 2010). Moreover, EE can be calculated based on the values of metabolic equivalents (METs), which are computed depending on the performed PA (see Appendix A.1.1). A MET represents the amount of oxygen consumed at rest (being one liter of oxygen equal to 5 kcal, a MET is approximately 3.5 ml $O_2/kg/min$, which is 1.2 $kcall/min$ for a 70-kg person), and is defined as the resting metabolic rate Jette et al. (1990). Energy expenditure is calculated from the METS values using the following equation (Kawahara et al., 2009):

$$EE(kcal) = 1.05 \times METs \left(\frac{kcal}{kg \times h} \right) \times duration(hour) \times weight(kg) \tag{2.3}$$

Furthermore, both oxygen uptake and heart rate increase linearly with increasing exercise intensity. To estimate EE, it is determined the individual HR-VO$_2$ relationship. Thus, HR can be used to estimate VO$_{2max}$ and EE, assuming a linear relationship between HR and VO$_2$. However,
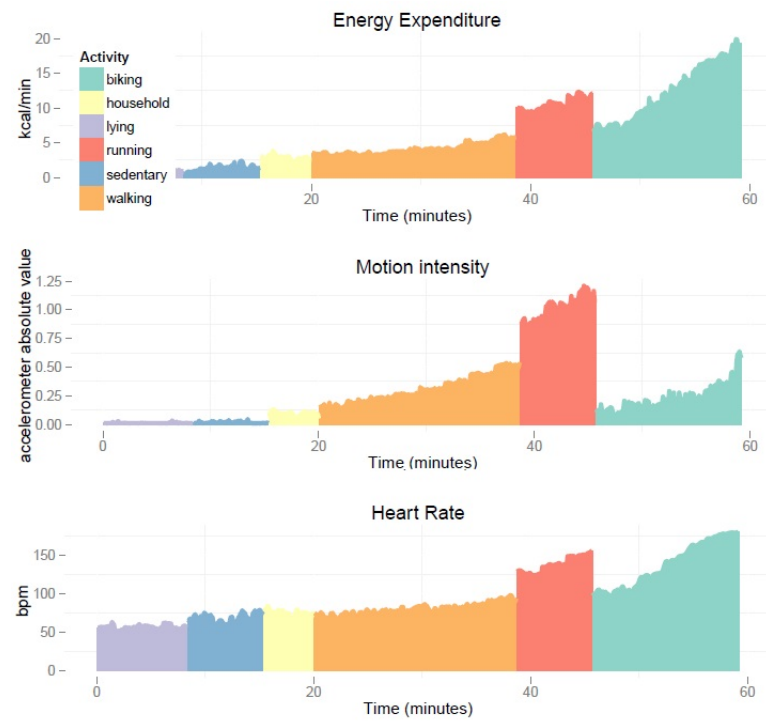
Figure 2.5: Relationship between accelerometer and EE, and between heart rate and EE data for a series of activities performed in laboratory conditions. Walking, running and biking activities are performed at increasing intensities (Altini, 2015).

during very low and very high intensities, this relationship becomes non-linear, leading to some errors (Achten and Jeukendrup, 2003). Since HR increases so that oxygen can be delivered to the body, it is verified that, during exercise, there is also a correlation and a linear relationship between speed and HR. When HR reaches its maximum, VO_{2max} is reached and there can be no further increase in exercise intensity. Estimating the oxygen volume and subsequently EE from heart rate presents some advantages, compared to established metabolic equations, since the heart rate changes during exercise reflect the volume of oxygen whereas metabolic equations assume a fixed expenditure rate for a specific intensity (Magalhães, 2016). To derive a reliable EE estimate, it is necessary to normalize HR according to an individual's cardiorespiratory fitness (CRF) level. Thus, a normalized HR could be used as independent variable in EE regression models and its normalization can be obtained using information on CRF (Altini et al., 2015). In Appendix A.1.2, a model proposed by Altini (2015) to automatically estimate the heart rate normalization factor can be seen.

As depicted in Figure 2.5, the heart rate is as higher as the physical effort required by the physical activity performed, which is confirmed by the energy expenditure per minute in each activity type. Accelerometer data shows a strong relation with EE for weight bearing activities such as walking at different speeds. However, the relation between accelerometer and EE gets very weak for non-weight bearing activities, such as biking. The heart rate is highly correlated

with energy expenditure during moderate and vigorous activities such as walking, running and biking, but during lying or sedentary activities this relationship is weaker (Altini, 2015).

Thus, EE is typically estimated using both acceleration and heart rate data (Altini et al., 2015). The estimation of EE from the heart rate is sport-specific and depends on the PA and posture. Altini (2015) proposed activity-specific EE linear models (see Appendix A.1.3), which use anthropometric characteristics, accelerometer and HR features.

Brage et al. (2004) suggested a multi-linear regression equation that was derived and expressed in terms of both activity counts and heart rate values. The model uses the same equations as those that were used in the study by Thompson et al. (2006), where accelerometer counts and heart rate were used to estimate EE (see Appendix A.1.4).

2.4 Human Activity Recognition Methodologies

Human activity recognition (HAR) is performed just like any other machine learning application. Pattern recognition is a sub-field of the machine learning and its main objective is to learn to distinguish patterns of interest from their background, using techniques based on probabilistic and statistical arguments (Freixo, 2015).

In the ideal case, an activity is recognized independently of the environment where it is performed in, or the performing person. It is based on sensor and/or video observation data, as well as on knowledge about the context within which the observed activities take place (Ranasinghe et al., 2016). This work focus on physical sensor based HAR, in which physical sensors are attached to the body of humans to infer their activity.

Wearable sensors based activity recognition is a recent field of study (back to 1990s) due to its requirements on the power of sensors and a light-weight hardware, allowing mobile systems to be worn by a single person (Starner et al., 1999). It has been used in healthcare and in interactive applications, such as medical applications (monitoring and diagnosis, rehabilitation, correlation between movement and emotions, child and elderly), home monitoring and assisted living (tracking, monitoring and emergency, assistance for people with cognitive disorders or chronic conditions) and sports and leisure applications, since it demonstrated good performance in applications which require explicit motion analysis (Avci et al., 2010). However, it is not able to distinguish similar actions, for instance, making tea and coffee (Guan et al., 2011).

In Figure 2.6 are presented the common phases in an HAR process. These include the two main stages of training and testing. The training stage starts with a time series dataset of measured attributes from individuals performing each activity, which are split into time windows to apply feature extraction. Then, relevant information is used by learning methods to generate an activity recognition model. In testing stage, the same type of attributes are collected in order to extract defined features to be evaluated in the previously trained learning model (classifier), generating a predicted activity label. The classifier can be evaluated by comparing its result with the ground truth. Each phase of HAR process is described next.
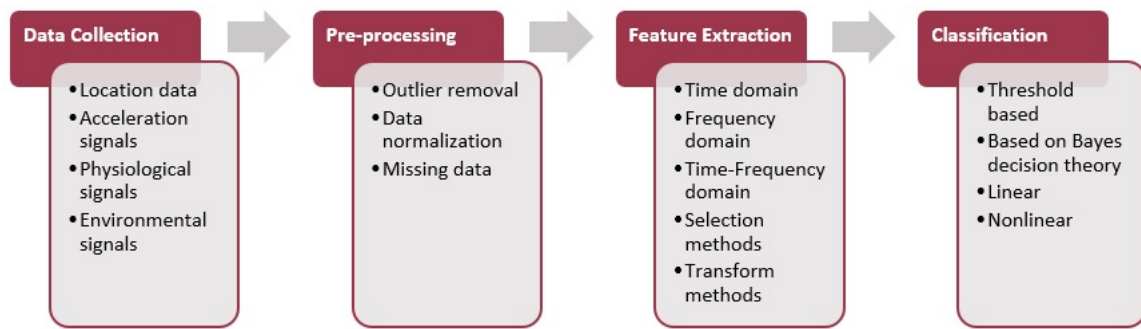
Figure 2.6: Common steps for human activity recognition process (Lara and Labrador, 2013; Avci et al., 2010).

2.4.1 Data Collection and Pre-processing

HAR process begins with the collection of relevant information on human behavior. These information corresponds to the raw data of a sensor. In HAR, the most used data provides from environmental attributes, acceleration signals, location data and physiological signals (Lara and Labrador, 2013). Pre-processing is a key step, since it allows to remove artifacts, noise and redundancy which could distort the final classification. Furthermore, pre-processing allows to perform data aggregation and normalization, and correct missing data. Finally, a segmentation step is often used to retrieve important and useful information from continuous stream of sensor data (Avci et al., 2010).

2.4.2 Feature Extraction and Dimensionality Reduction

Once the components are representative of the activity performed, the main characteristics of features are extracted. Statistical and structural approaches have been proposed to extract features from time series data. Structural approaches take into account the interrelationship among data, applying, for example, linear, polynomial, exponential or sinusoidal functions. Statistical methods, use quantitative characteristics of the data to extract features (Lara and Labrador, 2013). These features are measurable properties which enable the characterization of the movement/activity, such as time domain, frequency domain and time-frequency domain features. Also, heuristic features (signal magnitude area, signal vector magnitude and inter-axis correlation) are often used, since these features have been derived from a fundamental understanding of how a specific movement would produce an unique sensor signal (Avci et al., 2010).

In order to increase the quality of the features and reduce the computational effort needed for the classification, a dimensionality reduction should be performed. If features with little discrimination power are selected, the subsequent design of a classifier would lead to poor performance. Also, the number of features extracted should not be too large, in order to the data not became minimal relatively to the features dimensionality. However, a short amount of features may not provide sufficient information to fully describe the performed activity (Lara and Labrador, 2013).

Selected features should take distant values in the different classes and closely located values in the same class (Theodoridis and Koutroumbas, 2003). Thus, feature selection methods and feature transform methods can be used.

In feature selection methods, one possibility is to examine the features individually and discard those with little discriminatory capability (statistical hypothesis testing). Another one is to examine them in combinations (class separability measures). Unlike the former, the latter takes into account the correlation that exists among the various features (Theodoridis and Koutroumbas, 2003). The selection itself can be performed by different methods, such as forward-backward sequential search, correlation-based feature selection (CFS) approach, K-Means clustering, support vector machine (SVM) based feature selection, bayesian information criterion (BIC), minimum description length (MDL), minimum redundancy and maximum relevance (MRMR), among others (Theodoridis and Koutroumbas, 2003; Avci et al., 2010; Lara and Labrador, 2013).

The application of a linear or nonlinear transformation to a feature vector sometimes may lead to a new one with better discriminatory properties. Applying transform-based features, an appropriately chosen transform can exploit and remove information redundancies, which usually exist in the set of samples obtained by the measuring devices. Fourier coefficients as features are often used, because the low-energy, high frequency coefficients can be neglected, with little loss of information (Theodoridis and Koutroumbas, 2003). Principal component analysis (PCA) is a widely used statistical analysis method which transforms the original features into a lower dimensional space (Avci et al., 2010). Other methods such as independent component analysis (ICA), local discriminant analysis (LDA) and discrete cosine transform (DCT) might be used (Theodoridis and Koutroumbas, 2003; Avci et al., 2010; Lara and Labrador, 2013).

2.4.3 Classification and Evaluation

Based on the extracted features, the classification of the segments is performed in order to identify activities. Two learning approaches can be considered: supervised and unsupervised learning, which deal with labeled and unlabeled data, respectively. This work is more focused on supervised learning, since a HAR system usually consists of inferring a decision rule from labeled training data, such as "walking", "running", etc. Concerning, for example, the movement of the arm, supervised algorithms associate an observation (or features) of movement to possible movement states in terms of the probability of the observation, i.e., they use statistical schemes. Supervised learning includes a training phase and a test phase. The selection and training of the classifier is done in the training phase. A labeled dataset is used to create a model to classify unlabeled objects of data. The test phase is used to evaluate the algorithm performance.

Statistical schemes include threshold-based techniques, Bayes-based classifiers, including Naive Bayes (NB) classifier, Gaussian mixture model (GMM) and hidden Markov model (HMM), linear classifiers, such as support vector machines (SVM), and nonlinear classifiers, which include K-Nearest Neighbours (kNN) classification, decision trees and artificial neural networks (ANN) (Yang and Hsu, 2010; Avci et al., 2010; Lara and Labrador, 2013).

Threshold-based techniques are widely used to distinguish activities with various intensities. K-Nearest Neighbours algorithms are used for classification of activities based on the closest training examples in the feature space (Avci et al., 2010). Decision trees build a hierarchical model which uses a tree-like model of decisions and their outcomes, and costs (Avci et al., 2010). In this model, the attributes are mapped to nodes, and edges represent the possible attribute values, being each branch a classification rule (Lara and Labrador, 2013). Decision trees usually generate models that are easy to understand by humans.

Naïve Bayes is a simple probabilistic classifier based on the theorem of Bayes (Avci et al., 2010), which calculate posterior probabilities for each class using estimated conditional probabilities from the training set (Lara and Labrador, 2013). In a HAR, it determines activities according to the probabilities of the signal pattern of the activities (Yang and Hsu, 2010). The main disadvantage of Bayesian methods relies on the fact that it is necessary to make assumptions on the independence among features. It assumes that all features are conditionally independent given a class value, however, such assumption does not hold in many cases (Lara and Labrador, 2013). In fact, acceleration signals are highly correlated, as well as physiological signals such as heart rate.

In GMM approach, the likelihood function is not a typical Gaussian distribution. GMMs are parametric representations of probability density functions, based on a weighted sum of multivariate Gaussian distribution (Avci et al., 2010). The weights and parameters describing probability of activities are obtained by the expectation-maximization algorithm. The HMM is a statistical model applied to determine unknown states at any time according to observable activity features corresponding to the states. A Markov chain represents the likelihood (probability) of transitions between possible activities (states), thus it can describe transitions between activities (Yang and Hsu, 2010). However, GMM and HMM approaches are usually used in the unsupervised context, trying to directly construct models from unlabeled data.

SVMs represent kernel functions that project all instances to a higher dimensional space in order to find a linear decision boundary (i.e., a hyperplane) to partition the data. Artificial neural networks replicate the behavior of biological neurons in the human brain. Activation signals are propagated to codify knowledge in the network links. Although ANNs are universal function approximators, showing good results on HAR, a high computational cost is needed, as well as a large amount of training data. In both support vector machines and artificial neural networks, knowledge is hidden within the model, which may be prejudicial to the analysis and incorporation of additional logical information. Moreover, SVM and ANN do not provide a set of rules understandable by humans (Lara and Labrador, 2013).

The output of several classifiers can be combine in order to improve classification accuracy. However, this approach is computationally much more expensive.

To evaluate HAR systems, two analysis have been proposed based on the dependency on the subject: subject-dependent and subject-independent evaluations. In the subject-dependent analysis, a classifier is trained and tested for each individual with his/her own data, and the average accuracy for all subjects is computed, while in the subject-independent evaluation only one classifier is built splitting the data of all individuals into a training set and a testing set (Lara et al.,

2012). Then, a large set of metrics can be applied to evaluate the algorithm performance. These include confusion matrices, measurement of accuracy, recall, precision and F-Measure, and receiver operating characteristic (ROC) curves (Lara and Labrador, 2013).

Chapter 3

Literature Review

This Chapter provides a review of the existing studies in human activity recognition which can be applied to sports field, using wrist-worn sensors, such as smartwatches, bracelets or other type of sensors. Estimation of energy expenditure methods, using acceleration and heart rate data, are also reviewed, as well as works concerning the analysis of the running symmetry. The following keywords and combinations were used in the search: recognition, movement, activity, smartwhatches, wearables, wrist-worn, upper-limb, sports, accelerometer, inertial sensors, heart rate, heart rate variability, photoplethysmography, energy expenditure, physical activity, exercise training, running, symmetry.

Furthermore, it is made a review of current wrist-worn devices and mobile applications in sport context which use inertial and heart rate sensors in order to provide useful information to their users.

Finally, some public datasets which might be used in the development of this project are described.

3.1 Pattern Recognition of Movement and Activity

Wearable activity sensors can be placed on different parts of a human body whose movements are being studied. When it is necessary to measure the whole-body movement, the sensors are commonly placed on the sternum, lower back and waist. Most studies adopted waist-placement for motion sensors since it is close to the center of mass of a whole human body, so the accelerations measured by a single sensor can better represent the major human motion (Yang and Hsu, 2010). Some systems require the user to wear two or more accelerometers (Tapia et al., 2007; Ermes and Parkka, 2008; Ghasemzadeh et al., 2009; Riboni and Bettini, 2011; Reiss and Stricker, 2012; Garcia-Valverde et al., 2014), or carry a rucksack with recording devices (Ermes et al., 2008). However, such approach may be uncomfortable, causing constraint in body movement and discomfort, mainly during sport activities.

In order to improve comfort and reduce complexity and energy consumption, it is important to minimize the number of sensors required to recognize activities (Lara and Labrador, 2013).

Accuracy of sensors placed on wrist used to classify physical activities was compared with sensors placed on other parts of the body, such as hip (Bao and Intille, 2004; Liu et al., 2012; Mannini et al., 2013), waist (Fergus et al., 2015), thigh, upper arm and ankle (Bao and Intille, 2004; Mannini et al., 2013), and the accuracy results obtained were close, although sometimes lower. However, these seem to be reliable for sports purposes. A sensing platform that can be worn as a sport watch was presented by Maurer et al. (2006) and Lester et al. (2006), using an accelerometer (ACC), a light sensor, microphone, compass, temperature and barometer sensors. Furthermore, single ACCs placed on wrist were used in PA recognition (Yang et al., 2007, 2008; Chen et al., 2008; Siirtola et al., 2009; Kao et al., 2009), as well as sensors from smartwatches combined with sensors from smartphones (Riboni and Bettini, 2011; Garcia-Valverde et al., 2014; Ramos et al., 2016), or only a smartwatch (Chernbumroong et al., 2011). Table 3.1 presents a summary of the literature review done for this topic, including the devices and sensors used, their body placement and the sampling rates.

Maurer et al. (2006) analyzed the impact of the sensor specifications, such as the accelerometer sampling rate, which lies between 4 Hz (Lester et al., 2006) and 100 Hz (Yang et al., 2007, 2008; Chen et al., 2008; Siirtola et al., 2009; Kao et al., 2009; Reiss and Stricker, 2012), and they found that no significant gain in accuracy is achieved above 20 Hz for ambulation activities.

Vital signs data (e.g., heart rate, respiration rate, skin temperature, skin conductivity, ECG, etc.) have also been considered in a few works (Tapia et al., 2007; Liu et al., 2012; Lara et al., 2012; Reiss and Stricker, 2012; Lara and Labrador, 2013; Garcia-Valverde et al., 2014; Ríos-Aguilar et al., 2015; Altini et al., 2015). Tapia et al. (2007) proposed an activity recognition system that combines data from five triaxial ACCs and a HR monitor, concluding that the heart rate is not useful in a HAR context, since results only improved 1-2%. Contrariwise, some authors combined acceleration data with vital signs to achieve highly accurate activity recognition (Liu et al., 2012; Lara et al., 2012; Garcia-Valverde et al., 2014).

Physical activities, including walking, strolling, running, ascending or descending stairs, jogging, standing still and cycling can be classified according to the accelerations and heart rate signals measured from a wrist-worn device. Movement classification through machine learning techniques has been widely studied. Walking, for instance, can be identified by frequency-domain analysis of acceleration signals. It is characterized by a variance of over 0.02 g in vertical acceleration and frequency peak within 1–3 Hz in the signal spectrum. Discrete wavelet transform is used to distinguish walking on a level ground and walking on a stairway (Yang and Hsu, 2010).

Movement classification through supervised machine learning procedure had been applied using different classifiers: k-nearest neighbors classification, support vector machines, Naive Bayes classifier, Gaussian mixture model, hidden Markov model, decision trees and artificial neural networks. Tables 3.2 and 3.3 present a summary of the literature review done for pattern recognition of human movement and activity, including pre-processing, feature extraction, selection and classification methods, test mode and the accuracy obtained by the different works. Implementing activity recognition in mobile devices becomes challenging because they are still constrained in terms of processing, storage, and energy. Therefore, feature extraction and learning methods

Table 3.1: Literature review of the devices and sensors, their body placement and the sampling rates used for pattern recognition of human movements and physical activities.

References	Sensors and Devices	Body Placement	Sampling Freq. (Hz)
Bao and Intille (2004)	5 ACC	Wrist, Ankle, Thigh, Upper Arm	76.25
Maurer et al. (2006)	eWatch: ACC, Light Sensor	Wrist	50 and lower
Lester et al. (2006)	Wristwatch: Temperature,Micophone, Compass, Barometer, Light Sensor, ACC	Wrist	4
Tapia et al. (2007)	5 ACC and Heart Rate Monitor	Wrist, Hip, Ankle, Upper Arm, Thigh, Chest (HRM)	30
Yang et al. (2008), Chen et al. (2008), Kao et al. (2009), Siirtola et al. (2009)	ACC	Wrist	100
Ermes et al. (2008)	4 ACC	2 on Wrist, Ankle, Chest	50
Ermes and Parkka (2008)	ACC, GPS	Wrist, Hip and a Rucksack (GPS)	20
Ghasemzadeh et al. (2009)	ACC and Gyroscope	Upper Body, Upper Arm, Wrist and 2 on club	30 and 50
Chernbumroong et al. (2011)	eZ430-Chronos watch: ACC	Wrist	33
Riboni and Bettini (2011)	Smartphone: ACC, GPS, Smartwatch: ACC	Wrist and Pocket	16
Reiss and Stricker (2012)	3 IMU and Heart Rate Monitor	Chest, Wrist, Ankle	100
Lara et al. (2012)	BioHarnessTM: Vital Signals, Heart Rate, ACC	Chest	30 (ACC) 1 (Vital Signals)
Liu et al. (2012)	Ventilation Sensor (breathing) and 2 ACC	Hip and Wrist	30
Mannini et al. (2013)	4 ACC	Wrist, Thigh, Hip, Upper Arm, Ankle	90
Ramos et al. (2016), Garcia-Valverde et al. (2014)	Smartphone, Smartwatch: ACC,Gyroscope, Heart Rate Monitor	Wrist and Pocket	-
Altini et al. (2015)	ECG Necklace: ACC, Heart Rate	Neck and Chest	256 (ECG), 32 (ACC)
Fergus et al. (2015)	4 ACC	2 on Wrist, 2 on Hip	-

should be carefully chosen to guarantee a reasonable response time and battery life (Lara and Labrador, 2013).

Riboni and Bettini (2011) developed a system for automatic activity recognition based on the integration of hybrid statistical and ontological reasoning, COSAR. The use of the COSAR technique considerably improves the recognition rate with respect to the solely statistical techniques (error reduction of 45.43% with respect to the statistical technique, and of 29.32% with respect to the statistical-hist technique). COSAR avoids many misclassifications between activities characterized by similar body movements but different contexts (e.g., location). The historical variant of COSAR further improves classification results, gaining a recognition rate of 93.44% (error reduction of 39.26% with respect to the COSAR technique).

Regarding ACC data, statistical feature extraction is employed and, in most of the cases, either time- or frequency-domain features. Techniques like Principal Component Analysis (Ghasemzadeh et al., 2009; Yang et al., 2008) are used to handle the high variability inherent to acceleration signals. Also, some studies apply Linear Discriminate Analysis to transform features (Maurer et al., 2006; Yang et al., 2007; Chen et al., 2008; Kao et al., 2009; Ghasemzadeh et al., 2009). Bao and Intille (2004) and Ermes et al. (2008) extracted frequency domain entropy to discriminate activities with similar energy values, such as biking and running. Moreover, the peak frequency of the PSD is used to detect cyclic activities (walking, running and cycling). Ermes et al. (2008) used the signal variance to estimate the intensity of an activity. Bao and Intille (2004) suggested that some common everyday activities in naturalistic settings could be detected using fast FFT-based feature computation and a decision tree classifier algorithm. Decision trees are slow to train but quick to run, so, a pre-trained decision tree should be able to classify user activities in real-time on emerging mobile computing devices with fast processors and wireless accelerometers.

Before ACC features are extracted and/or derived, the signal is often high pass filtered to remove any baseline offset (Yang et al., 2008) and interpolated using cubic spline interpolation (Tapia et al., 2007; Fergus et al., 2015) for missing values. Moving average filters are also used to remove the random noise (Ghasemzadeh et al., 2009; Chernbumroong et al., 2011; Garcia-Valverde et al., 2014). Altini et al. (2015) applied a bandpass filter between 0.1 and 10 Hz to isolate the dynamic component due to body motion and a low-pass filter at 1 Hz. Mannini et al. (2013) used signal magnitude vectors (SMV[1]) which were low pass filtered using a 15 Hz cut-off 4th order Butterworth filter. This way, he limited the bandwidth of the signal to the frequencies common in human motion, removing high frequency noise. This work also investigated the effect of removing wavelet based features from the training set. These features provide not only good frequency resolution at low frequencies, but also better time resolution at higher frequencies, however, they require substantial processing. The authors concluded that the improvement of 0.6 percentage points is at the cost of a 12% increase in computation time. Thus, wavelet based features might be excluded.

Since vital signs have much lower variability than acceleration signals, Lara et al. (2012)

---

[1]$SMV = \sqrt[2]{ACC_x^2 + ACC_y^2 + ACC_z^2}$

proposed structure detectors, i.e., linear and non-linear functions, to extract features. Moreover, they used the magnitude of change and the trend of the vital signs to discriminate among activities during periods of vital sign stabilization, overcoming the transient period issue (e.g. the interval of time after stop running in which vital signs remain as if running).

To dimensionally reduce the number of features, a common method is the Minimum Redundancy and Maximum Relevance (Liu et al., 2012). In contrast, Maurer et al. (2006) and Chernbumroong et al. (2011) applied a Correlation-based Feature Selection approach, which works under the assumption that features should be highly correlated with the given class but uncorrelated with each other (Lara and Labrador, 2013).

In the work by Mannini et al. (2013), the author concluded that one of the limitations of previous studies was the fact that the algorithms have been trained and evaluated on small pools of participants with little data per participant. Moreover, some studies used 50% overlapping windows, which leads some of the same data to appear in two windows, potentially inflating recognition results, especially if this overlapping window technique is applied jointly with n-fold validation. In fact, the measured time series if often divided in time overlapping time windows, which are intended to handle transitions more accurately. This information is included in the "pre-processing" column of the Table 3.2, and it can be seen that many windows lengths are used among the different studies.

Some authors pointed out that specific recognition model should be built for each individual, since people perform activities in a different manner due to age, gender, weight, fitness level, and so on (Bao and Intille, 2004; Tapia et al., 2007; Reiss and Stricker, 2012). On the other hand, authors prefer a monolithic recognition model, flexible enough to work with different users. Therefore, two types of analysis have been proposed to evaluate activity recognition systems: subject-dependent and subject-independent evaluations (Lara and Labrador, 2013). In the second one, only one classifier is built for all individuals using *n*-fold cross validation (Maurer et al., 2006; Lester et al., 2006; Siirtola et al., 2009; Chernbumroong et al., 2011; Riboni and Bettini, 2011; Lara et al., 2012; Ramos et al., 2016) or leave-one-individual-out analysis (Bao and Intille, 2004; Yang et al., 2007; Tapia et al., 2007; Chen et al., 2008; Yang et al., 2008; Ermes et al., 2008; Liu et al., 2012; Altini et al., 2015).

Mannini et al. (2013) compared the two subject-independent approaches. In the *n*-fold cross validation, data are randomized and divided, and the algorithm is trained on *n-1* subsets and tested on the remaining one. This process is performed *n* times, alternating circularly the test subset. The leave-one-subject-out cross validation is a specific case of *n*-fold, with *n* equal to the total number of data. The subsets correspond to data from the various participants, and data from all subjects are used to train except one that is used for test phase. Results were better using leave-one-subject-out, since it avoids the problem of *n*-fold cross validation which can encourage the algorithm to overfit the data.

Table 3.2: Literature review for pattern recognition of human movements and physical activities. Continued in Table 3.3.

References	Pre-processing	Features Extracted	Feature Selection and Classification	Test mode	Accuracy (%)
Bao and Intille (2004)	SW with 50% overlap (6.7 s)	Mean, Energy, Entropy, Correlation	DT C4.5, NB	LOSO, SPEC	C4.5: 71.58±7.4(*SPEC*) 84.26±5.19(*LOSO*)
Maurer et al. (2006)	SW	Variance, RMS, SD, ZCR, Interquartile, MAD, MCR, Mean, Cumulative Histogram	LDA, CFS, DT, NB, KNN	5 cross	DT: 87
Lester et al. (2006)	0.25s Windows	FFT freq. coefficient, BPF coefficient, Correlation, Entropy, Integral, Mean, Variance	Exclude features, Static, HMM	4 cross	HMM: 87, HMM, ACC: 45
Tapia et al. (2007)	ACC: SW with 50% overlap (4.2s), CSI HR: AF, 30s Window	AUC, Variance, Mean, Entropy, MDA, Correlation, FFT peaks, Energy, Number Heart Beats>Resting HR	DT, NB	SPEC (10 cross), LOSO	SPEC: 94.6 LOSO: 56.3
Yang et al. (2007)	SW with 50% overlap (5.24s)	Mean, Correlation, Interquartile, MAD, RMS, SD, Variance, Energy	LDA, FSS, NFC	LOSO	FSS: 83.41±5.93 LDA: 92.86±5.91
Yang et al. (2008)	HPF overlap Window	Mean, MAD, RMS, Correlation, SD, Variance, Energy, SMA	PCA, ANN, KNN	LOSO	ANN: 95.24, KNN: 87.18
Ermes et al. (2008)	SW with 50% overlap	Average, Variance, PSD peak, Entropy	DT	-	94
Ermes and Parkka (2008)	-	Mean, Variance, Median, Skew, Kurtosis, Percentil, PSD peak, Speed	Custom DT, Automatic generated DT, ANN, HM	LOSO	HM: 89
Chen et al. (2008), Kao et al. (2009)	SW with 50% overlap	Mean, Correlation, Energy, MAD, Interquartile, RMS, Variance, SD	LDA, FBF	LOSO	93 and 94.71
Siirtola et al. (2009)	Data compression	Mean, SD, Percentil Variance,y-Average change	Clustering based, DT	10 cross	85
Ghasemzadeh et al. (2009)	5-point MAF	Mean, Variance, SD, MAD, RMS	PCA, LDA, LR	-	-

Table 3.3: Continued from Table 3.2.

References	Pre-processing	Features Extracted	Feature Selection and Classification	Test mode	Accuracy (%)
Chernbumroong et al. (2011)	MAF, SW with 50% overlap	Minimum, Differences, Mean, Coefficient Sum, Energy, Entropy, SD, Variance, Correlation	CFS, DT, ANN	5 cross	DT: 94.13, ANN: 90.45
Riboni and Bettini (2011)	-	Mean, Variance, Correlation, Kurtosis, other	DT, NB, MLR, SVM, COSAR	4 cross	COSAR: 93
Reiss and Stricker (2012)	SW 5.12s	Mean, Variance, Energy. HR: Mean, Gradient	Boosted DT, Bagging DT, DT, NB, kNN	SPEC (9 cross), LOSO	KNN, Boosted DT: 90 and over
Lara et al. (2012)	SW with 50% overlap (5s, 12s, 20s)	Mean, Variance, SD, Correlation, Interquartile, MAD, RMS, Energy	NB, DT, ANN, ALR	5x2 cross	12s Window, ALR: 95.7
Liu et al. (2012)	Micro-controller	ACC: Mean, SD, Median, Correlation, Energy, Entropy, Percentil; Breathing: freq.	MRMR, SVM, kNN, NB	LOSO	SVM: 76 (Wrist ACC), 88 (all)
Mannini et al. (2013)	LPF and 12.8s, 4s, 2s Windows	Mean and SD of SMV, PSD, Wavelet Transform, Minimum, Maximum	Sets' combination, SVM	N cross, LOSO	12.8s Window, LOSO: 95.0 (Ankle), 84.7 (Wrist)
Garcia-Valverde et al. (2014)	MAF	Time domain features	Sets' combination, KNN, Boosted DT	-	DT: 99.7, KNN: 99.3
Altini et al. (2015)	ACC: BPF (1-10Hz)	ACC: Mean, Variance, SD, Median, MAD, MDA, Interquartile, Correlation, RR interval freq.	Clustering based, SVM + HMM	LOSO	SVM + HMM: 92.3
Fergus et al. (2015)	CSI	ACC: Mean. direct observation BMI, EE, VO_2, HR	MLP, SVM, DT, NB, ANN	cross feature	MLP: 74 (Wrist and HR)
Ramos et al. (2016)	-	Mean, SD, Mean + SD	Sets' combination, DT, NB, SVM	10 cross	SVM: 89.63 (Mean + SD)

3.2   Estimation of Energy Expenditure

Energy expenditure can be estimated by measuring physical activities. Studies by Liu et al. (2012), Altini et al. (2012) and Garcia-Valverde et al. (2014) estimated EE after recognition of the physical activities involved using methods mentioned on the previous section.

The doubly labeled water (DLW) method, which is done by administering a dose of DLW and then measuring the elimination rates of deuterium and oxygen-18 in the subject over time, and indirect calorimetry, that measures oxygen uptake, carbon dioxide production and cardiopulmonary parameters, are regarded as the gold-standard references of EE (Yang and Hsu, 2010). These are often used as ground truth to compare with results from more recent methods, which use ACC and/or HR data (Thompson et al., 2006; Staudenmayer et al., 2009; Assah et al., 2010; Altini et al., 2012; Santos et al., 2014), and can replace the gold-standard techniques, which are expensive, require a controlled laboratory environment and are not convenient in a free-living environment (Yang and Hsu, 2010).

Metabolic Equivalent Tasks equations, derived or validated for different accelerometers, have been used to better match exact EE of physical activities among subjects (Thompson et al., 2006; Staudenmayer et al., 2009; Assah et al., 2010; Duclos et al., 2016).

Staudenmayer et al. (2009) developed two artificial neural networks to apply to PA data collected with a Actigraph uniaxial ACC. The first ANN model estimated physical activity METs (i.e. energy expended in PA), and the second ANN identified activity type. They correctly classified activity type (low-level activities, locomotion, vigorous sports, and household/other activities) 88.8% of the time, showing that they could successfully estimate activity METs and identify activity type using ANN analytic procedures, which simpler regression-type methodologies would not.

To predict EE associated with each activity, Liu et al. (2012) implemented a regression version of the SVM, the support vector regression, to estimate METs and obtained an accuracy of 93.4% using an ACC on the wrist. However, their previous results for activity recognition with SVM were 75.8% accurate. Many factors affect the accuracy of EE estimation using accelerometry, for instance, the location and attachment of ACCs, external vibration, gravitational artifact and the types of activity performed (Yang and Hsu, 2010). Moreover, Staudenmayer et al. (2009) suggested that multiple accelerometers and subject-specific models would better identify specific activities.

Therefore, another promising possibility is the use of both heart rate and accelerometry measures to recognize human activities and estimate energy expenditure, as proposed by many (Assah et al., 2010; Altini et al., 2012; Santos et al., 2014; Garcia-Valverde et al., 2014; Altini et al., 2015; Duclos et al., 2016). Thompson et al. (2006) earlier suggested that combined accelerometry and heart rate provides an accurate estimate of criterion EE, whereas a simple motion sensor does not.

Assah et al. (2010) and Santos et al. (2014) examined the validity of Actiheart, a combined HR and motion sensor (uni-axial ACC), in estimating PA EE. Both works showed that combined sensor measures did not significantly differ from the DLW method.

Assah et al. (2010) used branched equation modelling and, compared with the combined models, the separate ACC or HR models were less accurate in predicting DLW measures. In this work, accelerometer data was converted to EE using group calibrated accelerometry equations, corresponding to level walking or running acceleration, and a group calibration HR equation, modified from the equation published by Brage et al. (2004), was used to assess the additional benefit of using individual calibration compared with group calibration. Results showed that the mean bias doubled for group compared with individual calibration of HR.

Both works concluded that combined HR and movement sensing is a valid method for estimating free-living PA EE. The main problems were the small sample size of the validation study and the possibility of Actiheart electrodes become loose. Moreover, Santos et al. (2014) concluded that this method had limited usefulness to assess EE in a population with high levels of physical activity due to the high rate of equipment failure.

In the study by Santos et al. (2014), accelerometry models provided the highest individual errors. It underestimated EE which is in accordance with Brage et al. (2004), that stated that accelerometry models tend to underestimate PAI, mainly due to the variability of the sources of movement and the assumptions about the efficiency of the work performed. The use of HR is not error free also, as its relation with PAI may be affected by several factors. It is then expected that EE models that consider both accelerometry and HR data will present better accuracy. Santos et al. (2014) further concluded that individual heart rate calibration is not necessary when using combined heart rate and motion sensor in a very active population.

Altini et al. (2012) combined static METs with activity-specific regression equations, applying four steps to derive an EE model: 1) categorize activities into clusters meaningful for EE estimates; 2) separate sedentary and non-sedentary activities; 3) examine the motion patterns of non-sedentary clusters to select the best independent variables for the prediction models and, when no differences in motion were distinguishable within one cluster, physiological signals were used to discriminate between different levels of EE; 4) include anthropometric characteristics to take into account differences in body size. They used a necklace which combines ACC and HR data. Since HR signals differ greatly at the individual level, they required individual calibration or normalization. The heart rate above rest was used as the only heart rate feature, to reduce between subject differences in HR during different activities. Measures of motion intensity outperformed HR for low to medium intensity activities, while activities where whole body motion is not representative of EE, such as biking, were better modeled by methods using HR as well. Walking patters were predicted accurately by methods using ACC only features when differences in EE could be explained by motion patterns alone. Overall, combining manually selected ACC and HR features, representative of variations in EE within a cluster, showed significant improvements compared to other methods (with increases in accuracy from 18 to 31%).

Altini et al. (2015) determined activity composites and used them to optimize the correlation to HR normalization parameters. Also, individual-specific HR normalization parameters were used to normalize HR, which was then included in activity-specific regression models to estimate EE. The HR normalization minimizes the effect of individual fitness differences from entering

in EE regression models. HR normalization provided optimal results for moderate to vigorous activities, especially the ones where ACC data is not indicative of EE due to lack of whole body movement (as shown by the highest reduction in root mean square error for EE estimation when biking, 18.0%). Other activities such as rowing and walking uphill would most likely benefit as well, due to the inability of ACCs alone to estimate EE accurately.

Duclos et al. (2016) proposed an acceleration vector variance based method, which consists of a function which takes into account data from the smartphone or the smartwatch (or both devices, depending on the activities), personalized categories from acceleration variance, and age, gender, weight and height of participants. They compared the EE given by a smartphone and a smartwatch with that produced by Armband, and the mean error of EE obtained between the proposed function and Armband was less than 4%. This work defined a new predictive mathematical function of EE, which competes with the non-public function used in dedicated costly devices such as Armband. In addition, it demonstrated the potential of wearable technologies.

3.3   Running Symmetry Analysis

As mentioned before, accelerometer and heart rate monitoring are useful to evaluate the physical demands of an activity. Markers such as running symmetry might also be considered in evaluation of injury occurrence and sports performance (Saba, 2016).

To study the running symmetry is necessary to evaluate the human movement parameters. Satkunskiene et al. (2009) performed a biomechanical analysis of walking and running using an accelerometer placed at different body positions to find out its optimal position to determine what components of acceleration are most valuable. To evaluate the quality of walking/running they obtained the parameters such as speed, rate, steps duration and length and symmetry index which is commonly used for evaluation of gait symmetry during walking, running and stair stepping. Results showed that the vertical component of acceleration measured on the hip is most informative.

Running asymmetries can also be detected through wearable sensors placed on tibia (Moran et al., 2015) and trunk (Saba, 2016). A running symmetry is a ratio of the synchronization of the right and left lower limbs during the gait cycle (Saba, 2016). The highest impact accelerations/loads are produced in *y*-axis direction, thus Moran et al. (2015) concluded that the sum of impact accelerations along the tibial longitudinal *y*-axis was best able to identify asymmetries and was able to identify asymmetry in all participants. For each step, they captured accelerations and segment angular velocities, from which discrete features of interest were extracted in all three planes (minima and maxima, the sum of the signal over one step cycle, and the cycle's standard deviation). To determine an asymmetry value, the measures were subsequently subtracted (right-left). Work by Saba (2016) showed that a trunk-mounted unit, that incorporates GPS, accelerometer, and magnetometer housed in a waterproof case, can be reliably used to monitor running symmetry and to detect asymmetrical gait patterns. The magnitude of asymmetry detected was similar to that detected by ankle-mounted sensors. Moreover, it was confirmed that

running symmetry is affected by varying work out intensities due to fatigue, leading to increased gait asymmetry.

Worn on feet, TUNE (specifications in Appendix B) measures speed, each foot's ground-contact time, heel-contact time and balance/symmetry during a full run. It provides both real-time data during the run, as well as a post-run analysis that shows the evolution of the runner's form throughout a run, and over a longer period of time. This provides the runner with an accurate view of their progression and allows to better understand how certain conditions (uphill, downhill, fatigue, etc.) affect their running form.

No studies were found integrating wrist-worn sensors information to detect running asymmetries. However, some studies used wrist-worn sensors for arm's tracking (Shen et al., 2016; Pereira, 2016) and recognition of upper limb movements (Biswas et al., 2014, 2015). Arm symmetry in swimming was studied by Stamm et al. (2012) through a wearable sensor placed on the lower back. Here, the recorded acceleration data was filtered using a 0.5Hz high-pass Hamming windowed finite impulse response filter to gain the sensor orientation. The signal was then analyzed using a zero-crossing detection algorithm to find the individual stroke rates and the differences between left and right arm stroke durations (asymmetry). The comparison of the accelerometer with the video derived results proofed that the sensor is capable of measuring the arm stroke symmetry as accurate as the video method.

These studies might be important to integrate data from wrist-worn sensors in the detection of running asymmetries, since the movement described by the arms during a run plays an important role in its proper execution. Pereira (2016) developed an inertial tracking system to obtain upper limb joint positions and trajectories in 3D using two inertial measurement units (IMU) placed at elbow and wrist. An extended Kalman filter was used as a sensor fusion method that fuses data from accelerometers, gyroscopes and magnetometers, in order to obtain the orientation of each segment. Lastly, a set of equations was defined to represent the upper and lower segments to reconstruct position and trajectory (motion) of the upper limb. Results demonstrated an acceptable performance in different movements, however, a sensor-to-body transformation process had to be developed in order to overcome errors due to the alignment of the sensors.

Furthermore, Shen et al. (2016) tracked the 3D posture of the entire arm (wrist and elbow) using the motion and magnetic sensors on smartwatches. The challenge of using only one smartwatch, a single point on the wrist, as overcame due to the fact that the pointing direction of the forearm is strongly coupled to the arm's posture. A system that fuses IMU sensors and the anatomy of arm joints into a modified hidden Markov model was developed and achieved around 9.2 cm of median error for free-form postures and 13.3 cm for a real time version, when compared with Kinect 2.0. To note that a particle filter was first implemented, but resulted in a high-dimensional system and the estimator could hardly converge, thus the authors aborted the effort and focused on reducing the state space of the system for good tracking accuracy.

3.4 Wrist-Worn Devices and Mobile Apps in Sports

Health and fitness trackers have been developed to record activity and monitor vital signs, such as calorie consumption, fitness activity, pulse, weight and heart rate. To track oxygen intake and activity pattern along with calorie burning rate, such trackers use 3D accelerometers to identify movement and transform it to calories burnt. Many studies concluded that majority of wearable devices produce invalid measures of energy expenditure, overestimating the measures. However, the successful use of these devices, both in sports and health applications, is due to the implementation of sensor fusion methods, combining 3D accelerometers, pedometers and heart rate monitors, which present many advantages when compared to activity monitor systems (El-Amrawy and Nounou, 2015; Magalhães, 2016).

Many wrist-worn fitness devices include embedded heart rate monitors, which measure HR by using light to track the blood (PPG based). These can be smartwatches or wristbands, such as Apple Watch 1 and 2[2], Motorola Moto 360[3], Samsung Gear S2 and Fit2[4], PulseOn[5], Garmin Vívosmart HR, Vívosmart HR+, and Vívoactive H[6], Polar M600[7], TomTom Spark 3 Cardio[8], and Fitbit Charge 2, Blaze and Surge[9]. Table 3.4 compares available wrist-worn fitness devices, which have both heart rate and accelerometer sensors, in terms of price, compatibility, battery life, and other specifications. All of them allow to monitor activity and heart rate, including basic features such as step counting, calories burned, distances and heart rate zones. Furthermore, these devices transmit data to smartphones or other devices via Bluetooth connection.

Recent study by El-Amrawy and Nounou (2015) evaluated the accuracy, precision, and overall performance of seventeen wearable devices currently available compared with direct observation of step counts and heart rate monitoring. With regards to the step count evaluation, the accuracy of the tested devices ranged between 79.8% (Samsung Gear 2) and 99.1% (MisFit Shine), while the precision ranged between 4% (MisFit Shine and Qualcomm Toq) and 17.5% (Jawbone UP). Concerning heart rate measurements, the accuracy ranged from 99.9% (Apple Watch) to 92.8% (Motorola Moto 360), and precision ranged from 5.9% (Apple Watch) to 20.6% (Samsung Gear S). They conclude that the accuracy and precision of the selected fitness trackers are reasonable and can indicate the average level of activity and thus average energy expenditure.

PulseOn design reduces artefacts and improves HR reliability, moreover, movement artefacts are reduced by adaptive movement-cancellation algorithms and optimized mechanics, which stabilize the sensor-to-skin contact (Delgado-Gonzalo et al., 2015).

---

[2]http://www.apple.com/pt/watch/

[3]https://www.motorola.com.br/products/moto-360-sport

[4]http://www.samsung.com/pt/wearables/gear/

[5]http://pulseon.com/

[6]https://buy.garmin.com/pt-PT/ES/cIntoSports-c571-atFILTER_FEATURE_HEARTRATE_01-p1.html?sorter=featuredProducts-desc

[7]https://www.polar.com/pt/produtos/sport/M600

[8]https://www.tomtom.com/pt_pt/sports/fitness-trackers/gps-fitness-watch-cardio-spark3/black-large/

[9]https://www.fitbit.com/eu

Table 3.4: Comparison of available wrist-worn fitness devices. *Only iOS and Android systems are considered.

Fitness Tracker	Price (€)	Compatibility*	Battery Life	Wi-Fi	GPS
Smartwatch					
Apple Watch 1	349	iOS	18h	yes	no
Apple Watch 2	449-999+	iOS	18h	yes	yes
Motorola Moto 360	300	Android	1 day	yes	yes
Samsung Gear S2	350	Samsung	2-3 days	yes	no
Vívoactive HR+	270	Android & iOS	13h (GPS)	no	yes
Polar M600	349	Android & iOS	8.5h (GPS)	yes	yes
Fitbit Blaze	200	Android & iOS	5 days	yes	no
Fitbit Surge	250	Android & iOS	10h (GPS)	yes	yes
Spark 3 Cardio	199	Android & iOS	11h (GPS)	no	yes
Wristband					
Samsung Gear Fit2	170	Samsung	9h (GPS)	yes	yes
PulseOn	186	Android & iOS	7 days	no	no
Vívosmart HR	149	Android & iOS	5 days	no	no
Vívosmart HR+	220	Android & iOS	8h (GPS)	no	yes
Fitbit Charge 2	160	Android & iOS	5 days	no	no

The battery life of these devices is very limited, mainly due to GPS. In the case of TomTom Spark 3 Cardio, although it has a battery life of 11h using GPS, it can go up to 3 weeks in activity tracking mode, without GPS.

Garmin devices include performance, activity tracking and running features, such as auto pause (pause and resume timer based on speed), auto lap (automatically start a new lap), auto goal (learn your activity level and assigns a daily step goal), time/distance alert (trigger alarm when you reach the goal), save personal records and compute heart rate-based calorie. Moreover, Garmin Vivoactive HR has built-in sport Apps which include features for cycling, swimming (lengths, distance, pace, stroke count/rate, calories), golfing (calculates exact yardage for shots from anywhere on course, calculates distance to front, middle and back of green, and has a digital scorecard), ski/boarding, cross country skiing and stand-up paddle boarding.

The Polar M600 allows to choose from over a hundred sports profiles and has a Smart Calories feature that provides an accurate calorie output based on the maximum heart rate and training intensity.

Fitbit devices detect and record workouts in the Fitbit App, and show simplified heart rate zones. Charge 2 monitors cardio fitness level and performs guided breathing sessions based on the heart rate, which helps the user to return breathing to normal after a workout. Like the Blaze, the Charge 2 automatically tracks exercises like basketball, biking, hiking, running, and more.

However, it takes upwards of 10 to 15 minutes to register that the user is doing an activity. Fitbit App syncs with the recorded workouts by the Fitbit trackers so that the user can see all exercise stats, their impact on overall day, and how is the performance improving. Also, users can check their cardio fitness level, which is basically a breakdown of the heart rate data (resting, average, and peak) and estimated VO_{2max}. Several Apps use Fitbit trackers to assess PA and HR, however, Fitbit does not allow to access the data in real-time (Magalhães, 2016).

Moto 360 has a built-in activity tracker, Moto Body App, to monitor daily efforts and offers coaching advice to help users meet their goals.

Apple Watches include the Workout App, where users can choose from 12 indoor and outdoor workouts, Activity App, to track all the activity throughout the day, and allow to connect with Third-Party Workout Apps.

Google Play Store and App Store offer several apps related to Health & Fitness, being the most popular the Google Fit App[10], and the Apple Health App[11], respectively. Users can access to their data in real-time and anywhere, since their progress can be tracked from the smartphone/iPhone, tablet/iPad, Android Wear Watch/Apple Watch, or web. Furthermore, they consolidate health data from third-party apps to monitor fitness, nutrition, sleep and weight data: Nike +, Runkeeper, Strava, MyFitnessPal, Lifesum, Basis, Withings and Xiaomi Mi Band, among many others.

Most of the devices which monitor heart rate present heart rate training zones to help the users track their heart rate during exercise. These zones are defined based on the maximum heart rate (FHR-age) as depicted in Figure 3.1[12]. Some also use heart rate together with speed and personal info (such as age, sex and weight) to estimate VO_{2max}, since the better the aerobic fitness, the more oxygen can pass into body.

EXERCISE ZONES									
				AGE					
20	25	30	35	40	45	50	55	65	70
100% 200	195	190	185	180	175	170	165	155	150
VO₂ Max (Maximum effort)									
90% 180	176	171	167	162	158	153	149	140	135
Anaerobic (Hardcore training)									
80% 160	156	152	148	144	140	136	132	124	126
Aerobix (Cardio training / Endurance)									
70% 140	137	133	130	126	123	119	116	109	105
Weight control (Fitness / Fat burn)									
60% 120	117	114	111	108	105	102	99	93	90
Moderate activity (Maintenance / Warm up)									
50% 100	98	95	93	90	88	85	83	78	75

Figure 3.1: Heart rate zone training with wearables.

---

[10]https://play.google.com/store/apps/details?id=com.google.android.apps.fitness

[11]http://www.apple.com/ios/health/

[12]http://gadgetsandwearables.com/2017/01/13/benefits-of-heart-rate-zone-training/

3.5 Datasets

Some of the previous works used public datasets in order to evaluate human activity recognition techniques and to monitor physical and aerobic activities. To predict the activity being performed and energy expenditure, acceleration and heart rate variability patterns are used.

COSAR-DS-1.0[13] dataset was acquired to evaluate activity recognition techniques under the Pal-SPOT Project and it was used in the work by Riboni and Bettini (2011). For the experimental evaluation of activity recognition techniques, 5-hours activity data were collected by two Pal-SPOT (Small Programmable Object Technology) sensors placed on the left pocket of the subjects, plus a GPS, and another on their right wrist. Data from the accelerometer of each sensor was collected at 16 Hz and, for each activity instance, accelerometer readings were merged to build a feature vector composed of 148 features, including means, variances, correlations, kurtosis, and other statistical measures. Six volunteers, three men and three women of ages ranging from 30 to 60 years old and with different levels of athletic preparation, recorded 10 different activities (brushing teeth, climbing up, climbing down, riding a bicycle, jogging, standing still, strolling, walking downstairs, walking upstairs, writing on a blackboard) performed both indoor and outdoor.

The Activity Recognition Repository[14] presents 6 *arff* files containing information of 4 physical activities (walking, standing, sitting and driving) collected from 3-axis accelerometers of a smartphone (Sony Smartphone Xperia Z1) and a smartwatch (Sony SmartWatch 2 SW2) in order to study their usage in HAR (Ramos et al., 2016). This dataset includes arithmetic mean and standard deviation features. The subjects were thirteen, twelve males and one female, aged from 20 to 35 years old and without any physical disability.

The Heterogeneity Dataset[15] for Human Activity Recognition from Smartphone and Smartwatch sensors consists of two datasets created to investigate the impact of sensor heterogeneities on HAR algorithms (Stisen et al., 2015). It contains the readings of accelerometers and gyroscopes, sampled at the highest frequency the respective device allows. Reading were recorded from nine users while executed 6 different activities (biking, sitting, standing, walking, walking downstairs and walking upstairs) carrying 4 smartwatches (2 LG watches, 2 Samsung Galaxy Gears) and 8 smartphones (2 Samsung Galaxy S3 mini, 2 Samsung Galaxy S3, 2 LG Nexus 4, 2 Samsung Galaxy S+).

The public datasets PAMAP and PAMAP2[16] include both activity and heart rate data and were used in works by Reiss and Stricker (2012) and Magalhães (2016). The PAMAP dataset was recorded with an early system prototype developed in the PAMAP (Physical Activity Monitoring for Aging People) project to identify basic aerobic activities and estimates their intensity level. Eight volunteers, 7 male and 1 female, aged from 25 to 31 years old, were subjected to a predefined data collection protocol of about one hour each, which makes approximately 8 hours of data

---

[13]http://everywarelab.di.unimi.it/palspot

[14]https://goo.gl/Y8NXP1

[15]https://archive.ics.uci.edu/ml/datasets/Heterogeneity+Activity+Recognition

[16]http://www.pamap.org/demo.html

collected. The subjects wore 3 Colibri wired IMUs on wrist, chest and ankle, and a HR-monitor on the chest. The PAMAP2 dataset was recorded to physical activity monitoring and includes data from nine volunteers subjects, 8 male and 1 female, aged from 25 to 31 years old, wearing the same sensors as in PAMAP dataset, and performing 18 different activities. Over 10 hours of data were collected altogether, from which nearly 8 hours were labeled as one of different 18 activities. Both datasets include outdoor (walking, running, cycling, playing soccer and rope jumping) and indoor (lying, sitting, standing, vacuum cleaning, ironing and ascending/descending five flights of stairs) activities, and transient activities (e.g. going from one location to the next activity's location, or waiting for the preparation of some equipment).

The dataset mHealth[17] was recorded to benchmark techniques dealing with human behavior analysis based on multimodal body sensing. Ten volunteers of diverse profile worn 3 Shimmer2 sensors placed on chest, right wrist and left ankle, which acquired acceleration, rate of turn and magnetic field orientation data. The sensor positioned on the chest also provided 2-lead ECG measurements. All data was acquired at 50 Hz and during 12 different activities (standing still, sitting and relaxing, lying down, walking, climbing stairs, waist bends forward, frontal elevation of arms, knees bending, cycling, jogging, running, jump front and back) of 1 minute or 20 repetitions, depending on the activity (Banos et al., 2014, 2015).

Among these datasets, ACC data acquired from wrist-worn sensors was useful during the development phase of this project. Also, the heart rate data present in the datasets was useful to compare with HR data acquired using smartwatches to infer on its reliability.

---

[17]https://archive.ics.uci.edu/ml/datasets/MHEALTH+Dataset

Chapter 4

Research and Development Methodology

This Chapter presents the work developed in this dissertation, including the research methodology and the development of a system which fuses inertial and heart rate sensors to be implemented in wearables. The system was implemented in a smartwatch to track the upper limb and physiological signals in order to obtain measures of physical activity and energy expenditure, and to recognize patterns of movement and activity. The system was then integrated with TUNE, allowing runners to get motor learning and training feedback information, reduce potential for injuries, increase motivation and improve their running experience. The technologies and methodologies used are explained in detail.

4.1 System Overview

Figure 4.1 depicts the architecture of the developed system. Each module is described in detail in the following sections. A wearable system, composed of TUNE and the smartwatch Moto 360, was used to measure relevant movements and physiological signals in running context (Data Acquisition module in Section 4.2). The movement of the upper limb was measured through the acceleration sensor of the smartwatch, and the heart rate was measured trough its photoplethysmography (PPG) sensor. The movement of the lower limbs was obtained through TUNE, which monitors both feet using force sensitive resistor (FSR) sensors and GPS data to analyze symmetry during a full recording.

The signals provided by the smartwatch were pre-processed as described in Section 4.3, in order to remove random noise and isolate the frequencies of interest.

Acceleration signals were used to perform activity recognition. Section 4.4 describes the features extracted, their selection and the classification techniques used. The result of this module was used to estimate energy expenditure, which was calculated according to the activity being performed, the heart rate measures, the personal information of the subject and the GPS data from TUNE, as described in Section 4.5.
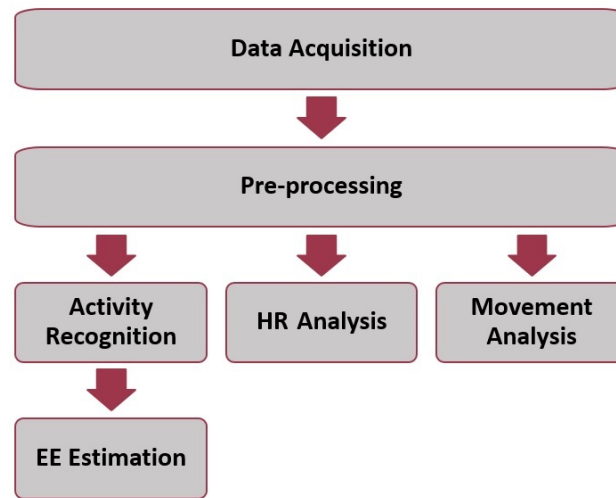
Figure 4.1: System flowchart.

Heart rate signal was also used to determine HR zones of exercise and training intensity, as mentioned in Section 4.6.

To analyze the movement of the arm (Section 4.7), the peaks of the acceleration signal were detected to count steps and to calculate the amplitude of the arm in terms of acceleration. These measurements can be compared with TUNE data, such as step counting and ground contact time in order to relate movements of the arms and feet.

Android Studio and SDK Tools were used to build an application for both wearable and mobile devices in order to obtain and save acceleration and heart rate signals from the smartwatch and to record data from TUNE. Python was used to evaluate the signals and test all the methodologies described, which were later implemented in Android to build a wearable application, as described in Section 4.8.

4.2 Data Acquisition

4.2.1 Smartwatch

Motorola Smartwatch Moto 360[1] placed at the dominant wrist was used to acquire acceleration and heart rate signals. Both signals were saved in real time together with their time stamp (the time in nanosecond at which each event happened). Moto 360 has bluetooth and Wi-Fi communication and the operative system Android Wear^{TM} is compatible with Smartphones Android^{TM} 4.3 or higher. It was design for sports, with barometric altimeter, accelerometer, ambient light sensor, gyroscope, vibration/haptics engine and heart rate sensors. Heart rate is obtained through an optical heart rate monitor (PPG) and Moto 360 allows to continuously track heart rate during a run to monitor performance.

---

[1]https://www.motorola.com.br/products/moto-360-sport

Moto 360 includes a built-in activity tracker to monitor users daily efforts and offers coaching advice to help them meet their goals (Moto Body). It has built-in GPS that works seamlessly with Moto Body to measure performance, and it allows to track distance travelled, pace, lap times, and more. For running and fitness, Moto 360 uses Moto Body software to record workout data and sync seamlessly with Android apps like Fitbit, MapMyRun, and Under Armour Record. Plus, cyclists can use the GPS-supported Strava app right on their Moto 360 Sport.

4.2.1.1 Accelerometer Sensor

The ACC sensor of Moto 360 was used to measure the linear acceleration of the arm caused by its movement. This sensor was set to record data with a sampling frequency of 50 Hz, however, events can be received faster or slower than the specified rate. Figure 4.2 shows the coordinate system relative to the device that is used by the ACC sensor API.
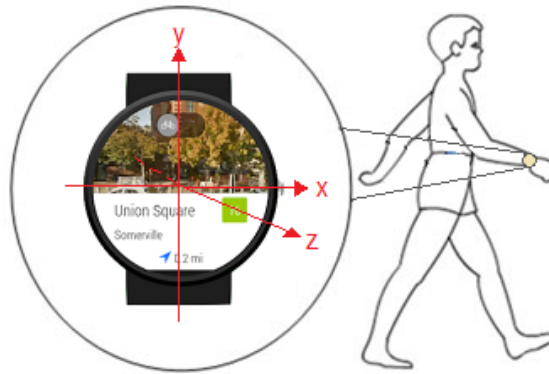
Figure 4.2: 3-axis coordinate system of the ACC sensor relative to the smartwatch. When placed on the wrist, with the arm in the same position as this figure: the *x*-axis is horizontal and points backwards, the *y*-axis is vertical and points down, and the *z*-axis points right, toward the outside of the screen face. In this system, coordinates behind the screen have negative *z* values.

4.2.1.2 Heart Rate Sensor

The HR sensor of Moto 360 was used to obtain the heart rate measurements of the users. This sensor does not allow to establish a constant reading rate, thus the HR sampling frequency was set to *SENSOR_DELAY_NORMAL*, an Android pre-defined parameter. The heart rate data is recorded with a variable frequency, from every 1 to 20 seconds, depending on the activity and effort required from the watch system.

4.2.2 TUNE

TUNE (see specifications in Appendix B) was used to monitor both feet in terms of stance, swing, pace, speed, cadence, number of steps, step length, foot's ground-contact and heel-contact time. Such parameters allow this device to analyze balance/symmetry during a full recording. TUNE

has bluetooth communication and it is compatible with Android^{TM} 4.3 or higher. Its 4 FSR sensors acquire at a sampling rate of 1.000 Hz. Moreover, TUNE provides information on latitude, longitude, altitude, mean velocity, distance and duration through GPS data.

The gait cycle is divided into stance (while foot is in contact with the ground) and swing (while foot is in the air). The flight time (when neither foot is touching the ground) is incorporated in the swing of a foot and happens at the beginning and at the end of the swing phase. The gait cycle time is equal for both feet due to this interaction between them. A lower percentage of time spent in the stance phase and a shorter gait cycle time, means a faster run. The ground contact time, or stance time, indicates the duration of the stance phase, reflecting the capacity to produce force when the foot is on the ground and to use elastic energy stored in the muscles to propel the body of the ground. The percentage of stance time that a runner has their heel on the ground is the heel percentage. The stance time is directly affected by cadence and speed variations. The time in propulsion during the stance phase is given by the the stance dynamics index, and, the higher this index, the better the runner is using the ground underneath his feet to move forward and to avoid excessive vertical oscillation. The heel strike measurement shows the percentage of strides landed with the heel first.

4.3 Signal Pre-Processing

4.3.1 Acceleration

The acceleration provided by the smartwatch includes the force of gravity (g) applied to the device according to the following relationship:

$$A_d = -g - \sum F/mass \tag{4.1}$$

, where $g = 9.81 m/s^2$, A_d is the acceleration applied to the device, and F is the force caused by body movement. Therefore, an high-pass filter was applied to obtain the real acceleration of the device. First, a low-pass filter was used to isolate the force of gravity, which was then subtracted to the raw signal.

Moreover, a low-pass filter with a cut-off frequency of 15Hz was applied to isolate the common frequencies observed in human motion (Mannini et al., 2013) and a 5-point Moving Average Filter was implemented to remove random noise (Ghasemzadeh et al., 2009).

4.3.2 Heart Rate

The heart rate signal was filtered by a Moving Average Filter using a kernel with size of 5 samples in order to smooth noisy data. To assume an equidistant sampling, a cubic spline interpolation at 1Hz was applied to the heart rate signal (Tapia et al., 2007).

4.4   Activity Recognition

Only acceleration signals were used to perform activity recognition, since the recognition will be performed in real time, and heart rate does not respond immediately to changes in physical activity (Magalhães, 2016). It was verified in the preliminary work of this dissertation that a sudden increase in work effort will not result in an immediately increase of the values of heart rate, as shown in Figure 4.3. On the other hand, when the work effort decreases, the heart rate values remain high for some time and gradually return to rest values. However, acceleration is in close agreement with the activity being performed, thus, acceleration signals were used to recognise the activity.
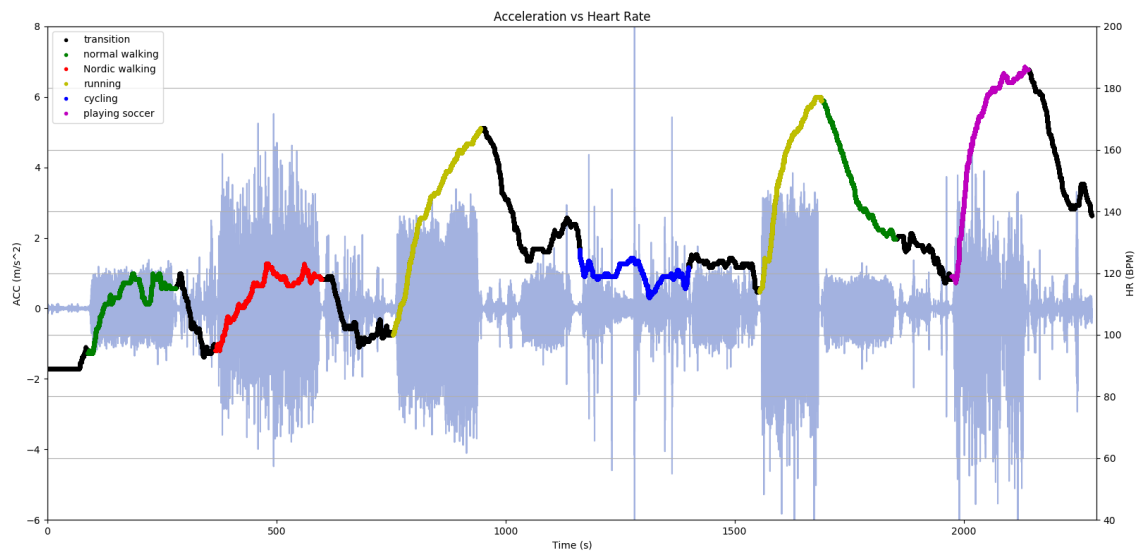
Figure 4.3: Relationship between heart rate values and physical effort (acceleration signal represented in bluish gray color) during a different set of activities being performed. This data is relative to a subject of PAMAP dataset and was acquired outdoor.

4.4.1   Feature Extraction and Selection

All features extracted are present in Table 4.1 and the mathematical formulas are presented in Appendix C, Section C.1. Each feature was extracted from the total acceleration, *x*-axis acceleration, *y*-axis acceleration and *z*-axis acceleration signals, except the last two which were only extracted from the total acceleration signal, given a total of 54 features. Features were computed for each window of 5 seconds with 50% overlap.

To select and reduce feature's dimension, four methods from the feature selection module of scikit-learn software[2] implemented in Python were tested: Recursive Feature Elimination (RFE), Principal Component Analysis (PCA), Linear Discriminant Analysis (LDA) and Extra Trees Classifier (ETC).

---

[2]http://scikit-learn.org/stable/modules/feature_selection.html

Table 4.1: Features extracted from acceleration signals. Mathematical formulas are presented in Appendix C, Section C.1.

Domain	Features	
Time	Mean	Median Absolute Deviation (MAD)
	Median	Interquartile Range (IQR)
	Maximum	Energy
	Minimum	Zero Crossing Rate (ZCR)
	Root Mean Square (RMS)	Skewness
	Standard Deviation (SD)	Kurtosis
Frequency	Spectral Entropy	
	Power Spectral Density (PSD) Peak	
	Total Average Power (TAP)	

RFE selects features by recursively considering smaller and smaller sets of features. Weights are assigned to each feature and those whose absolute weights are the smallest are eliminated from the current set. At each iteration, 1 feature was set to be removed. The procedure is recursively repeated on the eliminated set until the desired number of features to select is eventually reached. RFE was tested for the top 20, 10 and 6 features.

PCA performs a linear dimensionality reduction using singular value decomposition of the data to project it to a lower dimensional space, replacing the original features with a new set of variables that can be ranked in the order of their importance. The LDA model fits a Gaussian density to each class, assuming that all classes share the same covariance matrix. The model is used to reduce the dimensionality of the input by projecting it to the most discriminative directions. Thus, this technique aims to maximize the between-class scatter, while minimizing within-class scatter (Ghasemzadeh et al., 2009). Both PCA and LDA were tested to obtain 20, 10 and 6 components.

Extra tree classifiers implements a meta estimator that fits a number of randomized decision trees (a.k.a. extra-trees) on various sub-samples of the dataset and use averaging to improve the predictive accuracy and control over-fitting. Decision tree is a hierarchical model that recursively separates the input space into class regions. It composes of decision nodes and leafs in which each node has a test function. The test function is applied to the input and, depending on the output, one of the branches is taken Chernbumroong et al. (2011). It aims to find the smallest tree possible and, in order to achieve that, it finds the best attribute that would make the data after the split pure as possible. Gini impurity measure was used to find that attribute [3]. This a measure of how often a randomly chosen element from the set would be incorrectly labeled if it was randomly labeled according to the distribution of labels in the subset. The number of features to consider when looking for the best split was set to be equal to the square root of the total number of features.

---

[3] http://scikit-learn.org/stable/modules/generated/sklearn.ensemble.ExtraTreesClassifier.html

4.4.2 Classification

To classify each activity, 9 classifiers used in supervised learning from scikit-learn software[4] implemented in Python were tested: Logistic Regression, Linear Discriminant Analysis, K-Nearest Neighbours, Decision Trees, Gaussian Naive Bayes, Support Vector Machine, Linear SVM, Multi-layer Perceptron Classifier and Bagging Classifier.

Logistic regression is a linear model for classification where the probabilities describing the possible outcomes of a single trial are modelled using a logistic function. Logistic regression was used with L2 regularization. As an optimization problem, binary class L2 penalized logistic regression minimizes a cost function (Bishop, 2006).

Using K-Nearest Neighbours, classification is computed from a simple majority vote of the nearest neighbours of each point, i.e, a point is assigned the data class which has the largest number of representatives amongst the nearest neighbours of the point (Bishop, 2006). The model chose implements learning based on the k nearest neighbours of each point and was set to use 5 neighbours weighted equally.

Decision tree classifier was applied to create a model that predicts the value of a target variable by learning simple decision rules inferred from the data features. Gini impurity was again used with decision tree classifier to measure the quality of a split.

With regard to the Support Vector Machines classifiers, two classes were tested: C-support vector classification (SVC) and linear SVC. SVMs have the advantage of being effective in high dimensional spaces, even if the number of dimensions is greater than the number of samples. However, they are likely to give poor performances if the number of features is much greater than the number of samples, and probability estimates are calculated using an expensive five-fold cross-validation (Wu et al., 2004). Both classifiers were set with all classes having weight one. SVC was set to use the *rbf* kernel function[5] with a kernel coefficient equal to the inverse of the number of features, and to use the shrinking heuristic. Linear SVC is similar to SVC but with a linear kernel.

The multi-layer perceptron classifier is a model based on supervised neural networks, which optimizes the log-loss function using LBFGS or stochastic gradient descent [6]. This classifier was set to use 100 neurons in the hidden layer and to use *relu* function[7] as the activation function for the hidden layer. The solver for weight optimization was set to a stochastic gradient-based optimizer.

Bagging methods are part of ensemble methods' family, whose goal is to combine the predictions of several base estimators built with a given learning algorithm in order to improve robustness over a single estimator. Bagging Classifier builds several estimators independently and average their predictions, reducing the variance of a base estimator (Breiman, 1996). A decision tree was used as the base estimator to fit on random subsets of the dataset, and 10 base estimators were used in the ensemble. The number of samples and the number of features to drawn from the

---

[4]http://scikit-learn.org/stable/supervised_learning.html

[5]$rbf : exp\left(-\gamma\left|x - x^{'}\right|^{2}\right) \cdot \gamma, \gamma > 0$

[6]http://scikit-learn.org/stable/modules/generated/sklearn.neural_network.MLPClassifier.html

[7]$relu$: The rectified linear unit function, returns $f(x) = max(0, x)$

dataset to train each base estimator were set to the length of the dataset and to the total number of features present, respectively, and samples were drawn with replacement.

The PAMAP dataset acquired outdoor was used to train and test each classifier with each feature selection/reduction method, and the best combination was chose. The activities classified were "walk very slow", "normal walk", "running", "cycling" and "rope jumping". For evaluation, a subject-independent analysis was made using 10-fold cross validation.

4.4.3   Results and Discussion

The best feature selection methods proved to be RFE and LDA, however, RFE method with top 10 features was chose due to its higher computational efficiency. Figure 4.4 presents the results obtained for all classifiers using RFE with top 10 features as the selection method. The results of the remaining selection methods can be found in Appendix C (Section C.2).
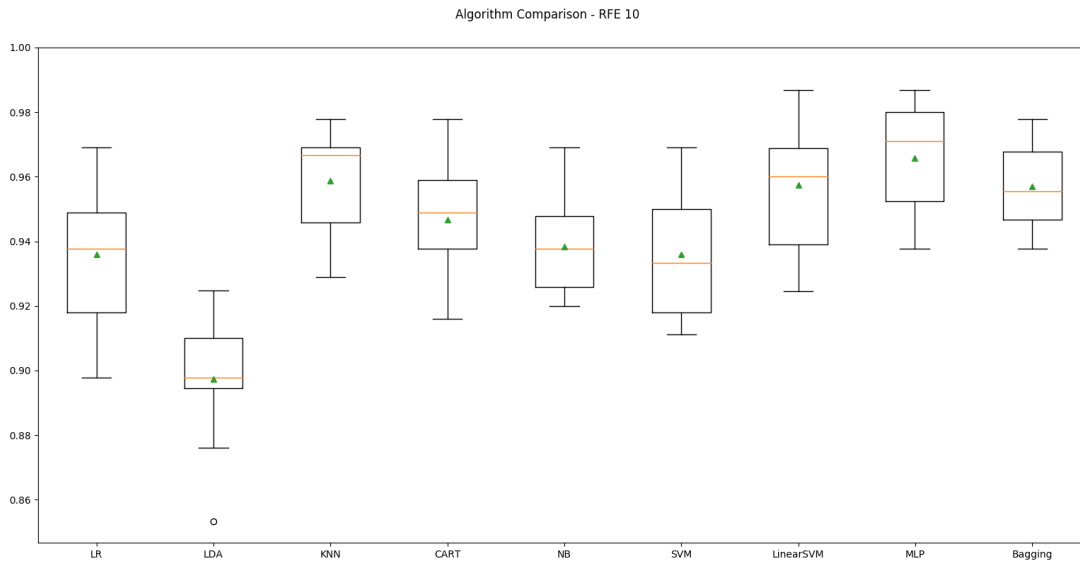
Figure 4.4: Classification's accuracy results using RFE method for 10 top features. Classifiers from *left* to *right*: Logistic Regression, Linear Discriminant Analysis, K-Nearest Neighbours, Decision Trees, Gaussian Naive Bayes, Support Vector Machine, Linear SVM, Multi-layer Perceptron Classifier and Bagging. The *vertical lines* represent non-outlier data points that extend to the most extreme (whiskers), the *circle* represents data that extend beyond the whiskers, the *green triangles* represent the mean value, and the *orange lines* represent the median of each box.

The top 10 features selected using RFE method were: median of the x-axis acceleration, root mean square of x-axis acceleration, standard deviation of x-axis and y-axis accelerations, interquartile range of x-axis, z-axis and total accelerations, and zero-crossing rate of x-axis, y-axis and z-axis accelerations.

The x-axis acceleration features were the most effective to distinguish between activities, and time-domain features are sufficient for different physical activities, as had also been conclude by Yang et al. (2008). Interquartile range is used when the mean values of different classes are

similar, representing the dispersion of the data and avoiding the effect on range caused by extreme values in the data. Root mean square and standard deviation measure the magnitude of a varying quantity in the ACC data (Yang et al., 2008). RMS measures central tendency while SD is a dispersion measure (Lara and Labrador, 2013; Avci et al., 2010), thus SD differentiates activities with different intensities, such as running *vs* others (Reiss and Stricker, 2012). Also, ZCR has more impact in running and rope jumping activities, which are more vigorous activities.

As depicted in Figure 4.4, the best classifier applied after the RFE selection method is MLP classifier, with an accuracy score of 95%. The correspondent confusion matrix is present in Table 4.2, and the main classification metrics of precision, recall and F1 score for each class are present in Table 4.3.

Running activity was the most precise, which may attribute to their distinct characteristics in generation acceleration among other activities, since it generates very large accelerations. Walking very slow was the less precise, revealing similarities with other movements, mainly with normal walk. Since they are very similar movements, there is an overlap in terms of features, being hard to control acceleration differences between the two. Rope jumping was the worst classified, due to the less representative acceleration generated with a sensor on wrist. Its false negative goes most to walking activities.

Table 4.2: Normalized confusion matrix of MLP classifier using RFE method for 10 top features.

		Predicted				
		Walk very slow	Normal walk	Run	Cycle	Rope jump
	Walk very slow	**0.99**	0.00	0.00	0.01	0.00
	Normal walk	0.06	**0.93**	0.00	0.01	0.00
True	Run	0.02	0.01	**0.95**	0.00	0.02
	Cycle	0.02	0.00	0.02	**0.97**	0.00
	Rope jump	0.05	0.05	0.00	0.03	**0.88**

Table 4.3: Main classification metrics results (precision, recall and F1-score for each class) of MLP classifier using RFE method for 10 top features.

Class	**Precision**	**Recall**	**F1-score**
Walk very slow	0.83	0.99	0.90
Normal walk	0.98	0.93	0.96
Run	0.99	0.95	0.97
Cycle	0.97	0.97	0.97
Rope jump	0.92	0.88	0.90
Average/Total	0.95	0.95	0.95

4.5 Energy Expenditure Estimation

As mentioned before in Section 3.2, "Energy Expenditure Estimation", of the "Literature Review" Chapter, the use of both heart rate and accelerometry measures to estimate energy expenditure showed to be a promising method. In the present work, the equation structure proposed by Brage et al. (2004), in Appendix A.1.4, for the combination of accelerometry and heart rate, was adapted. The author suggested a multi-linear regression equation that was derived and expressed in terms of both activity counts and heart rate values, where weighting factors were used to discriminate between activity and rest, to discriminate between walking and running activities, and to discriminate between the existence of movement or not during inactive states (Magalhães, 2016).

In this procedure, weighting factors were used to discriminate between the studied activities: walking, running, cycling and rope jumping. Heart rate proved to be a very reliable measure of energy expenditure during running, while activity measures are less reliable since it does not increase linearly with speed (Magalhães, 2016). Thus, the weighting factor relative to the HR-EE relationship is set to a higher value than the one relative to activity-EE relationship. The same was applied to rope jump activity, since movement registration is not relevant. On the other hand, during resting activities the heart rate is a poor measure, while movement registration is more reliable (Brage et al., 2004). Since, in this work, walking and cycling are less vigorous activities, movement and heart rate were equally weighted, as proposed by Brage et al. (2004) and Crouter et al. (2008).

Thus, energy expenditure was computed for running and rope jumping activities giving weighting factors of 0.9 to heart rate derived measures and 0.1 to activity-derived measures, whereas for walking and cycling activities both measures where given a weighting factor of 0.5 (Equation 4.2).

$$EE = \begin{cases} 0.9 \times EE_{HR} + 0.1 \times EE_{METs}, & \text{if } \textit{running or rope jumping} \\ 0.5 \times EE_{HR} + 0.5 \times EE_{METs}, & \text{if } \textit{walking or cycling} \end{cases} \tag{4.2}$$

Activity-EE relationship (EE_{METs}) was computed through metabolic equivalents values (Kawahara et al., 2009):

$$EE_{METs} = 1.05 \times METs \times duration \times weight \tag{4.3}$$

METs were computed depending on the performed physical activity, as described by Equation 4.4. METs values for cycling and rope jumping activities were computed based on Jette et al. (1990), who adapted METs values from an expert committee report submitted to the Canada Fitness Survey. Values for cycling vary with speed, and MET value for rope jump was set to 10.0, which corresponds to a workout of around 70 jumps per minute. METs values for running and walking were adapted from Ryu et al. (2008), who used a model that depends on activity and speed, but does not takes into account the grade. The influence of the grade was incorporated in the model by adding a vertical component: each *m/min* of vertical rise consumes an additional 1.8

$mL/Kg/min$ for each m/min of speed (Plowman and Smith, 2013).

$$MERs = \begin{cases} 0.093 \times speed - 4.7 + grade \times speed \times 1.8, & \text{if } running \\ 0.0272 \times speed + 1.2 + grade \times speed \times 1.8, & \text{if } walking \\ 0.25 \times speed \times 3.6 + 2.2, & \text{if } cycling \\ 10.0, & \text{if } rope\,jumping \end{cases} \quad (4.4)$$

HR-EE relationship (EE_{HR}) was computed through Equation 4.5, which uses a gender-dependent parameter (Magalhães, 2016). This parameter (HR_{param}) is obtained based on the relationship between heart rate, weight and age, depending on gender, as present in Equation 4.6. This model was predicted by Keytel et al. (2005), as result of the need of a model without a measure of fitness, such as VO_{2max}, since it is not always available. The model developed achieved a correlation coefficient of 0.857. The authors concluded that, after adjusting for age, gender and body mass, it is possible to estimate physical activity EE from heart rate in a group of individuals with a great deal of accuracy.

$$EE_{HR} = \frac{HR_{param}}{4.184} \times 60 \times duration \quad (4.5)$$

$$HR_{param} = \begin{cases} -55.0969 + (0.6309 \times HR) + (0.1988 \times weight) + (0.2017 \times age), & \text{if } male \\ -20.4022 + (0.4472 \times HR) - (0.1263 \times weight) + (0.074 \times age), & \text{if } female \end{cases} \quad (4.6)$$

4.6   Heart Rate Analysis

Heart rate measurements over time were used to determine heart rate zones of exercise and training intensity (Criner et al., 2009). The heart rate zones are obtained through the training intensity (I), the heart rate reserve ($HR_{reserve}$) and the resting heart rate (HR_{rest}), as present in equation (4.7). The heart rate reserve is calculated as present in equation (4.8), where the heart rate at rest is obtained by taking the pulse in the morning (ideally the average of 5 days), and the maximum heart rate (HR_{max}) depends on gender, or fetal heart rate, and age through equation (4.9).

$$HR_{zones} = I \times HR_{reserve} + HR_{rest} \quad (4.7)$$

$$HR_{reserve} = HR_{max} - HR_{rest} \quad (4.8)$$

$$HR_{max} = \begin{cases} 220 - age, & \text{if } man \\ 226 - age, & \text{if } woman \end{cases} \quad (4.9)$$

The training intensities were set from 45% to 100%, with intervals of 5%, of the maximum effort and they define the heart rate zones as depicted in Figure 4.5, in which the heart rate zones are defined for a male subject with 20 years and a heart rate at rest of 60 BPM. During exercise, the measured heart rate will correspond to one of the zones, indicating the intensity achieved by the subject as a measure of fitness.

Fitness can also be assessed by measuring resting heart rate and compare it to a fitness chart[8]. The resting heart rate varies with the fitness level, age and gender, and, the fitter the person is, generally the lower the resting heart rate. This is due to the heart getting bigger and stronger with exercise, and getting more efficient at pumping blood to the body, so, at rest, more blood can be pumped with each beat, and therefore less beats per minute are required. In accordance with these parameters, resting heart rate can be evaluated as "Athlete", Excellent", "Good", "Above Average", "Average", "Below Average" or "Poor", as depicted in the Tables present in Appendix D.

Figure 4.5: Heart rate training zones for a male subject with 20 years and a heart rate at rest of 60 BPM. For different subjects, the values of beats per minute that define the heart rate zones would vary according to equation (4.7).

4.7   Movement Analysis

Figure 4.6 depicts the relation between TUNE information and ACC information during a gait cycle when running. Peaks in the *x*-axis of the ACC signal correspond the the arm's swinging when running, and are related with specific occurrences on the feet in a gait cycle. The minimum peak corresponds to the the maximum amplitude achieve by the arm in front of the body, and the

---

[8]http://www.topendsports.com/testing/heart-rate-resting-chart.htm

maximum peak corresponds to the the maximum amplitude achieve by the arm behind the body (with the smartwatch placed on the right wrist).

Steps were counted using the total acceleration signal computed from acceleration signals of the smartwatch MOTO 360. Since a gait cycle encompasses two positive and two negative peaks, as depicted in Figure 4.6, the standard deviation along the acceleration signal was used as threshold to detect the peaks of interest. The difference between positive peaks and the successive negative peaks was computed to obtain the acceleration amplitude of the arm. The resulting signal is representative of the movement of the arms during a run.

Since arms and legs act synchronously, the movement of the arms might be linked with the movement of the feet through these two measurements from smartwatch's acceleration signal, in order to provide runners with real time measures of interest to improve running experience and their efficiency.
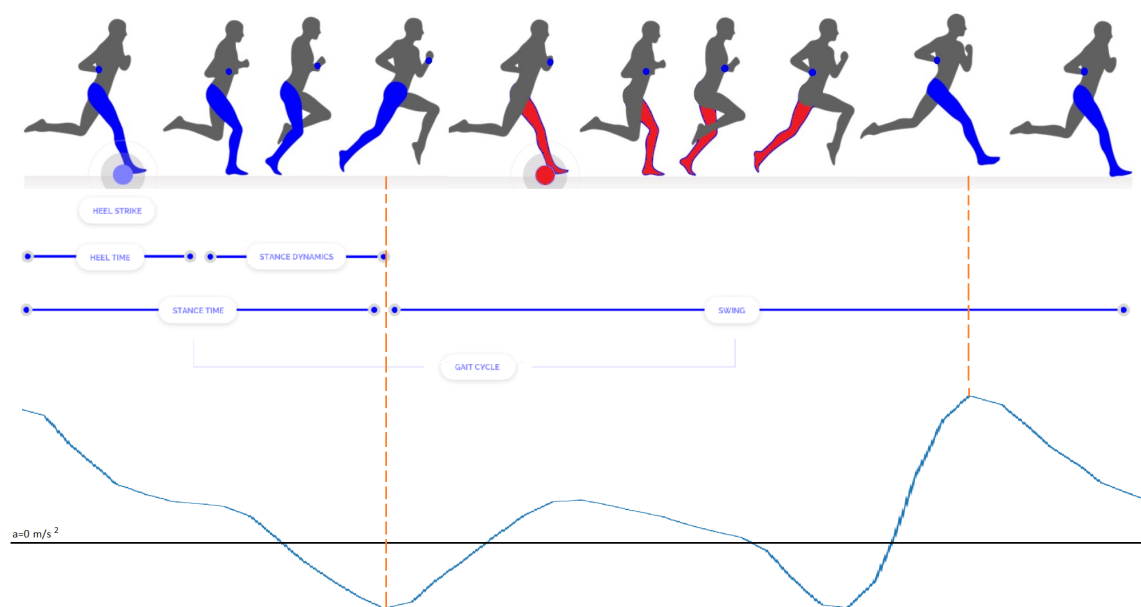
Figure 4.6: Representation of the relation between TUNE information and ACC information during a gait cycle when running. On *top*: Schematic representation of the information provided by TUNE. In *red* the left side of the body, and in *blue* the right side including a smartwatch. The *blue* and *red* circles represent right and left heel strikes, respectively. Heel time, stance dynamics, stance time and swing, i.e., a complete gait cycle, are represented for the right leg (*blue*). On *bottom*: Example of the *x*-axis of the ACC signal obtained from the smartwatch when running. The *orange dashed line* matches the peaks observed in the ACC signal with the correspondent moment in the gait cycle. The two peaks correspond to the maximum amplitude achieve by the arm in front and behind the body, respectively. The other two peaks between them correspond to the passage of the arm parallel to the body.

4.8   Android Wear Application

As depicted in the component diagram of Figure 4.7, TUNE system includes both a mobile APP
and a wear APP which receive data from TUNE devices. In order to take advantage of smartwatch
capabilities, which have been mentioned in this work, a Heart Rate Module was added to TUNE's
wear application. The developed module integrates the previous sections, from Data Acquisition
to Heart Rate Variability Analysis (Sections 4.2 to 4.6), as shown in the use case diagram of Figure
4.8.

Acceleration and heart rate built-in sensors were accessed through the Android sensor frame-
work, which provides several classes and interfaces to perform a wide variety of sensor-related
tasks. The pre-processing methodology described in Section 4.3 was applied to the sensors' raw
data. To perform activity recognition, the features resulting from the best selection method, men-
tioned in Sub-section 4.4.3, were computed. These features were then used by the classifier to
recognise the activity being performed in real time. The best classifier obtained during Research
and Development part of this work was the MLP, as discussed in Sub-section 4.4.3. The MPL clas-
sifier model built and trained in scikit-learn software was exported to Java, using sklearn-porter[9].
As result, a Class was built in Java and it was integrated in the Heart Rate Module to perform
activity recognition based on real-time acceleration signals acquired by the smartwatch.
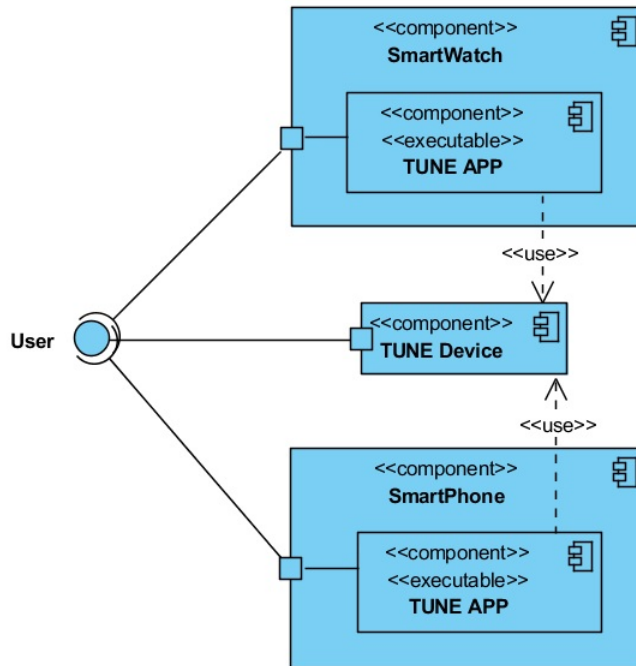
Figure 4.7: Component Diagram.

---

[9]https://github.com/nok/sklearn-porter
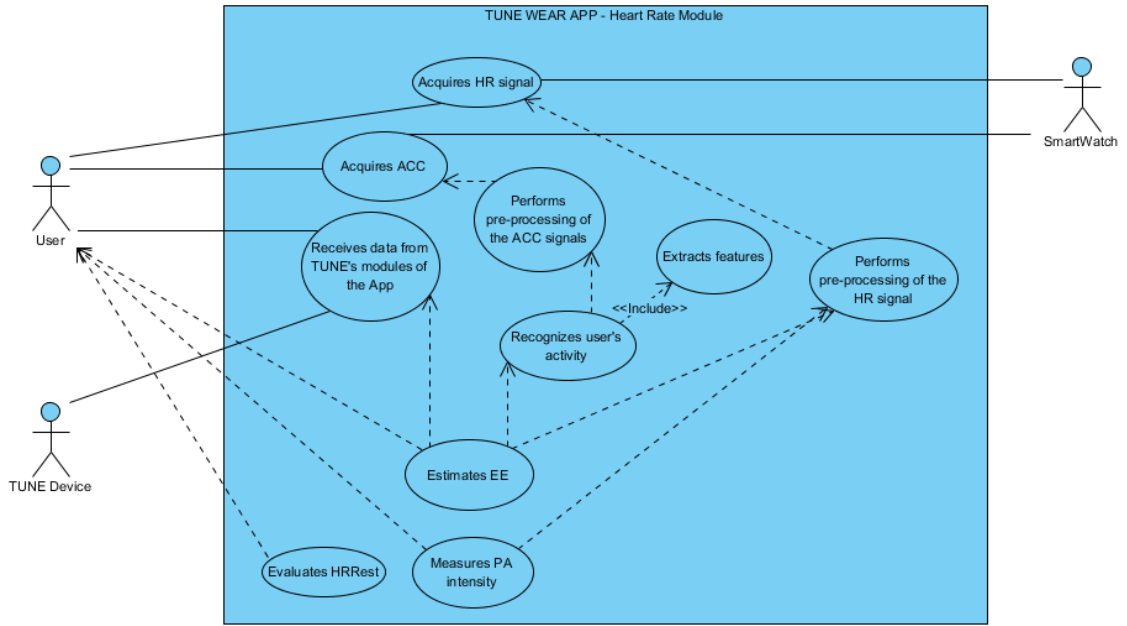
Figure 4.8: Use Case Diagram.

Energy expenditure is estimated as described in Section 4.5, depending on the activity being performed, heart rate measures, personal information of the subject and GPS data from TUNE. GPS data was used to obtain the values of distance and elevation, in order to compute the grade, and the values of speed (Equation 4.4). When the GPS connection fails, grade is set to 0 and velocity is computed using ACC information[10], integrating acceleration (a) over time (t) to get velocity (v):

$$v = \int a \cdot dt = v_0 + a \cdot t \tag{4.10}$$

Personal information of the subject includes age, gender, weight and resting heart rate. The physical activity intensity achieved by the subject is obtained as described in Section 4.6, using the resting heart rate value of the subjects and heart rate measures. Moreover, resting heart rate is evaluated as present in Section 4.6 and Tables in Appendix D. Such information is helpful with respect to how human body responds to physical activities and it is essential to improving performance. Analyzing this information, users can tailor their training to their specific goals, adjusting training intensity and following the evolution of their resting heart rate.

---

[10]http://www.analog.com/en/analog-dialogue/articles/enhancing-pedometers-using-single-accelerometer.html

Chapter 5

Experimental Work

This Chapter presents the experimental work of this dissertation, including the setup, the protocol and the datasets used and developed to validate the developed system. The statistics used to validate the system are described and the results obtained are present and discussed for each part of the work, including heart rate and movement analysis, activity recognition, and energy expenditure estimation.

5.1   Setup and Protocol

To validate the developed system, 4 subjects (see personal information in Table 5.1) performed the cycle *A* of activities present in Table 5.2, in a total of 8 minutes each cycle. With regard to health risk of the subjects, the body mass index (BMI) categorized subjects 1 and 2 as normal weight, subject 3 as overweight and subject 4 as underweight. However, all subjects are healthy and have a past in sports practice. The subjects performed 3 cycles *A*, with a break of 1 minute between each one. At the end, each subject performed the cycle *B*, running at a free speed during 3 to 5 minutes. The activities were performed outdoor with each subject using a smartwatch Moto 360 (right wrist), TUNE (feet) and COSMED K4b2 (chest, upper back and head). Tests were taken in collaboration with LABIOMEP[1], who provided the COSMED K4b2 system and technical support.

COSMED K4b2[2] was used to measure energy expenditure ground truth and to measure heart rate ground truth. The K4b2 is a portable system for pulmonary gas exchange measurement with true breath-by-breath analysis. Its technology and dimensions allow the user to measure physiological response to exercise without limitations. The K4b2 is provided with integrated GPS for speed, distance, altitude and position measurements, which are synchronized with Gas Exchange Data. Besides breath-by-breath exercise testing, which measures oxygen uptake (VO_2), K4b2 also performs indirect calorimetry, computing energy expenditure values (Cosmed, 1998). Energy expenditure is measured indirectly with a metabolic cart by analysis of respired gases (usually expired) to derive volume of air passing through the lungs, the amount of oxygen extracted from

---

[1]https://labiomep.up.pt/

[2]http://www.cosmed.com/en/products/cardio-pulmonary-exercise-testing/k4-b2-mobile-cpet

it (VO_2) and the amount of carbon dioxide, as a by-product of metabolism, expelled to atmosphere (i.e. carbon dioxide output, VCO_2). K4b2 was integrated with a wireless Polar heart rate chest strap[3] which transmitted HR measures to the K4b2 system. Data was recorded with variable frequency, since it depends on the individual breath-by-breath frequency.

Table 5.1: Subject information. The body mass index (BMI) is defined as the body mass divided by the square of the body height.

Subject ID	Gender	Age (*years*)	Height (*m*)	Weight (*kg*)	Resting HR (*bpm*)	BMI (kg/m^2)
1	Male	19	1.81	64	63	19.5
2	Male	23	1.79	66	59	20.6
3	Female	22	1.74	89	71	29.4
4	Female	23	1.61	45	60	17.4

Table 5.2: Data collection protocol.

Cycle	Activity	Description	Duration (min)
A	Walk very slow	Walking at a speed lower than 0.9m/s	1
	Normal walk	Walking at a speed of 1.3m/s to 1.5m/s	2
	Run	Running at a speed of 2.0m/s to 3.0m/s	2
	Cycle	Bicycling at a speed lower than 4.5m/s	2
	Rope jump	Around 70 jumps/minute	1
B	Run	Running at a free speed	3-5

5.2 Datasets

Among the datasets described in Section 3.5 of the Literature Review chapter, the public dataset PAMAP is the one that best suits this project, since it has the complete signals obtained during recordings, allowing to extract the same type of features extracted in the signals used in this project. Moreover, acceleration signals include recordings from an IMU placed on wrist, which is similar to a smartwatch, and the HR monitor used provides heart rate signals instead of ECG signal. Only the outdoor recordings were used, including the activities walking, running, cycling, playing soccer and rope jumping. However, the playing soccer activity was not taken into account, since it is not part of this project. The information on each of the 7 test subjects is present in Table 5.3 and the description of the performed activities in Table 5.4.

For the development of the experimental work, a dataset was developed with the acquired signals during the research and development part of this project, and during the validity of the system. This dataset includes recordings of HR and ACC signals from the smartwatch MOTO 360, data obtained from TUNE (right and left devices, and GPS data) and the activity recognition and EE results. The information of the test subjects and the description of the performed activities during

---

[3]https://www.polar.com/us-en/products/accessories/T31_transmitter

the validity of the system is present in Tables 5.1 and 5.2 of the previous section, respectively. The dataset includes recordings of two more subjects, which collected data during the research and development part of this project. Table 5.5 presents the information of each subject available in the dataset. Subjects 1 to 4 correspond to the ones in Table 5.1 and subjects 4 and 5 correspond to subjects used in tests performed during the research and development part of this project, thus they do not have information on activity and EE results, and they only performed cycle *B*, with a duration of more than 10 minutes per run. During validation tests, one of the TUNE devices failed, thus TUNE information is missing for subjects 1 and 4, and for subject 2 during cycle *A*.

The developed dataset and the PAMAP dataset were used for activity recognition purposes, and the developed dataset was used for energy expenditure estimation, heart rate analysis and movement analysis.

Table 5.3: Subject information of PAMAP outdoor dataset.

Subject ID	Gender	Age (*years*)	Height (*m*)	Weight (*kg*)	Resting HR (*bpm*)
2	Male	27	1.82	92	67
3	Male	30	1.68	62	56
4	Male	31	1.93	85	54
5	Male	25	1.80	70	69
6	Male	26	1.81	75	59
7	Male	29	1.74	91	56
8	Male	26	1.82	85	63

Table 5.4: Data collection protocol of PAMAP outdoor dataset.

Activity	Description	METs	Duration (min)
Walk very slow	Walking, < 0.9 m/s, level ground, strolling, very slow.	2.0	3
Normal walk	Walking, 1.3 m/s, level, moderate pace, firm surface; Walking, 1.5 m/s, level, brisk, firm surface, for exercise.	3.3-3.8	3
Run	Jogging, general; Running, 2.2 m/s.	7.0-8.0	3
Cycle	Bicycling, < 4.5 m/s, leisure, to work or for pleasure.	4.0	3
Rope jump	Rope jumping, moderate, general; Rope jumping, slow.	8.0-10.0	2

Table 5.5: Information present in the developed dataset. The ✓ means that the information is present in the dataset for the corresponding subject, and the × means that it is not present.

Subject ID	Cycle	ACC	HR	Activity	EE	GPS	TUNE	Total time (min)
1	A + B	✓	✓	✓	✓	✓	×	32
2	A + B	✓	✓	✓	✓	✓	✓ only cycle B	32
3	A + B	✓	✓	✓	✓	✓	✓	30
4	A + B	✓	✓	✓	✓	✓	×	30
5	B	✓	✓	×	×	✓	✓	66
6	B	✓	✓	×	×	✓	✓	148

5.3   Statistics

Heart rate and energy expenditure measures obtained by the developed system were compared with results from Polar HR chest strap and COSMED K4b2, respectively used as reference. The normalized root mean square error (NRMSE) was evaluated. NRMSE computes the similarity between the results obtained and the reference values using the root mean square error and the mean of the reference data. Further, it was also evaluated the percentage error and the Pearson correlation, to determine whether the values of two variables are associated.

Since this data does not follow a normal distribution, the Wilcoxon Signed Ranked test, a non-parametric test was applied, and the Kruskal-Wallis test, an extension of the Wilcoxon test, was used to test the hypothesis that a number of unpaired samples originate from the same population. In Kruskal-Wallis test, if the null-hypothesis, being the hypothesis that the samples originate from the same population, is rejected ($P<0.05$), then the conclusion is that there is a statistically significant difference between at least two of the subgroups. The subgroups used were the subjects for the HR measures, and the activities for the EE measures. In Wilcoxon test, if the resulting P-value is small ($P<0.05$) then it can be accepted that the median of the differences between the paired observations is statistically significantly different from 0.

Moreover, Scatter plots were created to represent graphically the relationship between the two variables, and Bland-Altman plots were created to compare the two measurements techniques. In Bland-Altman plots, the limits of agreement (LoA) are defined as the mean difference $\pm1.96SD$ of differences. If these limits do not exceed the maximum allowed difference between methods, the two methods are considered to be in agreement. Statistics were computed using MedCalc[4] software.

Activity recognition results were evaluated through confusion matrix and classification metrics of precision, recall and F1 score for each class. The classification obtained by the developed system was compared with direct observation.

With regards to step counting results, they were evaluated computing the error between the number of steps obtained with the developed system (using acceleration signals from Moto 360) and the number of steps given by TUNE.

5.4   Results and Discussion

This Section describes the results obtained with the developed system described in Chapter 4 and will provide the necessary information to evaluate its performance and discuss its benefices in the sports context to improve athletes' performance and to help them to follow an active and healthy lifestyle, using non-intrusive wearable smart devices. Furthermore, gaps that need improvement are identified and discussed.

---

[4]https://www.medcalc.org/statistics.php

5.4.1 Heart Rate Analysis

Table 5.6 presents statistical results obtained for heart rate measures, and Figure 5.1 depicts Scatter Plots and the Bland-Altman Plot for heart rate data results of all subjects. Moreover, Figures 5.2 and 5.3 depict the comparison between the Polar HR chest strap and smartwatch heart rate signals, including error signal (difference between Polar chest strap and Moto 360 measures).

It was obtained a Pearson correlation coefficient of 0.78 (P<0.0001, 95% CI 0.76 to 0.79), and, applying the statistical test for a significance level of 5%, it can be confirmed that there are significant differences between the heart rate obtained from the Polar HR chest strap and from the smartwatch Moto 360. Although the Bland-Altman Plot shows that both devices agreed in most part of the tests, with the majority of data being between the 95% limits of agreement, the mean of the percentage error (9.30%) and Figures 5.2 and 5.3 evidence errors above 10 BPM, which are not acceptable for reliability purposes, indicating the need to improve wrist worn systems to measure heart rate reliably. As depicted in Figures 5.2 and 5.3, measurements from Moto 360 seem to be underestimated in relation to Polar chest strap measures.

Applying the Kruskal-Wallis test, the null-hypothesis is rejected for subject 4, being the conclusion that there is statistical significant difference between this subject and the others. Moreover, it can be observed from Scatter and Bland-Altman Plots that subjects 1 and 4 presented the greatest dispersion. However, it must be noticed that the way each subject attached the smartwatch to their wrist influences the readings, and consequently, a wrong placement can be more propitious to dispersion.

As mentioned in Section 3.4, previous works concerning the reliability of smartwatches to monitor heart rate conclude that such devices are relatively accurate and beneficial, however, Moto 360 proved to be the least accurate with errors of 7.2% against the best error of 1% from Apple Watch (El-Amrawy and Nounou, 2015).

Although Polar HR chest strap is expectable to be more reliable since it is placed in chest, it is also susceptible to errors such as motion artefacts, not being the most trustful reference. In turn, the PPG method used by the smartwatch is susceptible to outside light errors sources and the wrist blood vessels expression might vary with the subjects, being very prone to movement artefacts (Magalhães, 2016). Furthermore, anatomical issues might also have influenced the results, since the subjects present different morphologies (as depicted in Table 5.1) and the the devices used were the same size for everyone. Hence, the devices might have adjusted better to some volunteer than others. Moreover, each subject placed on himself the chest strap and smartwatch, which might represent an error source.

Even though the results obtained show that Moto 360 does not have the best accuracy and reliability, mainly for medical purposes or to monitor cardiac patients, its reliability value is acceptable for heart rate monitoring of sportspeople who aim to improve their performance and follow an active and healthy lifestyle. Therefore, the errors obtained were decent enough to have the device showing correct readings most of the time during normal use and present some credibility to use it in a daily basis.

Table 5.6: Statistical results of heart rate measures. The mean of the percentage error (% Error) and normalized root mean square error (NRMSE) of the obtained heart rate measures for each cycle of the protocol and for each subject. Evaluation of the statistical difference between smartwatch Moto 360 and Polar HR chest strap, using data from all the participants (Correlation Coefficient and Wilcoxon Signed Ranked Test).

Subject ID	Cycle A		Cycle B		Correlation Coefficient	Wilcoxon Test
	% Error	NRMSE (%)	% Error	NRMSE (%)		
1	14.27	17.80	1.92	2.31		
2	8.20	10.27	6.12	7.43	0.78	P < 0.0001
3	5.26	7.80	2.81	4.28		
4	9.49	12.88	5.70	6.93		
Average	9.30	12.19	4.14	5.24		

(a) Scatter Plot (Subjects 1 and 2)

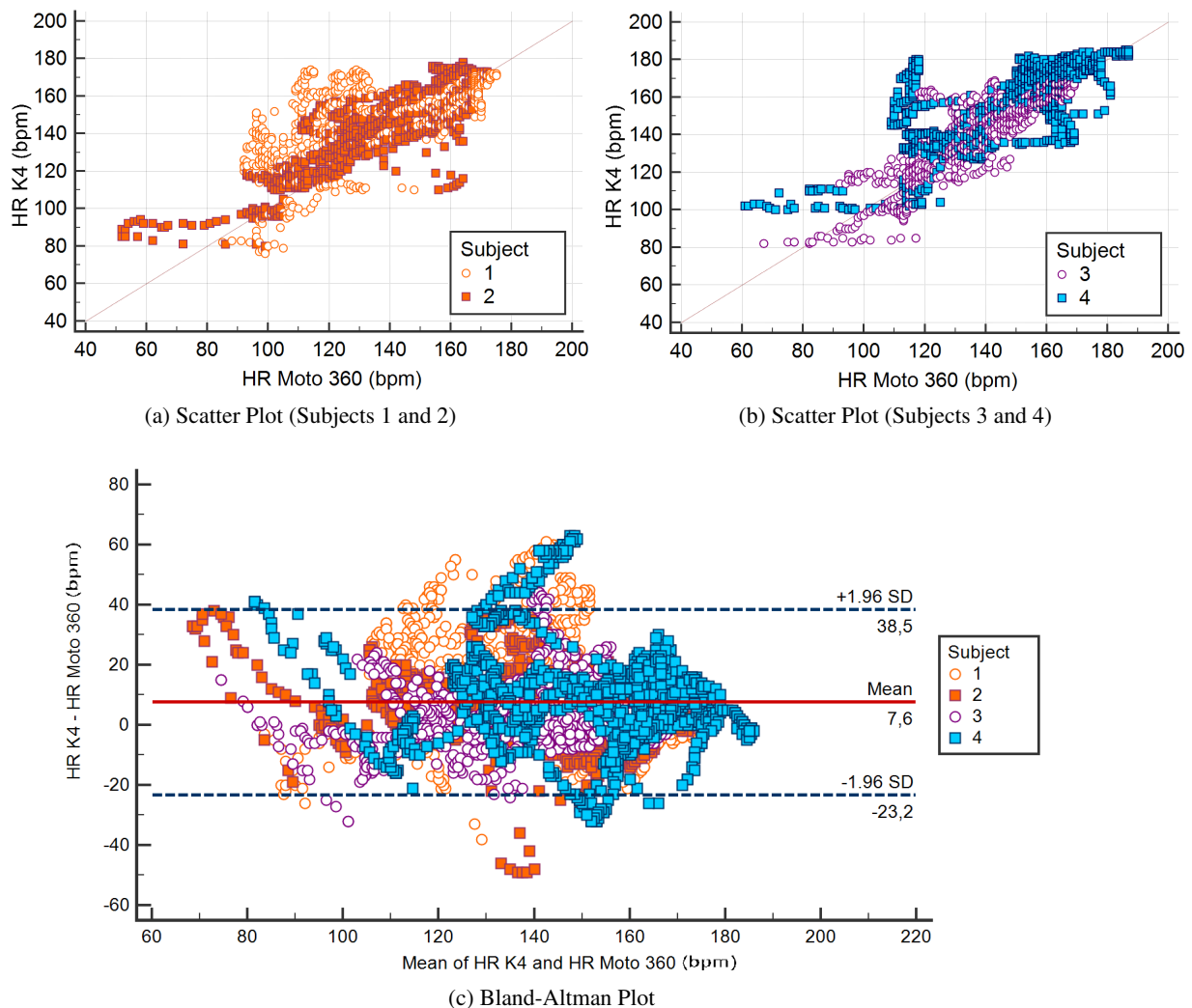(b) Scatter Plot (Subjects 3 and 4)

(c) Bland-Altman Plot

Figure 5.1: Scatter Plots for subjects 1 and 2 (*a*) and subjects 3 and 4 (*b*) and Bland-Altman Plot (*c*) for heart rate data results of all subjects, with the confidence interval $\mu \pm 1.96SD$ represented by the dashed lines.
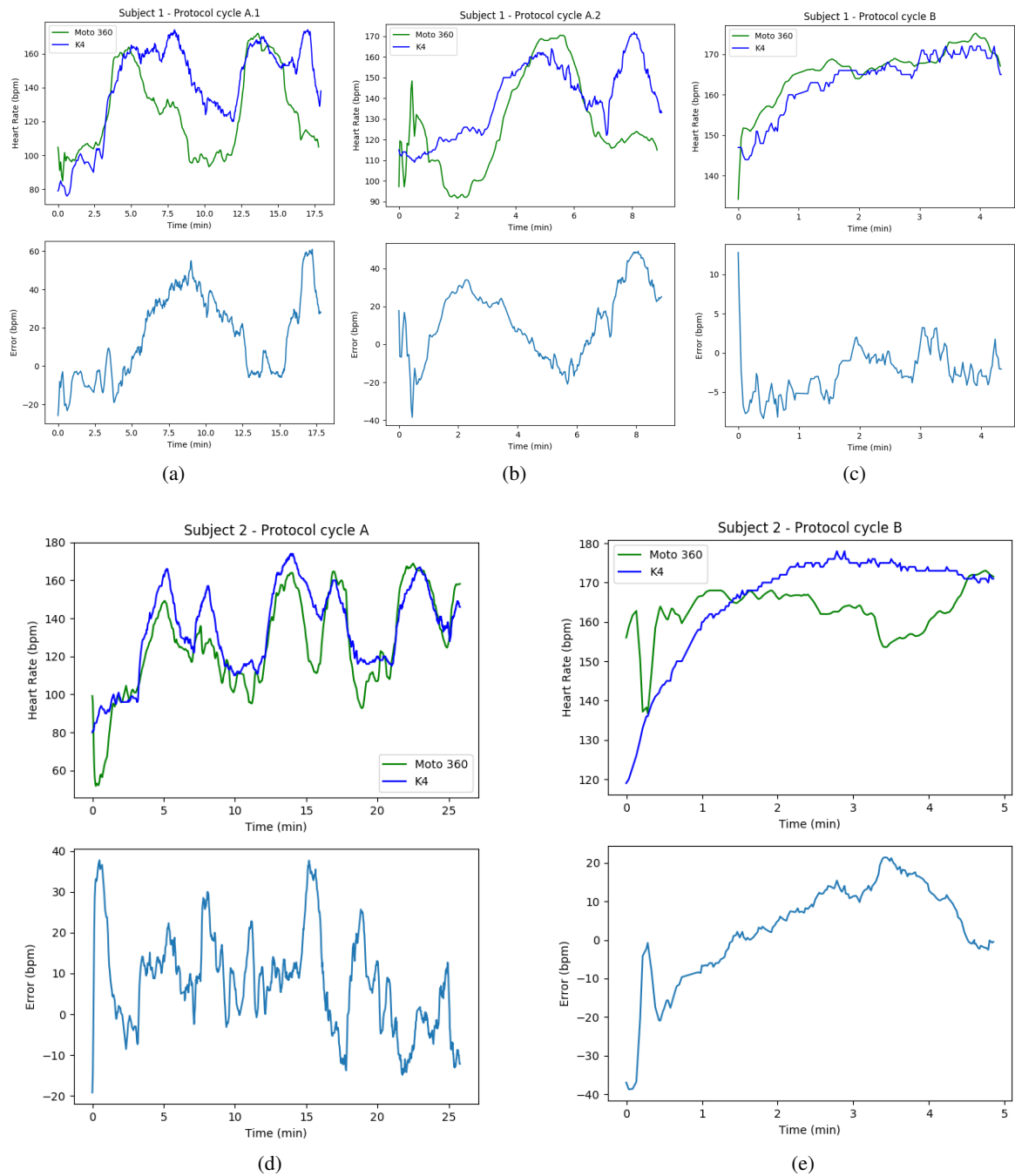
Figure 5.2: Results of heart rate measures obtained for subject 1 ((*a*), (*b*) and (*c*)) and subject 2 ((*d*) and (*e*)), for each cycle of the protocol. Comparison between the Polar HR chest strap and smartwatch heart rate signals.
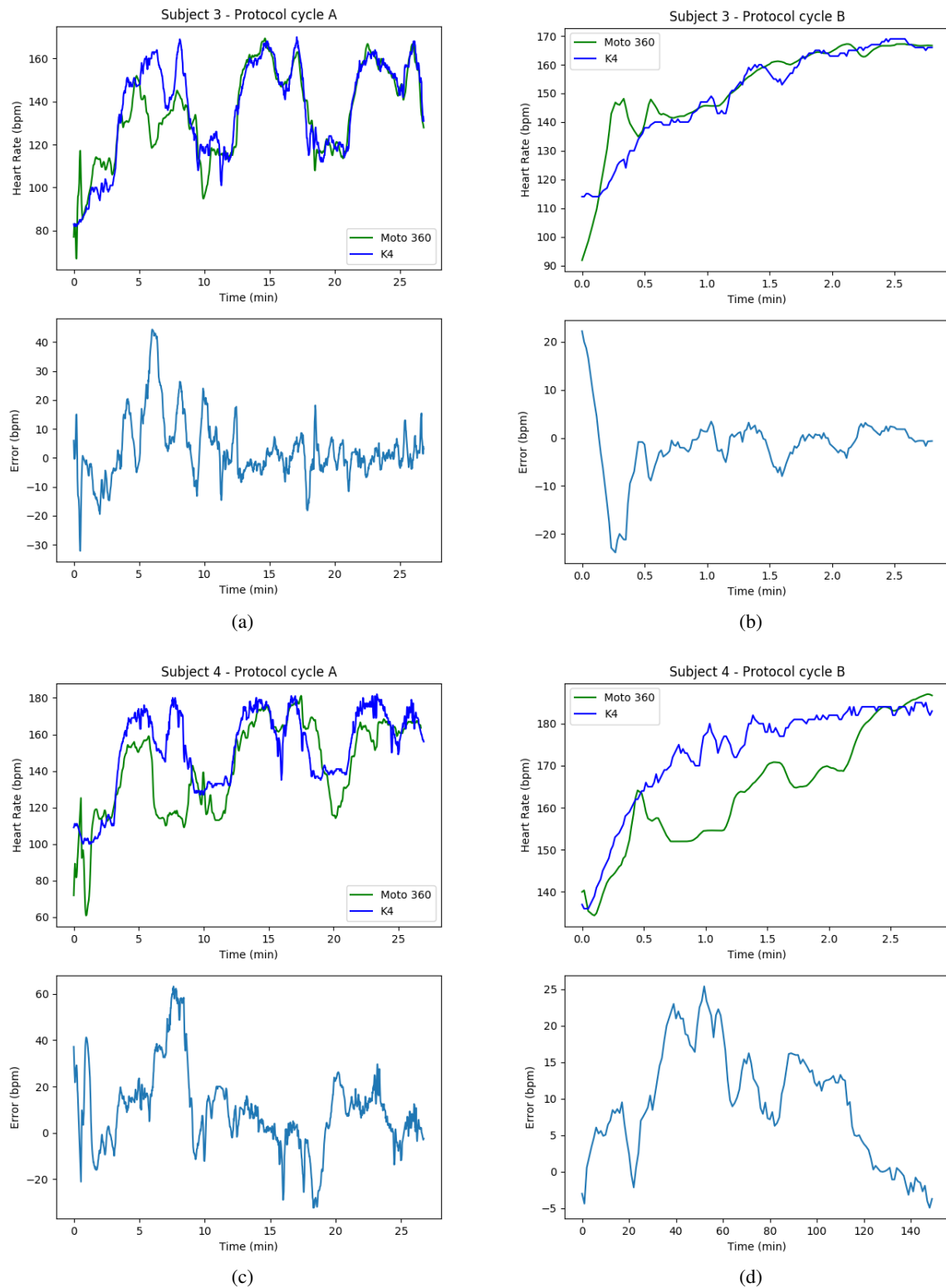
Figure 5.3: Results of heart rate measures obtained for subject 3 ((*a*) and (*b*)) and subject 4 ((*c*) and (*d*)), for each cycle of the protocol. Comparison between the Polar HR chest strap and smartwatch heart rate signals.

Recalling the protocol performed by the test subjects: walk very slow (1min), normal walk (2min), run (2min), cycle (2min), rope jump (1min) and rest (1min); the heart rate behaviour reflects the intensity and effort required by each activity and the responses of the autonomic nervous system. Although heart rate variability parameters were not computed in this work, since heart rate is the available data and not the ECG, the R-R interval would be computed as $60000/HR$, representing an inverse behaviour of the heart rate, i.e., the higher the HR, the shorter the inter-beat interval. Shorter intervals usually represent lower HRV, thus Figures 5.2 and 5.3 show that running and rope jumping are the most vigorous activities, presenting an higher HR value and, consequently, lower HRV. This behaviour expresses the lower influence of the PNS and the increased sympathetic stimulation, i.e, the ability of the heart to pump more blood and respond to body needs.

Table 5.7 presents an evaluation of the resting heart rate and training intensity during protocol cycle B for each subject. The relation speed-heart rate intensity is a measure of performance and it was normalized between 0 and 1 for this set of subjects (1 corresponds to the best performance). Figures 5.4 and 5.5 show the mean velocity and heart rate training intensity achieved by each subject during the performed protocol. Heart rate zones were computed as explained in Section 4.6 in order to obtain a measure of fitness.

Comparing these results with the physical/health information of the subjects (Table 5.1), there is a linear relationship between their *BMI* and the result obtained in $speed - HR intensity$ relation. Moreover, their resting heart rate also reflects their state of health. Subject 3, who presents an high BMI and resting heart rate, was the one who had most difficulty reaching high training intensities. In other words, training intensity evaluation is a valuable measure of the clinical state of the individuals and its regular monitoring can improve health risk and sports performance. The same happens with the monitoring of the resting heart rate, since a reduced resting HR is an indication of the effect of improved cardiovascular fitness.

These measures are also important to detect stages of fatigue. Without accumulated fatigue, HR intensity can easily rise above 70% during the first moments of exercise and the HR remains constant during exercise during several days. With accumulated fatigue, it becomes harder to achieve the 70% zone and the resting HR increases. To recover, it is recommended to train in HR zones lower than 70% or even stop exercising for some days.

Table 5.7: Resting heart rate and training intensity evaluation during protocol cycle B for each subject. The relation speed-heart rate intensity is a measure of performance and it was normalized between 0 and 1 for this set of subjects (1 corresponds to the best performance).

Subject ID	HR Rest Evaluation	Top HR Zone	Average HR Zone	Average Speed (m/s)	Speed-HR Int. Relation
1	Good (63 bpm)	Aerobic-intensive (80%)	Aerobic-extensive (71%)	3.03	0.87
2	Excellent (59 bpm)	Aerobic-intensive (80%)	Aerobic-extensive (73%)	3.38	1
3	Above Average (71 bpm)	Weight Control (70%)	Moderate Activity (60%)	2.23	0.55
4	Athlete (60 bpm)	Anaerobic (85%)	Aerobic-extensive (71%)	2.89	0.83

(a)

(b)

(c)

(d)

Figure 5.4: Mean velocity and heart rate training intensity achieved during the performed protocol for subject 1 ((*a*) and (*b*)) and subject 2 ((*c*) and (*d*)).

(a)
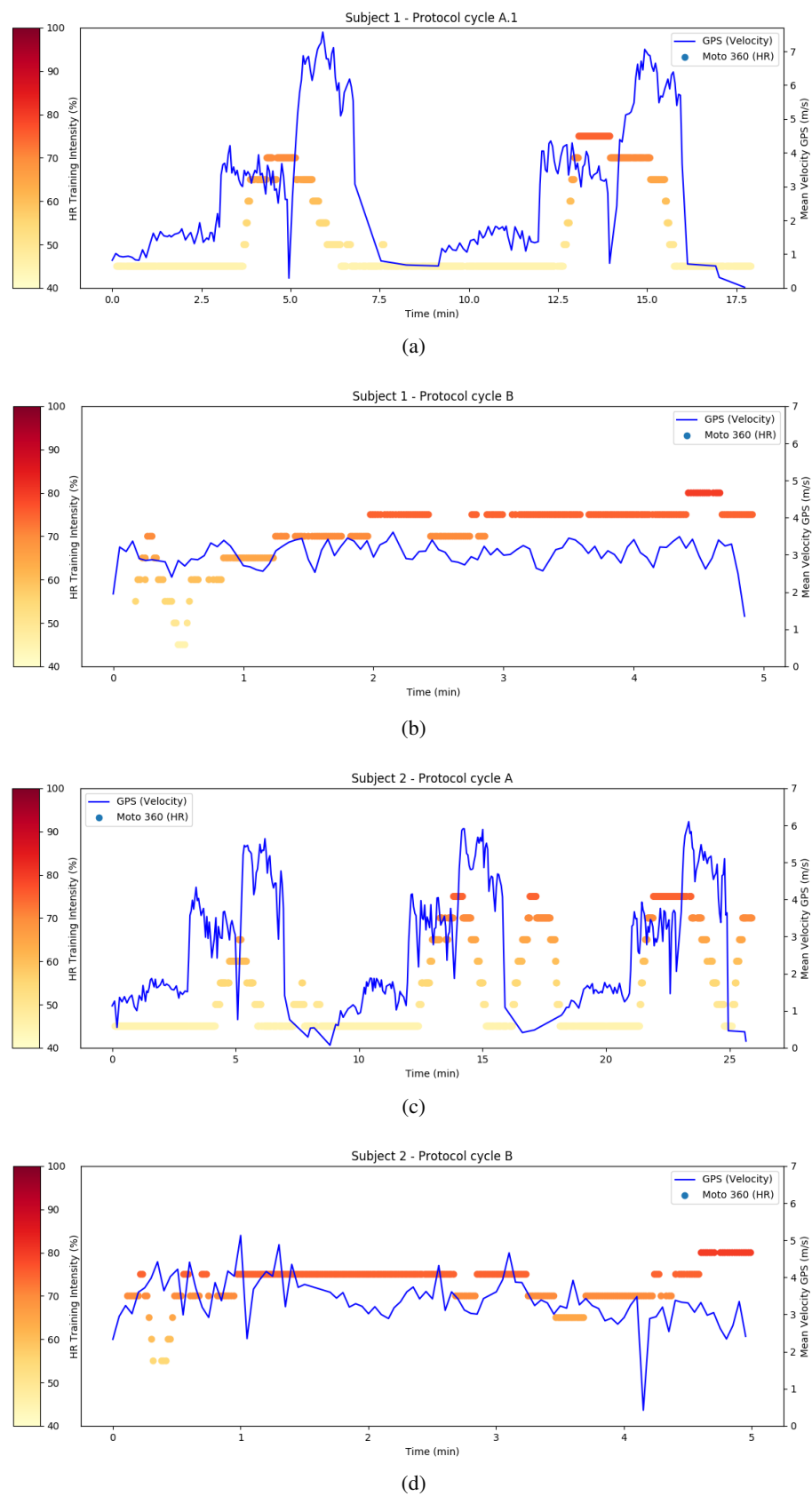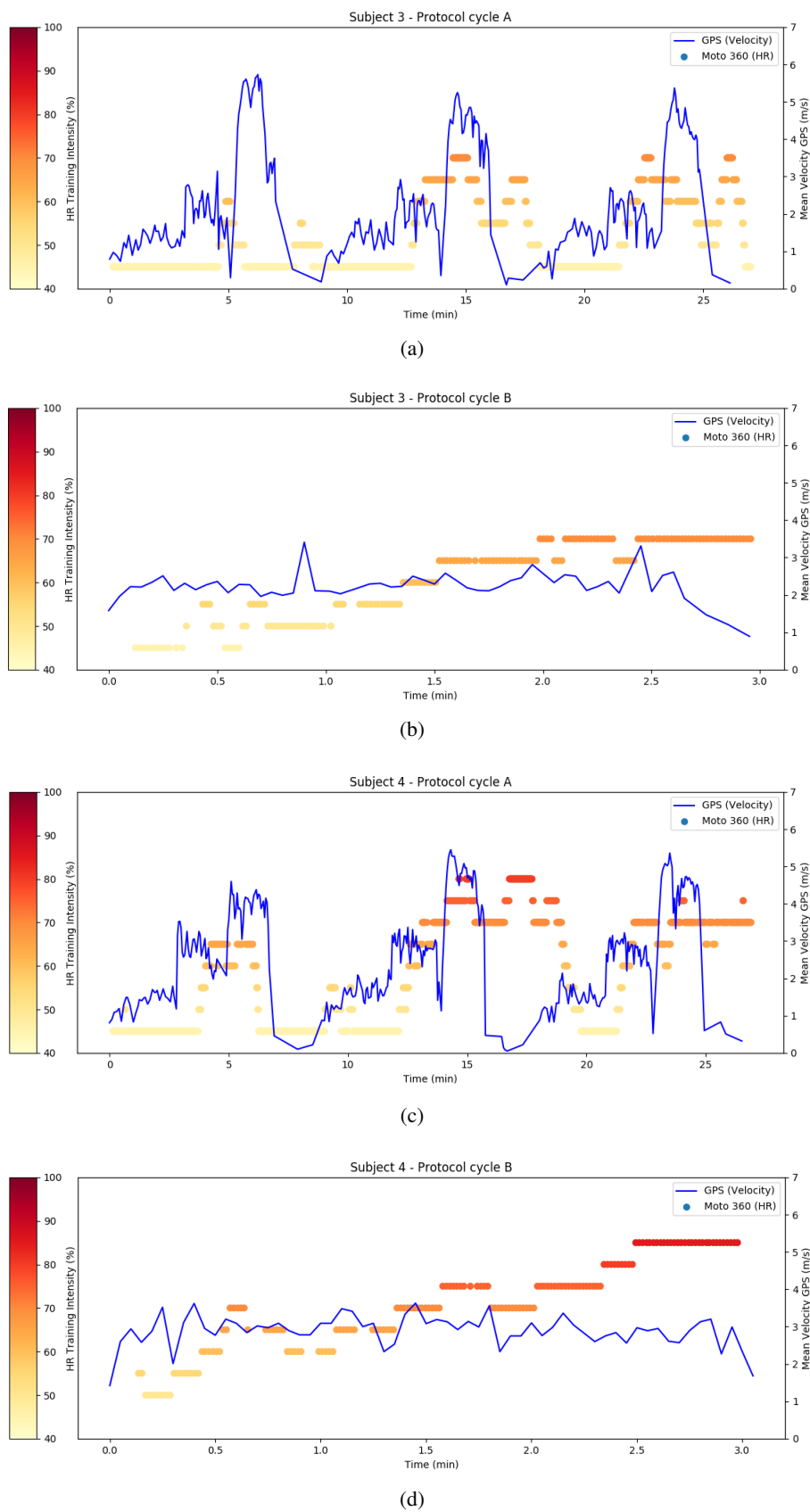

(b)

(c)

(d)

Figure 5.5: Mean velocity and heart rate training intensity achieved during the performed protocol for subject 3 ((a) and (b)) and subject 4 ((c) and (d)).

5.4.2 Activity Recognition

Table 5.8 presents the confusion matrix obtained for the activity recognition part of the work, and the classification metrics of precision, recall and F1 score for each class are present in Table 5.9.

All activities presented similar results to those obtained during the research and development part of this work, mentioned in Section 4.4. However, results were significantly worst concerning walking activities. Classifying walking activities was hard due to the difficulty controlling differences between the two in terms of acceleration. Since they are very similar movements, there is an overlap of the features. Walking very slow was most classified as normal walk mainly because the difference between walking very slow and normal walk was not well marked in terms of velocity and acceleration during tests, being hard to control such parameters. Moreover, the classifier was trained using PAMAP dataset and, although its protocol was similar to the one used in the test phase, the subjects performed the activities at a speed higher than expected, as confirmed by the mean velocity chart of Figures 5.4 and 5.5 in the previous sub-section.

Despite some errors, running, cycling and rope jumping activities achieved a precision of 97%, 99% and 90%, respectively. In what regards running activity, which is the main focus of this work, it was classified with 90% of accuracy. Overall, the results obtained were close to the ones presented by the previous works mentioned in Section 3.1 of the "Literature Review" Chapter.

Table 5.8: Normalized confusion matrix obtained for activity recognition during cycle A. Results are the average of the 4 subjects.

		Predicted				
		Walk very slow	Normal walk	Run	Cycle	Rope jump
	Walk very slow	**0.16**	0.83	0.00	0.00	0.00
	Normal walk	0.01	**0.97**	0.02	0.00	0.01
True	Run	0.02	0.03	**0.90**	0.00	0.06
	Cycle	0.17	0.19	0.01	**0.63**	0.01
	Rope jump	0.04	0.10	0.02	0.01	**0.84**

Table 5.9: Main classification metrics results (precision, recall and F1-score for each class) of activity recognition phase during cycle A. Results are the average of the 4 subjects.

Class	**Precision**	**Recall**	**F1-score**
Walk very slow	0.27	0.17	0.20
Normal walk	0.60	0.97	0.74
Run	0.97	0.92	0.94
Cycle	0.99	0.64	0.77
Rope jump	0.90	0.84	0.86
Average/Total	0.79	0.76	0.75

It is important to note that, in this work, only acceleration signals from a smartwatch were used, therefore the results obtained represent an improvement when compared with results of similar works: 87% (Maurer et al., 2006), 76% (Liu et al., 2012), 85% (Mannini et al., 2013; Siirtola et al., 2009), and 74% (Fergus et al., 2015). Better results were achieved by Chen et al. (2008), Kao et al. (2009) and Chernbumroong et al. (2011) with 94% of accuracy. The main problems detected which might had affected activity recognition were the small number of test subjects, the way subjects placed the smartwatch on their wrists, and the non-fulfilment of the protocol rigorously.

5.4.3 Energy Expenditure Estimation

Table 5.10 presents statistical results obtained for energy expenditure measures and Table 5.11 presents the total energy expenditure values of the developed system and COSMED K4b2, and the error between them, per activity and per subject. Figure 5.6 depicts Scatter and Bland-Altman Plots for energy expenditure estimation results of all subjects, for all activities performed, and Figure 5.7 depicts Bland-Altman Plots per activity. Moreover, Figures 5.8 and 5.9 depict the comparison between the developed system and COSMED K4b2 energy expenditure measures, including error signal (difference between K4 and the developed system measures). Note that the resting period of 1 minute between each cycle of the protocol was removed from these results.

It was obtained a correlation coefficient of 0.55 (P<0.0001, 95% CI 0.52 to 0.57). Applying the statistical test for a significance level of 5%, it can be confirmed that there are significant differences between the energy expenditure values obtained from the developed system and from the COSMED K4b2. Applying the Kruskal-Wallis test, the null-hypothesis is rejected for all activities, so there is statistical significant difference between these activities.

Table 5.10: Statistical results of the obtained energy expenditure measures. The mean of the percentage error (% Error) and normalized root mean square error (NRMSE) of the obtained EE measures for each cycle of the protocol and for each subject. Evaluation of the statistical difference between the developed system and COSMED K4b2, using data from all the participants (Correlation Coefficient and Wilcoxon Signed Ranked Test).

Subject ID	Cycle A		Cycle B		Correlation Coefficient	Wilcoxon Test
	% Error	NRMSE (%)	% Error	NRMSE (%)		
1	28.24	34.63	12.07	15.28		
2	36.36	42.03	17.92	19.81	0.55	P = 0.0059
3	26.71	33.75	16.76	20.03		
4	28.52	36.37	14.20	15.05		
Average	29.96	36.69	15.24	17.54		

Table 5.11: Total energy expenditure values, per activity and per subject, of the developed system and COSMED K4b2, and the error between them.

Activity	Method	Subject 1	Subject 2	Subject 3	Subject 4	Error (%)
Walk	Dev. system	970	1299	1989	1317	9.05
	COSMED K4b2	1068	1386	2047	1117	
Run	Dev. system	4094	3681	4553	2248	10.76
	COSMED K4b2	4301	4578	4326	2594	
Cycle	Dev. system	2303	2969	2943	2074	15.74
	COSMED K4b2	2028	2375	2676	1812	
Rope Jump	Dev. system	1040	1804	1753	856	18.79
	COSMED K4b2	1262	1591	1460	690	
Error (%)		11.29	16.06	9.54	17.46	**13.59**

Although the Bland-Altman Plot shows that both devices agreed in most part of the tests, with the majority of data being between the 95% limits of agreement, it can be observed that walking and running activities presented the greatest dispersions. However, it must be noticed that the amount of running samples was the highest and, consequently, the most propitious to dispersion. Moreover, errors in activity recognition have led to some activities being erroneously classified as walking, leading to propagation errors in the energy expenditure estimation. On the other hand, walking and running presented the best results in terms of total energy expenditure value, being the overall error of the developed system of 13.59%. Table 5.11 and Figures 5.8 and 5.9 show that the developed system mostly overestimates EE in cycling and rope jumping activities, and mostly underestimates EE in walking and running activities. In what regards running activity, expressed by the cycle B of the protocol, EE estimation achieved a NRMSE of 17.54%. This value increases when testing all activities, as expressed by the cycle A of the protocol, which achieved a NRMSE of 36.69%.

As mentioned before in Section 3.2 of the "Literature Review" Chapter, the combined HR-activity model had shown promising results estimating energy expenditure. In this work, results demonstrated that the model used still needs some improvements, as well as the wearable devices themselves. Using a similar EE estimation model, Magalhães (2016) achieved an NRMSE of 19.9%. However, the smartwatch used to measure HR was Fitbit Surge, which has an accuracy of 93.8% measuring heart rate, higher than the accuracy of the smartwatch Moto 360 used in this work; and the acceleration signals were provided by a smartphone placed on the belt of the subjects.

The high percentage error and the low correlation coefficient are mainly due to the propagation of errors of heart rate measurements and activity recognition. Furthermore, EE was estimated using group calibrated models, thus EE estimation could be improved using individual calibration, as proposed by Altini et al. (2015), who used individual-specific HR normalization parameters. However, such method is not suitable for generalized sports applications that are used by different

users, since it would required an individual calibration, which is time-consuming and not practical in the sports context. Therefore, the method presented in this work introduces a convenient way to monitor physical health with enough reliability.
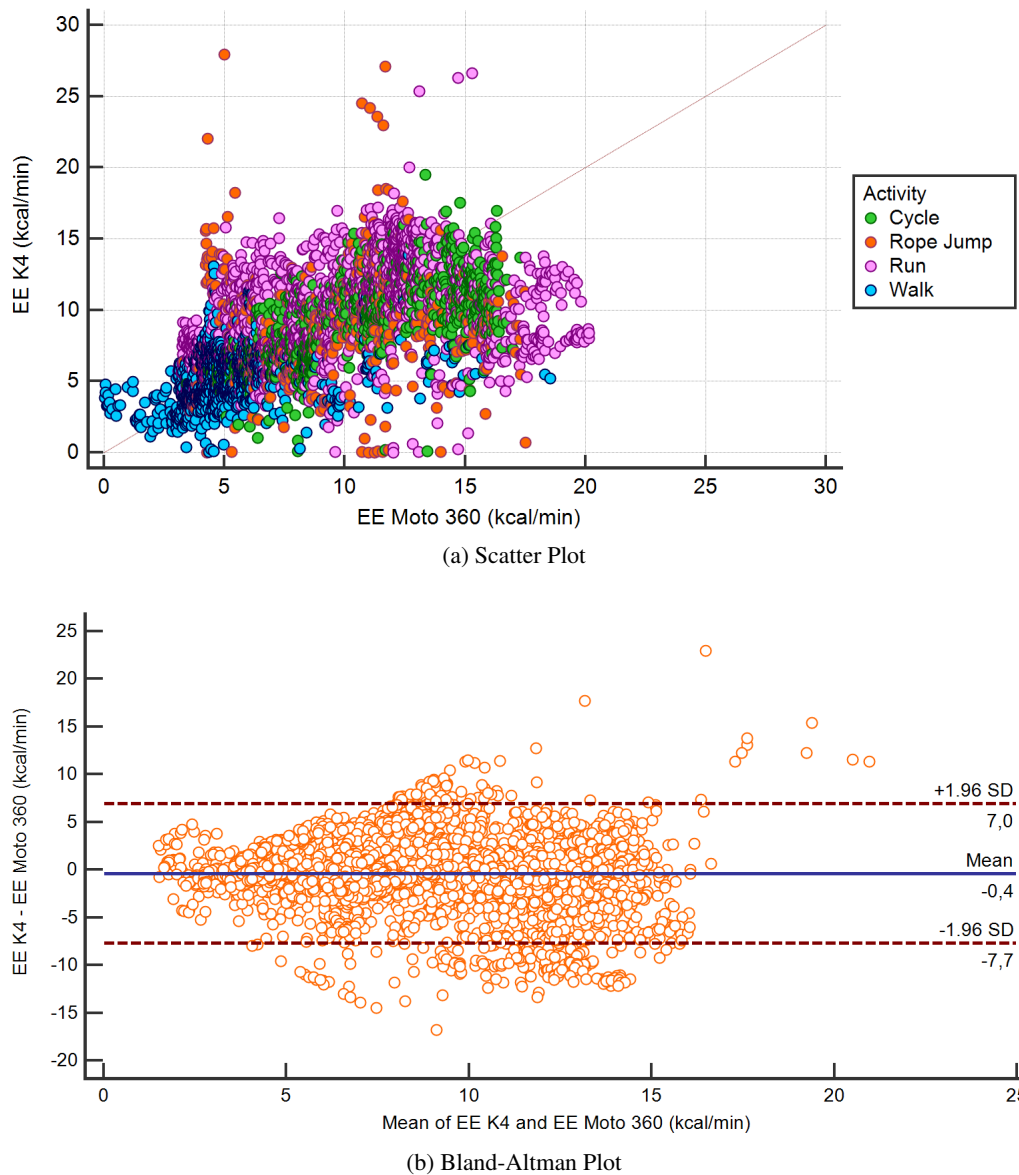

(a) Scatter Plot

(b) Bland-Altman Plot

Figure 5.6: Scatter Plot (*a*) and Bland-Altman Plot (*b*) for energy expenditure estimation results of all subjects, with the confidence interval $\mu \pm 1.96SD$ represented by the dashed lines.

(a) Walk
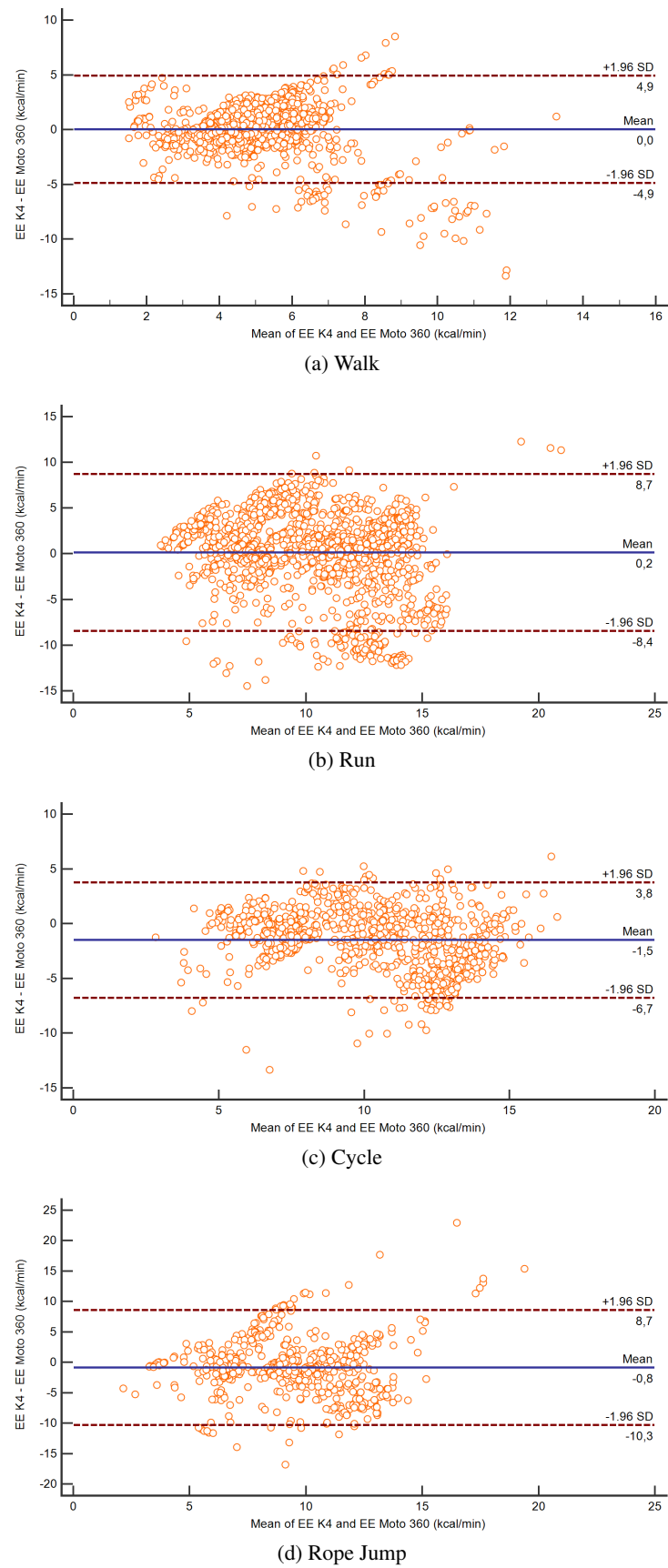

(b) Run

(c) Cycle

(d) Rope Jump

Figure 5.7: Bland-Altman Plots, with the confidence interval $\mu \pm 1.96SD$ represented by the dashed lines, for energy expenditure estimation results of all subjects, per activity: walk (a), run (b), cycle (c) and rope jump(d).
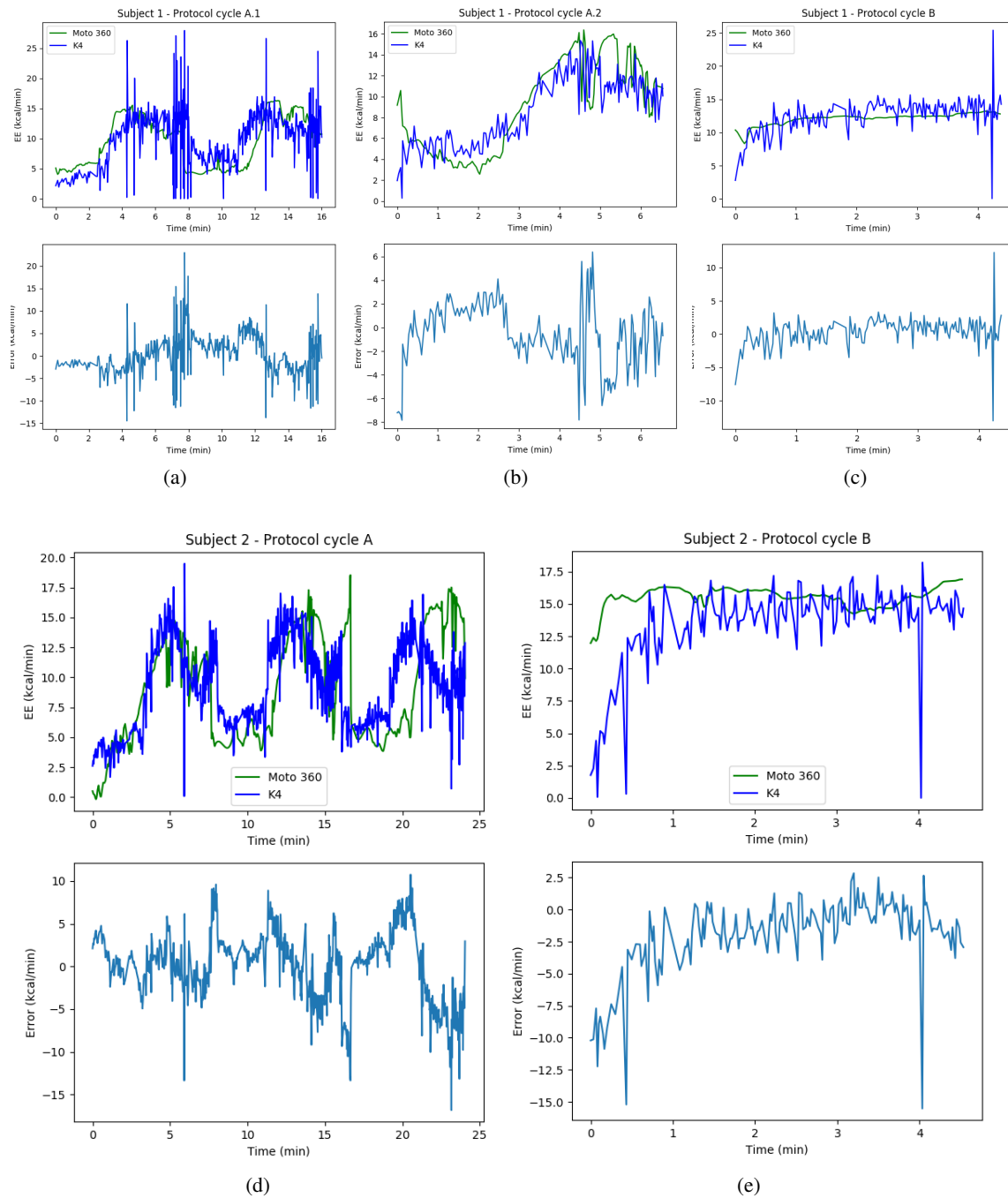
Figure 5.8: Results of energy expenditure measures obtained for subject 1 ((a), (b) and (c)) and subject 2 ((d) and (e)), for each cycle of the protocol. Comparison between the COSMED K4b2 and the developed system.
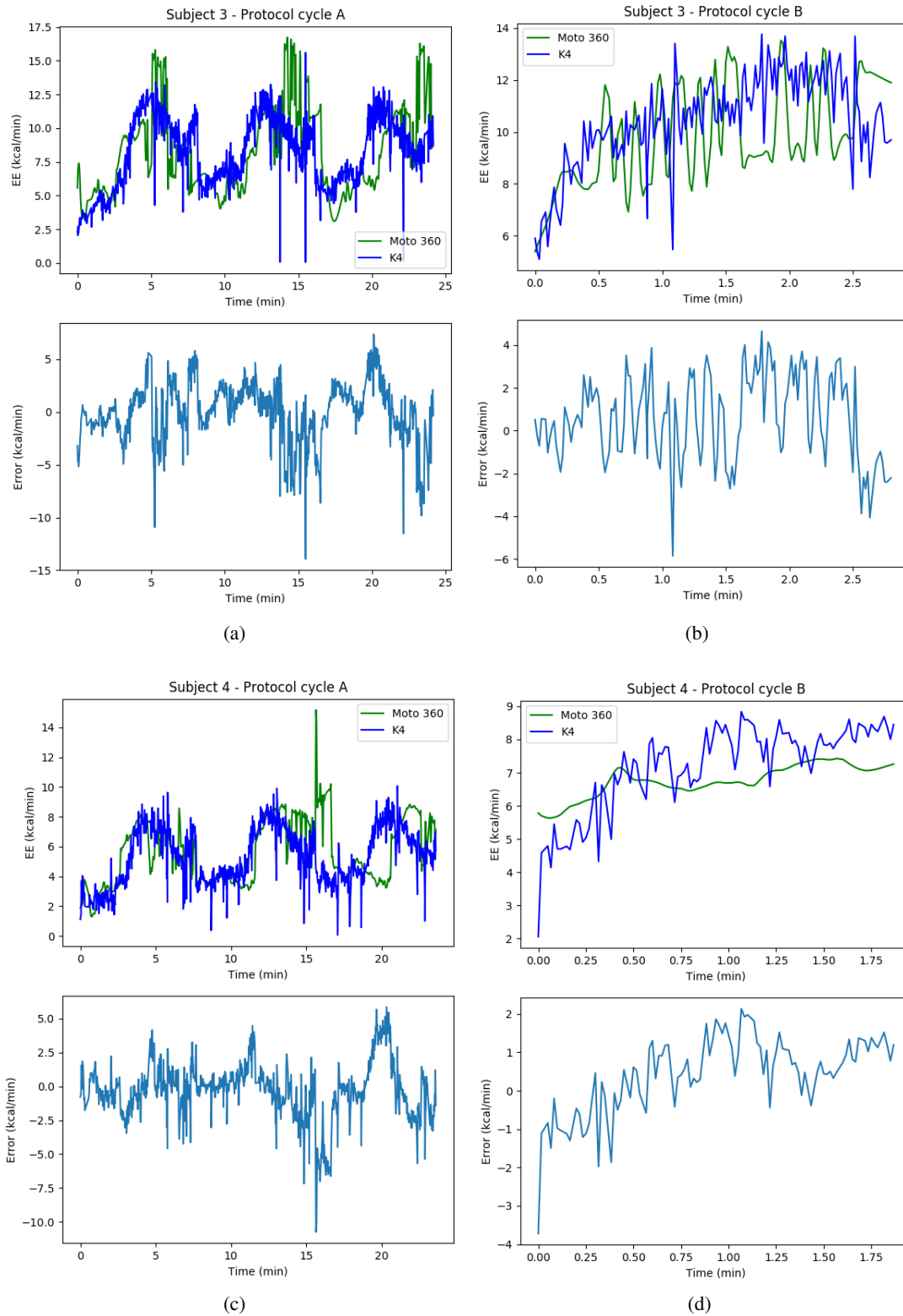
Figure 5.9: Results of energy expenditure measures obtained for subject 3 ((*a*) and (*b*)) and subject 4 ((*c*) and (*d*)), for each cycle of the protocol. Comparison between the COSMED K4b2 and the developed system.

5.4.4   Movement Analysis

Table 5.12 presents the results obtained for step counting by TUNE and by the developed system using acceleration signals from smartwatch Moto 360. The error obtained for the total number of steps counted was 1.10% and the average of the 9 measurements present in the table is 2.40%. El-Amrawy and Nounou (2015) reported that the accuracy of Moto 360 in step counting was 89%, thus, the proposed method represents an improvement of 9%.

Figure 5.10 shows the relation between ground contact time from TUNE left foot and the right arm acceleration amplitude of 3 of the measurements collected. Figure 5.10 (*a*) corresponds to 5 sets of running followed by going up and down stairs. Figure 5.10 (*b*) corresponds to a slow run followed by a faster run and Figure 5.10 (*c*) to sets of slow and fast runs. As shown in the figures, acceleration amplitude varies in indirect proportion with ground contact time, i.e., large accelerations of the arms are related to the rapid contact of the feet with the ground and therefore to a faster run. This behaviour reflects the increased ability to produce force when the foot is on the ground and to use elastic energy stored in the muscles to propel the body of the ground.

Although these graphs evidence a relation between the movement of the arm and the movement of the feet, it would be necessary more information to draw concrete conclusions. For instance, the comparable situations of running with and without moving the arms could be evaluated to infer about the importance of this movement in body balance while running, and to compute metrics that would evidence a better relation with metrics acquired from feet. Moreover, symmetry and synchronization of the arms was thought to be evaluated during this project, however another accelerometer would be necessary on the left wrist. The fusion of data from accelerometers, gyroscopes and magnetometers would be another option to evaluate the posture of the arm, however, a model would have to be design to overcame the issue of having only a single point on the wrist. Further, overlapping data of the activities represented in the figures (e.g. running and going up and down stairs), it would be possible to obtain a pattern for each movement that then could be compared with metrics acquired from feet. Thus, although results are promising, further work is needed to obtain consistent metrics that are able to describe the movement of the arm.

Table 5.12: Step counting results for running activity.

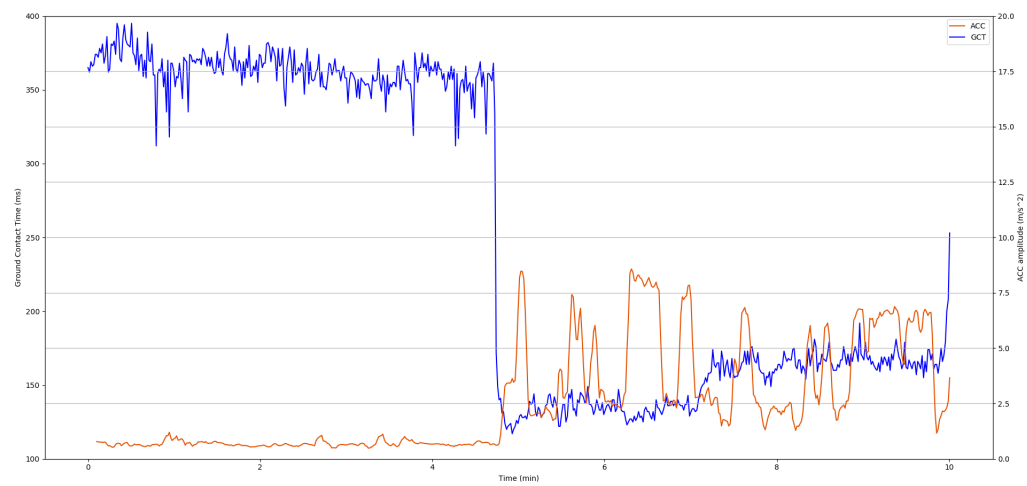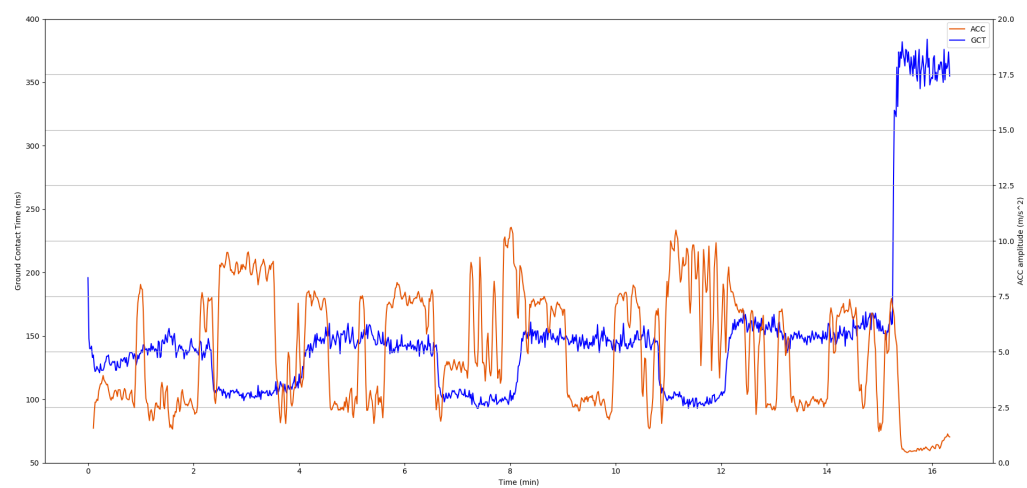| Subject ID	Moto 360 (steps)	TUNE (steps)	Error (%)
2	792	783	1.15
3	475	474	0.21
5	8780	8899	1.34
6_a	3884	3751	3.55
6_b	5388	5786	6.88
6_c	1366	1323	3.25
6_d	2823	2834	0.39
6_e	5273	5422	2.75
6_f	5424	5313	2.09
Total	34205	34585	1.10
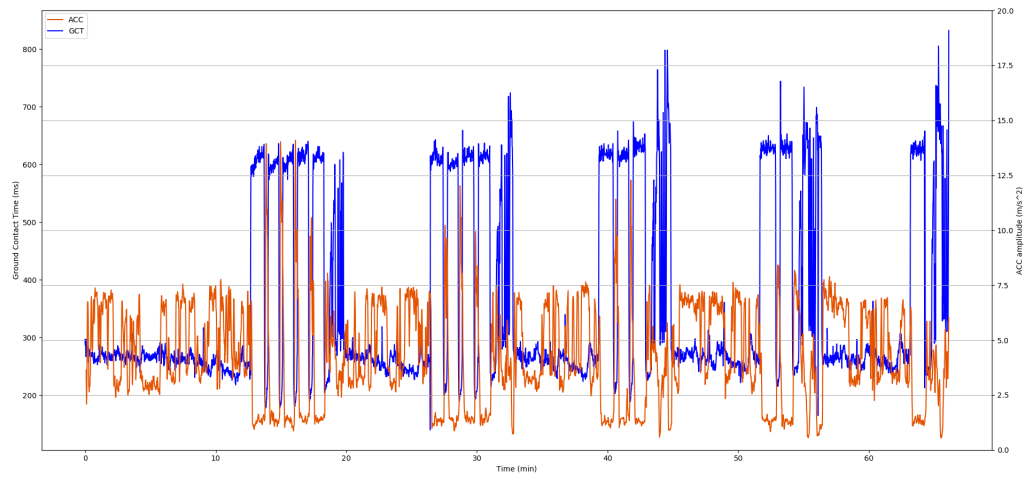
(a) Subject 5

(b) Subject 6_c

(c) Subject 6_d

Figure 5.10: Arm's acceleration amplitude (*orange*) obtained by Moto 360 and ground contact time from left foot (*blue*) obtained by TUNE device.

Chapter 6

Conclusions and Future Work

The ubiquity of wearable connected devices is mainly due to the growing popularity of fitness trackers. Athletes and health-conscious individuals are monitoring the physical parameters of their bodies by wearing health and fitness trackers. With the concern of such devices do not interfere in their performance, wristbands and watches with built-in GPS, activity sensors and heart rate monitors are on the top of their preferences. Heart rate is an important tool to access maximal oxygen uptake and energy expenditure values through wrist-worn devices, which are highly valued by athletes. Many authors suggested that the use of both heart rate and accelerometry/activity measurements improves the estimation of such parameters, when compared with both methods alone.

The aim of this work was to improve sport wearable solutions, allowing users to improve performance, reduce potential for injuries, increase motivation and improve their experience, as well as to promote a more effective, healthier and better performing sports practice. To do so, a wearable system, composed of TUNE and a smartwatch Moto 360, was used to measure relevant movements and physiological signals in sport context, namely in running. Heart rate and physical activity information were integrated in an energy expenditure estimation module.

EE computation was activity-specific, using activity recognition methods to distinguish between a set of physical activities including walking, running, cycling and rope jumping. Activities were recognized accurately with a simple and computationally inexpensive subject-independent method, applying supervised machine learning through Multilayer Perceptron Classifier to time features from acceleration signals. Running was classified with an accuracy of 90% and a precision of 97%. With regard to heart rate measurements, Moto 360 proved to not be reliable enough for medical purposes or to monitor cardiac patients, with an error of 9% comparing with Polar chest strap. However, taking into account that this chest strap is not the most reliable reference and that the smartwatch readings are influenced by many factors such as way of placement, anatomical issues and movement artefacts, the heart rate readings from Moto 360 were considered credible enough for sport proposes and for cardiac monitoring to improve physical activity. Energy expenditure estimation was expected to reflect errors from both activity recognition and heart rate measurements. EE estimation achieved a NRMSE of 18% for running activity, which increased

to 37% when testing all activities. Computing the total EE value, the developed system achieved an overall error of 14% when compared with COSMED K4b2. Although the results demonstrated that the model used still needs some improvements, as well as the wearable devices technology, the method presented in this work introduced a convenient way to monitor physical health with enough reliability.

Furthermore, heart rate zones of exercise and training intensity were analysed regarding personal information of the users. Such information is helpful with respect to how human body responds to physical activities and it is essential to improve performance. Results showed that there is a linear relationship between the body mass index and the result obtained in speed-HRintensity relation, and that the resting heart rate also reflects the state of health. It can be concluded that regular monitoring of training intensity and resting heart rate can improve health risk and sports performance, not only because they are a reflex of the cardiovascular fitness, but also because they can be used to detect stages of fatigue.

With regards to the movement of the arm, acceleration signals were used to count steps and to compute the amplitude of the arm in terms of acceleration. These measurements were linked with TUNE data, such as step counting and ground contact time. Steps were counted with an error of 2% and acceleration amplitude proved to vary in indirect proportion with ground contact time. Thus, movement analysis of the arm through a smartwatch is closely related to movement analysis of the feet.

TUNE allows for the detection of asymmetries between the left and right feet by monitoring both feet at the same time. Designed to help improve fitness and avoid injury on the track, it helps to improve the running style using customized workout routines based on the user data. Being an unique and powerful device on the market, its combination with a smartwatch proved to make running even more efficient, since the additional information on upper limb movement provides accurate metrics of activity and physiological information.

Therefore, this work successfully achieved the main objective of combining the symmetry of the feet and the movement of the arms with heart rate and acceleration measures, and physical activity and energy expenditure values, turning it in a valuable way of optimize sports performance without constraints. Furthermore, the possibility of leaving the smartphone behind is a major plus for running experience.

6.1   Future Work

Although the results were promising, further work is required to potentially improve sports experience using all the capabilities analysed in this dissertation. First of all, it is important to develop an user-interface associated with TUNE APP to present real-time metrics related to the movement of the arms and the physiological parameters such as heart rate, training intensity and energy expenditure. Moreover, it is essential to present the self-evolution of the users in terms of resting heart rate, ability to achieve higher heart rate training zones, calories burned and BMI evolution.

Another improvement would be taking advantage of heart rate measurements to study with more detail stages of fatigue and its influence on sports performance. Besides the resting heart rate and training intensity zones, heart rate variability is a powerful indicator of fatigue and cardiovascular health and it was not taken into account in this project due to time constraints.

Furthermore, this work could be expanded to other sports where the movement of the arms is crucial for a good performance, such as tennis and golf. Although patterns of movement are different, similar methodologies might be applied to monitor physiological behaviour and movement analysis in order to provide a better experience and improve performance.

In addiction, and following the idea of expansion to other sports, a more detailed study on arm movement would be opportune. To do so, and not forgetting body constraints, the fusion of data from accelerometers, gyroscopes and magnetometers from the smartwatch would be a way to infer about arm symmetry and posture without the need of extra devices attached to the body.

Last but not least, a very important improvement will be the technology evolution of the wearable devices, integrating sensors capable of more accurate and precise readings.

References

U. R. Acharya, K. P. Joseph, N. Kannathal, C. M. Lim, and J. S. Suri. Heart rate variability: a review. *Medical and biological engineering and computing*, 44(12):1031–1051, 2006.

J. Achten and A. E. Jeukendrup. Heart rate monitoring. *Sports medicine*, 33(7):517–538, 2003.

M. Altini. *Personalization of energy expenditure and cardiorespiratory fitness estimation using wearable sensors in supervised and unsupervised free-living conditions*. PhD thesis, Technische Universiteit Eindhoven, 2015.

M. Altini, J. Penders, and O. Amft. Energy expenditure estimation using wearable sensors: a new methodology for activity-specific models. In *Proceedings of the conference on Wireless Health*, page 1. ACM, 2012.

M. Altini, P. Casale, J. F. Penders, and O. Amft. Personalization of energy expenditure estimation in free living using topic models. *IEEE journal of biomedical and health informatics*, 19(5): 1577–1586, 2015.

F. K. Assah, U. Ekelund, S. Brage, A. Wright, J. C. Mbanya, and N. J. Wareham. Accuracy and validity of a combined heart rate and motion sensor for the measurement of free-living physical activity energy expenditure in adults in cameroon. *International journal of epidemiology*, page dyq098, 2010.

A. E. Aubert, B. Seps, and F. Beckers. Heart rate variability in athletes. *Sports medicine*, 33(12): 889–919, 2003.

A. Avci, S. Bosch, M. Marin-Perianu, R. Marin-Perianu, and P. Havinga. Activity recognition using inertial sensing for healthcare, wellbeing and sports applications: A survey. In *Architecture of computing systems (ARCS), 2010 23rd international conference on*, pages 1–10. VDE, 2010.

O. Banos, R. Garcia, J. A. Holgado-Terriza, M. Damas, H. Pomares, I. Rojas, A. Saez, and C. Villalonga. mhealthdroid: a novel framework for agile development of mobile health applications. In *International Workshop on Ambient Assisted Living*, pages 91–98. Springer, 2014.

O. Banos, C. Villalonga, R. Garcia, A. Saez, M. Damas, J. A. Holgado-Terriza, S. Lee, H. Pomares, and I. Rojas. Design, implementation and validation of a novel open framework for agile development of mobile health applications. *Biomedical engineering online*, 14(2):S6, 2015.

L. Bao and S. S. Intille. Activity recognition from user-annotated acceleration data. In *International Conference on Pervasive Computing*, pages 1–17. Springer, 2004.

C. M. Bishop. *Pattern recognition and machine learning*. springer, 2006.

D. Biswas, A. Cranny, N. Gupta, K. Maharatna, and S. Ortmann. Recognition of elementary upper limb movements in an activity of daily living using data from wrist mounted accelerometers. In *Healthcare Informatics (ICHI), 2014 IEEE International Conference on*, pages 232–237. IEEE, 2014.

D. Biswas, A. Cranny, N. Gupta, K. Maharatna, J. Achner, J. Klemke, M. Jöbges, and S. Ortmann. Recognizing upper limb movements with wrist worn inertial sensors using k-means clustering classification. *Human movement science*, 40:59–76, 2015.

E. Bosse, J. Roy, and D. Grenier. Data fusion concepts applied to a suite of dissimilar sensors. In *Electrical and Computer Engineering, 1996. Canadian Conference on*, volume 2, pages 692–695. IEEE, 1996.

S. Brage, N. Brage, P. W. Franks, U. Ekelund, M.-Y. Wong, L. B. Andersen, K. Froberg, and N. J. Wareham. Branched equation modeling of simultaneous accelerometry and heart rate monitoring improves estimate of directly measured physical activity energy expenditure. *Journal of Applied Physiology*, 96(1):343–351, 2004.

L. Breiman. Bagging predictors. *Machine Learning*, 24(2):123–140, 1996.

C. Chen, R. Jafari, and N. Kehtarnavaz. A survey of depth and inertial sensor fusion for human action recognition. *Multimedia Tools and Applications*, pages 1–21, 2015.

Y.-P. Chen, J.-Y. Yang, S.-N. Liou, G.-Y. Lee, and J.-S. Wang. Online classifier construction algorithm for human activity detection using a tri-axial accelerometer. *Applied Mathematics and Computation*, 205(2):849–860, 2008.

S. Chernbumroong, A. S. Atkins, and H. Yu. Activity classification using a single wrist-worn accelerometer. In *Software, Knowledge Information, Industrial Management and Applications (SKIMA), 2011 5th International Conference on*, pages 1–6. IEEE, 2011.

S. Cosmed. K4b2 user manual. *Rome, Italy: Cosmed SRL*, page 96, 1998.

G. J. Criner, P. Belt, A. L. Sternberg, Z. Mosenifar, B. J. Make, J. P. Utz, F. Sciurba, N. E. T. T. R. Group, et al. Effects of lung volume reduction surgery on gas exchange and breathing patter during maximum exercise. *Chest*, 135(5):1268–1279, 2009.

S. E. Crouter, J. R. Churilla, and D. R. Bassett. Accuracy of the actiheart for the assessment of energy expenditure in adults. *European journal of clinical nutrition*, 62(6):704, 2008.

R. Delgado-Gonzalo, J. Parak, A. Tarniceriu, P. Renevey, M. Bertschi, and I. Korhonen. Evaluation of accuracy and reliability of pulseon optical heart rate monitoring device. In *2015 37th Annual International Conference of the IEEE Engineering in Medicine and Biology Society (EMBC)*, pages 430–433. IEEE, 2015.

M. Duclos, G. Fleury, P. Lacomme, R. Phan, L. Ren, and S. Rousset. An acceleration vector variance based method for energy expenditure estimation in real-life environment with a smartphone/smartwatch integration. *Expert Systems with Applications*, 63:435–449, 2016.

S. Dufau, J. A. Duñabeitia, C. Moret-Tatay, A. McGonigal, D. Peeters, F.-X. Alario, D. A. Balota, M. Brysbaert, M. Carreiras, L. Ferrand, M. Ktori, M. Perea, K. Rastle, O. Sasburg, M. J. Yap, J. C. Ziegler, and J. Grainger. Smart phone, smart science: How the use of smartphones can revolutionize research in cognitive science. *PLoS ONE*, 6(9):1–3, 09 2011. doi: 10.1371/journal. pone.0024974. URL http://dx.doi.org/10.1371%2Fjournal.pone.0024974.

F. El-Amrawy and M. I. Nounou. Are currently available wearable devices for activity tracking and heart rate monitoring accurate, precise, and medically beneficial? *Healthcare informatics research*, 21(4):315–320, 2015.

W. Elmenreich. *Sensor Fusion in Time-Triggered Systems*. PhD thesis, Technischen Universität Wien, Fakultät für Technische Naturwissenschaften und Informatik, 2002.

eMarketer, AP. Smartphone users worldwide from 2014 to 2019 | statistic, 2015. URL https://www.statista.com/statistics/330695/number-of-smartphone-users-worldwide/.

Embedded-Lab. Easy pulse sensor (version 1.1) overview (part 1), 2013. URL http://embedded-lab.com/blog/easy-pulse-version-1-1-sensor-overview-part-1/.

M. Ermes and J. Parkka. Detection of Daily Activities and Sports With Wearable Sensors in Controlled and Uncontrolled Conditions. 12(1):20–26, 2008.

M. Ermes, J. Parkka, and L. Cluitmans. Advancing from offline to online activity recognition with wearable sensors. In *2008 30th Annual International Conference of the IEEE Engineering in Medicine and Biology Society*, pages 4451–4454. IEEE, 2008.

P. Fergus, A. Hussain, J. Hearty, S. Fairclough, L. Boddy, K. Mackintosh, G. Stratton, N. Ridgers, and N. Radi. A machine learning approach to measure and monitor physical activity in children to help fight overweight and obesity. In *International Conference on Intelligent Computing*, pages 676–688. Springer, 2015.

R. Freixo. Electromyography and inertial sensor-based gesture detection and control. Master's thesis, Faculdade de Engenharia da Universidade do Porto, 2015.

V. F. Froelicher, J. Myers, W. Follansbee, and A. Labovitz. Exercise and the heart. *Chest*, 118(1), 2000.

T. Garcia-Valverde, A. Muñoz, F. Arcas, A. Bueno-Crespo, and A. Caballero. Heart health risk assessment system: a nonintrusive proposal using ontologies and expert rules. *BioMed research international*, 2014, 2014.

Gfk. Wearables unit sales forecast north america 2014-2015, 2015a. URL https://www.statista.com/statistics/413297/wearables-north-america-unit-sales-forecast/.

Gfk. Wearables unit sales forecast western europe 2014-2015, 2015b. URL https://www.statista.com/statistics/413275/wearables-western-europe-unit-sales-forecast/.

H. Ghasemzadeh, V. Loseu, E. Guenterberg, and R. Jafari. Sport training using body sensor networks: A statistical approach to measure wrist rotation for golf swing. In *Proceedings of the Fourth International Conference on Body Area Networks*, page 2. ICST (Institute for Computer Sciences, Social-Informatics and Telecommunications Engineering), 2009.

D. Guan, T. Ma, W. Yuan, Y.-K. Lee, and A. Jehad Sarkar. Review of sensor-based activity recognition systems. *IETE Technical Review*, 28(5):418–433, 2011.

J. J. Guiry, P. van de Ven, and J. Nelson. Multi-sensor fusion for enhanced contextual awareness of everyday activities with ubiquitous devices. *Sensors*, 14(3):5687, 2014. ISSN 1424-8220. doi: 10.3390/s140305687. URL http://www.mdpi.com/1424-8220/14/3/5687.

A. C. Guyton and J. E. Hall. *TEXTBOOK OF MEDICAL PHYSIOLOGY*. Elsevier Inc., Philadelphia, 11th edition, 2006. ISBN 0721602401.

J. Hamill and K. M. Knutzen. *Biomechanical basis of human movement*. Lippincott Williams & Wilkins, 2006.

A. Hreljac. Impact and overuse injuries in runners. *MEDICINE & SCIENCE IN SPORTS & EXERCISE*, 2004. doi: 10.1249/01.MSS.0000126803.66636.DD.

M. Jette, K. Sidney, and G. Blümchen. Metabolic equivalents (mets) in exercise testing, exercise prescription, and evaluation of functional capacity. *Clinical cardiology*, 13(8):555–565, 1990.

T.-P. Kao, C.-W. Lin, and J.-S. Wang. Development of a portable activity detector for daily activity recognition. In *2009 IEEE International Symposium on Industrial Electronics*, pages 115–120. IEEE, 2009.

Y. Kawahara, N. Ryu, and T. Asami. Monitoring daily energy expenditure using a 3-axis accelerometer with a low-power microprocessor. *International Journal on Human-Computer Interaction*, 1(5):145–154, 2009.

L. Keytel, J. Goedecke, T. Noakes, H. Hiiloskorpi, R. Laukkanen, L. van der Merwe, and E. Lambert. Prediction of energy expenditure from heart rate monitoring during submaximal exercise. *Journal of sports sciences*, 23(3):289–297, 2005.

S. Kumar. Cardiac waveform: key to efficient heart rate monitoring, 2011. URL http://www.eetimes.com/document.asp?doc_id=1278714.

O. D. Lara and M. A. Labrador. A survey on human activity recognition using wearable sensors. *IEEE Communications Surveys & Tutorials*, 15(3):1192–1209, 2013.

Ó. D. Lara, A. J. Pérez, M. A. Labrador, and J. D. Posada. Centinela: A human activity recognition system based on acceleration and vital sign data. *Pervasive and mobile computing*, 8(5):717–729, 2012.

Y.-S. Lee and S.-B. Cho. Activity recognition using hierarchical hidden markov models on a smartphone with 3d accelerometer. In *International Conference on Hybrid Artificial Intelligence Systems*, pages 460–467. Springer, 2011.

J. Lester, T. Choudhury, and G. Borriello. A practical approach to recognizing physical activities. In *International Conference on Pervasive Computing*, pages 1–16. Springer, 2006.

S. Liu, R. X. Gao, D. John, J. W. Staudenmayer, and P. S. Freedson. Multisensor Data Fusion for Physical Activity Assessment. *IEEE Transactions on Biomedical Engineering*, 59(3):687–696, 2012.

V. Lugade, E. Fortune, M. Morrow, and K. Kaufman. Validity of using tri-axial accelerometers to measure human movement—part i: Posture and movement detection. *Medical engineering & physics*, 36(2):169–176, 2014.

H. J. Luinge, P. H. Veltink, and C. T. Baten. Ambulatory measurement of arm orientation. *Journal of biomechanics*, 40(1):78–85, 2007.

H. Mac Gillivray. Shape properties of the g-and-h and johnson families. *Communications in statistics-theory and methods*, 21(5):1233–1250, 1992.

J. Machek, J. Parak, and J. Havlik. Movement detection in the accelerometer data. *Conference on Advanced Methods of Biological Data and Signal Processing*, 1:2–6, 2012.

M. Magalhães. SHRAM-Smart Heart Rate and Activity Measurement. Master's thesis, Faculdade de Engenharia da Universidade do Porto, 2016.

A. Mannini, S. S. Intille, M. Rosenberger, A. M. Sabatini, and W. Haskell. Activity recognition using a single accelerometer placed at the wrist or ankle. *Medicine and science in sports and exercise*, 45(11):2193, 2013.

U. Maurer, A. Smailagic, D. P. Siewiorek, and M. Deisher. Activity recognition and monitoring using multiple sensors on different body positions. In *International Workshop on Wearable and Implantable Body Sensor Networks (BSN'06)*, pages 4–pp. IEEE, 2006.

J. Moores. Sports and fitness smart wearables market to be valued at \$44.2bn by 2021, 2016. URL http://www.sporttechie.com/2016/01/29/gadgets/sports-and-fitness-smart-wearables-market-to-be-valued-at-44-2bn-by-2021/.

K. Moran, C. Richter, E. Farrell, E. Mitchell, A. Ahmadi, and N. E. O'Connor. Detection of running asymmetry using a wearable sensor system. *Procedia Engineering*, 112:180 – 183, 2015. ISSN 1877-7058. doi: http://dx.doi.org/10.1016/j.proeng.2015.07.196. URL http://www.sciencedirect.com/science/article/pii/S1877705815014459.

T. Nieminen, M. Kähönen, T. Kööbi, K. Nikus, and J. Viik. Heart rate variability is dependent on the level of heart rate. *American heart journal*, 154(1):e13, 2007.

B. O'Donnell. The slow build: Smart wearables forecast, 2014-2020, 2015. URL http://www.technalysisresearch.com/downloads/TECHnalysis%20Research%20Smart%20Wearables%20Forecast%20Summary,%20May%202015.pdf.

M. S. Olufsen, A. V. Alston, H. T. Tran, J. T. Ottesen, and V. Novak. Modeling heart rate regulation—part i: sit-to-stand versus head-up tilt. *Cardiovascular Engineering*, 8(2):73–87, 2008.

A. Pereira. Inertial sensor-based 3D upper limb motion tracking and trajectories reconstruction. Master's thesis, Faculdade de Engenharia da Universidade do Porto, 2016.

S. A. Plowman and D. L. Smith. *Exercise physiology for health fitness and performance*. Lippincott Williams & Wilkins, 2013.

C. V. Putte, J. Regan, and A. Russo. *Seeley's essentials of anatomy & physiology*. McGraw-Hill Education, 2 Penn Plaza, New York, NY 10121, 9th edition, 2016. ISBN 978-0-07-809732-4.

F. Ramos, A. Moreira, A. Costa, R. Rolim, H. Almeida, and A. Perkusich. Combining Smartphone and Smartwatch Sensor Data in Activity Recognition Approaches: an Experimental Evaluation. *International Journal of Engineering and Technology*, 8, 2016. ISSN 23259086. doi: 10.18293/SEKE2016-040.

S. Ranasinghe, F. Al Machot, and H. C. Mayr. A review on applications of activity recognition systems with regard to performance and evaluation. *International Journal of Distributed Sensor Networks*, 12(8):1550147716665520, 2016.

A. Reiss and D. Stricker. Introducing a new benchmarked dataset for activity monitoring. In *2012 16th International Symposium on Wearable Computers*, pages 108–109. IEEE, 2012.

D. Riboni and C. Bettini. COSAR: Hybrid reasoning for context-Aware activity recognition. *Personal and Ubiquitous Computing*, 15(3):271–289, 2011. ISSN 16174909. doi: 10.1007/s00779-010-0331-7.

S. Ríos-Aguilar, J. Merino, A. Sánchez, and A. Valdivieso. Variation of the heartbeat and activity as an indicator of drowsiness at the wheel using a smartwatch. *International Journal of Artificial Intelligence and Interactive Multimedia*, 3(3):96–100, 2015.

N. Ryu, Y. Kawahawa, and T. Asami. A calorie count application for a mobile phone based on mets value. In *Sensor, Mesh and Ad Hoc Communications and Networks, 2008. SECON'08. 5th Annual IEEE Communications Society Conference on*, pages 583–584. IEEE, 2008.

D. J. Saba. *Validation of Running Symmetry Using Trunk Mounted Accelerometry: Clinical Trial and Case Study*. PhD thesis, Virginia Tech, 2016.

D. A. Santos, A. M. Silva, C. N. Matias, J. P. Magalhães, D. A. Fields, C. S. Minderico, U. Ekelund, and L. B. Sardinha. Validity of a combined heart rate and motion sensor for the measurement of free-living energy expenditure in very active individuals. *Journal of Science and Medicine in Sport*, 17(4):387–393, 2014.

D. Satkunskiene, V. Grigas, V. Eidukynas, and A. Domeika. 487. acceleration based evaluation of the human walking and running parameters. *Journal of Vibroengineering*, 11(3), 2009.

R. R. Seeley, T. D. Stephens, and P. Tate. *Anatomy and physiology. WCB*. MacGraw-Hill, 1998.

S. Shen, H. Wang, and R. R. Choudhury. I am a smartwatch and i can track my user's arm. In *Proceedings of the 14th annual international conference on Mobile systems, applications, and services*, 2016.

P. Siirtola, P. Laurinen, E. Haapalainen, J. Roning, and H. Kinnunen. Clustering-based activity classification with a wrist-worn accelerometer using basic features. In *Computational Intelligence and Data Mining, 2009. CIDM'09. IEEE Symposium on*, pages 95–100. IEEE, 2009.

H. B. Simon. *The Harvard Medical School guide to men's health*. Simon and Schuster, 2002.

O. Solomon Jr. Psd computations using welch's method. *NASA STI/Recon Technical Report N*, 92, 1991.

A. Stamm, D. A. James, R. M. Hagem, and D. V. Thiel. Investigating arm symmetry in swimming using inertial sensors. In *Sensors, 2012 IEEE*, pages 1–4. IEEE, 2012.

T. Starner, B. Rhodes, J. Weaver, and A. Pentland. Everyday-use wearable computers. In *International Symposium on Wearable Computers*, page 9, 1999.

J. Staudenmayer, D. Pober, S. Crouter, D. Bassett, and P. Freedson. An artificial neural network to estimate physical activity energy expenditure and identify physical activity type from an accelerometer. *Journal of Applied Physiology*, 107(4):1300–1307, 2009.

A. Stisen, H. Blunck, S. Bhattacharya, T. S. Prentow, M. B. Kjærgaard, A. Dey, T. Sonne, and M. M. Jensen. Smart devices are different: Assessing and mitigatingmobile sensing heterogeneities for activity recognition. In *Proceedings of the 13th ACM Conference on Embedded Networked Sensor Systems*, pages 127–140. ACM, 2015.

J. Sunny, S. George, and J. Kizhakkethottam. Applications and challenges of human activity recognition using sensors in a smart environment. *International Journal for Innovative Research in Science & Technology*, 2(4):50–57, 2015. URL http://www.ijirst.org/articles/IJIRSTV2I4024.pdf.

T. Tamura, Y. Maeda, M. Sekine, and M. Yoshida. Wearable photoplethysmographic sensors—past and present. *Electronics*, 3(2):282–302, 2014.

H. Tanaka, K. D. Monahan, and D. R. Seals. Age-predicted maximal heart rate revisited. *Journal of the American College of Cardiology*, 37(1):153–156, 2001.

E. M. Tapia, S. S. Intille, W. Haskell, K. Larson, J. Wright, A. King, and R. Friedman. Real-time recognition of physical activities and their intensities using wireless accelerometers and a heart rate monitor. In *2007 11th IEEE international symposium on wearable computers*, pages 37–40. IEEE, 2007.

S. Theodoridis and K. Koutroumbas. *Pattern Recognition*. Elsevier (USA), second edition, 2003. ISBN 0-12-685875-6.

D. Thompson, A. M. Batterham, S. Bock, C. Robson, and K. Stokes. Assessment of low-to-moderate intensity physical activity thermogenesis in young adults using synchronized heart rate and accelerometry with branched-equation modeling. *The Journal of nutrition*, 136(4): 1037–1042, 2006.

P. H. Veltink, H. B. J. Bussmann, F. Koelma, H. M. Franken, W. L. J. Martens, and R. C. V. Lummei. The feasibility of posture and movement detection by accelerometry. pages 4–5, 1993.

D. E. Warburton, C. W. Nicol, and S. S. Bredin. Prescribing exercise as preventive therapy. *Canadian Medical Association Journal*, 174(7):961–974, 2006.

T.-F. Wu, C.-J. Lin, and R. C. Weng. Probability estimates for multi-class classification by pairwise coupling. *Journal of Machine Learning Research*, 5(Aug):975–1005, 2004.

C.-C. Yang and Y.-L. Hsu. A review of accelerometry-based wearable motion detectors for physical activity monitoring. *Sensors*, 10(8):7772, 2010. ISSN 1424-8220. doi: 10.3390/s100807772. URL http://www.mdpi.com/1424-8220/10/8/7772.

J.-Y. Yang, Y.-P. Chen, G.-Y. Lee, S.-N. Liou, and J.-S. Wang. Activity recognition using one triaxial accelerometer: A neuro-fuzzy classifier with feature reduction. In *Entertainment Computing–ICEC 2007*, pages 395–400. Springer, 2007.

J.-Y. Yang, J.-S. Wang, and Y.-P. Chen. Using acceleration measurements for activity recognition: An effective learning algorithm for constructing neural classifiers. *Pattern recognition letters*, 29(16):2213–2220, 2008.

G. Zhang, C. Liu, L. Ji, J. Yang, and C. Liu. Effect of a percutaneous coronary intervention procedure on heart rate variability and pulse transit time variability: A comparison study based on

fuzzy measure entropy. *Entropy*, 18(7):246, 2016. ISSN 1099-4300. doi: 10.3390/e18070246. URL http://www.mdpi.com/1099-4300/18/7/246.

Appendix A

Mathematical Formulations

A.1 Energy Expenditure Estimation

A.1.1 Metabolic Equivalents Equations

The values of metabolic equivalents (METs) are computed from the equations in Table A.1.

Table A.1: Metabolic equivalents estimation per activity type (Kawahara et al., 2009; Magalhães, 2016). METs in $\frac{kcal}{kg \times h}$, speed in $\frac{km}{h}$ and constant multiplying by speed in $\frac{kcal}{kg \times km}$.

Activity	METs
Walking	$0.00163 \times speed + 1.2$
Running	$0.00558 \times speed - 4.7$
Sitting	Between 1.0 and 2.0
Standing	Between 1.2 and 2.3
Laying	Between 0.95 and 1.3

A.1.2 Heart Rate Normalization Factor

A multiple linear regression model (see Table A.2) was built by Altini (2015) to predict the normalization factor (i.e. an individual's HR while running at 10 km/h) using activities of daily living only.

Actual HR measurements are used after applying the HR normalization factor, derived with the normalization factor estimator, using the simple ratio (Altini, 2015):

$$NormalizedHR = \frac{CurrentHR}{NormalizationFactor} \tag{A.1}$$

Table A.2: Heart Rate Normalization Factor Estimation Model (R^2 0.87). The best model relies on HR while lying down resting and while walking at 4, 5 and 6 km/h, together with the individual height and age, as independent variables (Altini, 2015).

Variable	Coefficient
Intercept	66.91
HR at rest	0.29
HR 4 km/h	1.58
HR 5 km/h	-2.80
HR 6 km/h	2.18
Height	-0.17
Age	-0.23

A.1.3   Activity-Specific EE Linear Models

EE is estimated by first classifying the activity performed, by means of ACC features, and then applying an activity-specific EE linear regression model. Altini (2015) developed six multiple linear regression models, one for each cluster of activities (see Table A.3).

Table A.3: Activity-specific EE linear models, using anthropometric characteristics, ACC and HR features. Resting Metabolic Rate (*RMR*), motion intensity (*MI*), standard deviation (*SD*), median (*MED*), main frequency peak (*FFTpeak$_f$*) and its amplitude (*FFTpeak$_a$*), body weight (*BW*) and Normalized Heart Rate (*HRNorm*) (Altini, 2015).

Cluster	Model
Lying	$0.49 + 0.00068RMR - 29.66MI_x + 9.78SD_x + 0.11MED_x + 0.68MED_y$
Sedentary	$0.31 + 0.00061RMR + 8.42MI_x + 11.12MI_y - 2.37MI_z + 2.9SD_x +$ $2.48SD_y + 0.47MED_y - 0.14MED_z + 0.05FFT_{peak}Y_a$
Dynamic	$-3.43 + 5.95HRNorm + 0.035BW + 7.65MI_y + 8.59MI_{tot} + 4.80SD_x$
Walking	$-9.00 + 15.07HRNorm + 0.056BW + 3.91SD_x$
Biking	$-10.58 + 0.0029RMR + 16.75HRNorm - 37.66MI_x + 14.23MI_y -$ $54.37VAR_y + 26.22SD_x$
Running	$-8.73 + 11.50HRNorm + 0.12BW + 13.99MI_y - 5.28SD_y +$ $4.16MED_x - 3.70MED_z - 1.33FFT_{peak}X_f$

A.1.4   Multi-linear Regression Equation

In work by Thompson et al. (2006), accelerometer counts and heart rate were used to estimate energy expenditure using the following equations:

$$PAI = 5.95 \times HraS - 134 + 0.23 \times age(y) + 84 \times sex \tag{A.2}$$

$$PAI = 0.203 \times counts/min + 46 - 0.75 \times age(y) + 83 \times sex \qquad \text{(A.3)}$$

where *PAI* is the physical activity intensity in $J \cdot min^{-1} \cdot kg^{-1}$, *sex* is coded 0 for females and 1 for males, *HraS* represents heart rate above sleep, and *counts/min* represents accelerometer counts per minute.

Figure A.1 depicts the equation structure proposed by Brage et al. (2004) for the combination of accelerometry and heart rate. All physical activity intensity (*PAI*) relationships are determined by calibration. *P1*, *P2*, *P3* and *P4* are weighting factors, *X* refers to the accelerometer counts, which is used to discriminate between activity and rest. *Y* and *Z* behave as heart rate thresholds in the presence and absence of activity, respectively. *Y* is used to discriminate between walking and running activities and *Z* is used to discriminate between the existence of movement or not during inactive states (Magalhães, 2016).
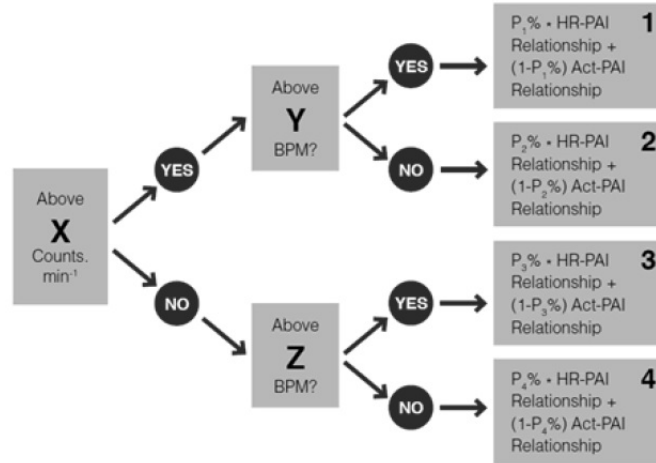
Figure A.1: Equation structure for the combination of accelerometry and heart rate (Magalhães, 2016).

Appendix B

TUNE specifications

![kinematix logo](making sense of body dynamics)	Tune Datasheet	Data: 12 / 01 / 2017 Version: V1.0
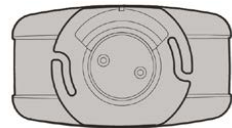
Picture 1 - Charger

Picture 2 - 2 x Device
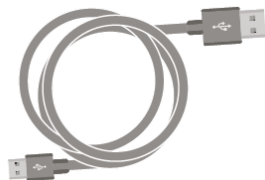
Picture 3 - Micro flat USB cable

Picture 4 – Insole start guide

TUNE Devices	
Weight	12g
Length	45mm
Thickness	12.65mm
Width	25mm

25 mm
0.98 inches

45 mm
1.77 inches
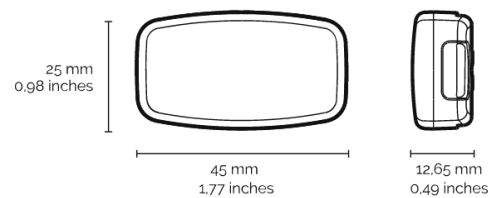
12.65 mm
0.49 inches

TUNE Charger	
Weight	10g
Length	45mm
Thickness	15.8mm
Width	12.65mm

25 mm
0.98 inches

15.8 mm
0.62 inches

45 mm
1.77 inches

![kinematix logo - making sense of body dynamics]	Tune Datasheet	Data: 12 / 01 / 2017 Version: V1.0

TUNE Functioning features	
Battery	3.7V (70mAH)
Battery Type	Li-ion polymer
Power	60 mW (max. 90 mW)
Transmission	ISM 2.4 GHz
Battery time on stand-by	30 days
Battery time in use	10 hours of continuous usage
Type of communication	Bluetooth Low Energy (BLE)
UBS Cable	1.5m
Charger connection	Micro USB (5V)

Picture 5 – Pair of insoles

Picture 6 – Insole start guide

TUNE Insole	
Weight	16g
Length	225mm to 300mm
Thickness	2mm
Width	12.65mm

TUNE Insole Dock	
Weight	6g
Length	29mm
Thickness (with clip)	12.10mm
Width	29mm

2

kinematix making sense of body dynamics	Tune Datasheet	Data: 12 / 01 / 2017 Version: V1.0

TUNE insole pressure sensors	
Number of sensors	4
Type of sensors	Piezo-resistive
Active area/sensor	600 mm2
Sampling rate	1000 Hz
Operating Range Temperature	-15°C to 45°C
Durability	> one million load cycles
Cable length	84.1mm to 98.3mm
Cable thickness	1.8mm
Cable wide	9.1mm

Tune System Requirements	
Android	4.3 or higher
Android Wear	4.3 or higher
IOS	8.4 or higher

Activity data provided by TUNE	
Duration	Duration of the test in hours, minutes and seconds.
Speed	Average speed for the test
Distance	Distance of the test in Km given by GPS
Stance time	Ground contact time: indicates the duration of stance phase
Stance dynamics	Measures the time in propulsion during the stance phase
Heel strike	Percentage of strides you land the heel first
Heel time	Time of the heel keep on the ground.
Fitness plan	Generated based on your last 4 races.

Appendix C

Activity Recognition Development

C.1 Feature Extraction Formulations

Mathematical formulas of the features extracted from acceleration signals are present below. x is the variable vector (total acceleration, x-axis acceleration, y-axis acceleration or z-axis acceleration) and N is the length of x.

C.1.1 Time Domain Parameters

$$Mean(x) = \frac{\sum_{n=1}^{N} x_n}{N} \tag{C.1}$$

$$Median(x) = \begin{cases} x_{\frac{N+1}{2}}, & \text{if } N \text{ is odd} \\ \frac{1}{2}\left(x_{\frac{N}{2}} + x_{\frac{N}{2}+1}\right), & \text{if } N \text{ is even} \end{cases} \tag{C.2}$$

$$Minimum(x) = MIN(x) \tag{C.3}$$

$$Maximum(x) = MAX(x) \tag{C.4}$$

$$RMS(x) = \sqrt{\frac{1}{N} \times \sum_{n=1}^{N} x_n^2} \tag{C.5}$$

$$SD(x) = \sqrt{\frac{1}{N} \times \sum_{n=1}^{N} (x_n - Mean(x))^2} \tag{C.6}$$

$$MAD(x) = Median\left(|x_n - Median(x)|\right) \tag{C.7}$$

$$IQR(x) = 75^{th} percentile(x) - 25^{th} percentile(x) \tag{C.8}$$

$$Energy(x) = \frac{\sum_{n=1}^{N} x_n^2}{N} \tag{C.9}$$

$$ZCR(x) = \frac{1}{N} \sum_{n=1}^{N} |(s_n) - (s_{n-1})|, \text{where } s = \begin{cases} 1, & \text{if } x_n > 0 \\ 0, & \text{otherwise} \end{cases} \tag{C.10}$$

$$Skewness(x) = 3 \times \frac{Mean(x) - Median(x)}{SD(x)} \tag{C.11}$$

Equation C.11 computes the skewness of a data set. For normally distributed data, the skewness should be about 0. A skewness value > 0 means that there is more weight in the left tail of the distribution (Mac Gillivray, 1992).

$$Kurtosis(x) = \frac{1}{N} \sum_{n=1}^{N} \left(\frac{x_n - Mean(x)}{SD(x)} \right)^4 \tag{C.12}$$

Equation C.12 computes the kurtosis using Pearson's definition of a dataset (with normal=3.0). Kurtosis is the fourth central moment divided by the square of the variance (Mac Gillivray, 1992).

C.1.2 Frequency Domain Parameters

$$SpectralEntropy(x) = -\sum s * log_2(s + 0.00000001) \tag{C.13}$$

where

$$s = \sum \frac{subWindows^2}{\sum_{n=1}^{N} (x_n^2) + 0.00000001} \tag{C.14}$$

and

$$subWindows = \begin{cases} x[0 : floor(N/10) * 10], & \text{if } N \neq floor(N/10) * 10 \\ x, & \text{otherwise} \end{cases} \tag{C.15}$$

Equation C.13 computes spectral entropy[1] through the spectral sub-energies (Equation C.14) of subwindows (Equation C.15).

$$PSDpeak(x) = MAX \left(\frac{1}{K} \sum_{k=1}^{K} P_k \right), k \in [0, N-1] \tag{C.16}$$

where

$$P_k = \frac{1}{\sum_{n=0}^{N} x_n^2} |X_k|^2, k \in [0, N-1] \tag{C.17}$$

---

[1] https://github.com/tyiannak/pyAudioAnalysis/blob/master/audioFeatureExtraction.py

where

$$X_k = \sum_{n=0}^{N-1} x_n \cdot e^{-i2\pi kn/N}, k \in [0, N-1] \tag{C.18}$$

Power spectral density was estimated using Welch's method[2], which computes it by dividing the data into overlapping segments, computing a modified periodogram for each segment and averaging the periodograms. It first computes discrete Fourier transform (DFT) at frequency of 50Hz for each segment (Equation C.18). Then, the periodogram value is calculated from DFT (Equation C.17) and its average is computed to obtain Welch's estimate of the PSD as in Equation C.16, where finally the peak is computed as PSD's maximum value (Solomon Jr, 1991).

Total Average Power (TAP) is given by the sum of the power spectral density (Equation C.19).

$$TAP(x) = \sum \left(\frac{1}{K} \sum_{k=1}^{K} P_k \right), k \in [0, N-1] \tag{C.19}$$
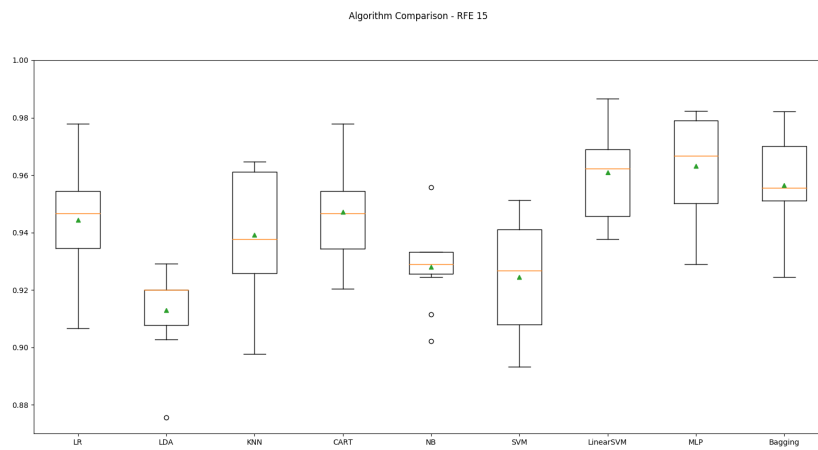
C.2 Activity Recognition Results

Figures C.1, C.2 and C.3 show the results obtained for all classifiers using different selection methods: RFE with top 20 and top 15 features, ETC, LDA with 20, 10 and 6 components, and PCA with 20, 10 and 6 components.
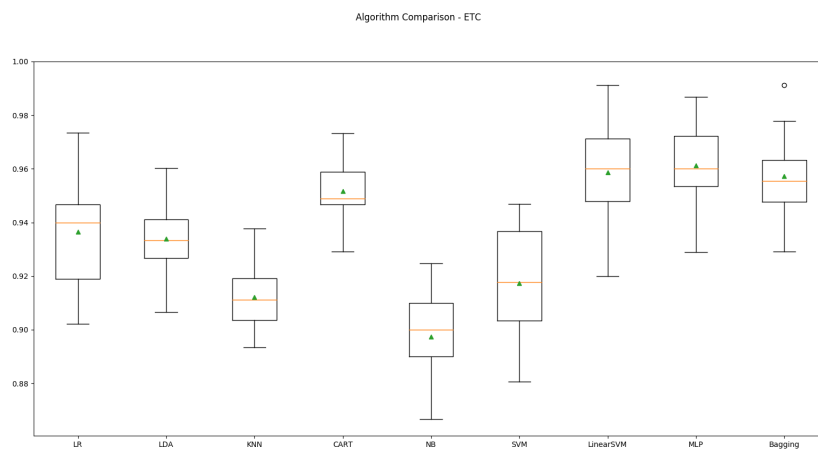
---

[2]https://docs.scipy.org/doc/scipy-0.14.0/reference/generated/scipy.signal.welch.html
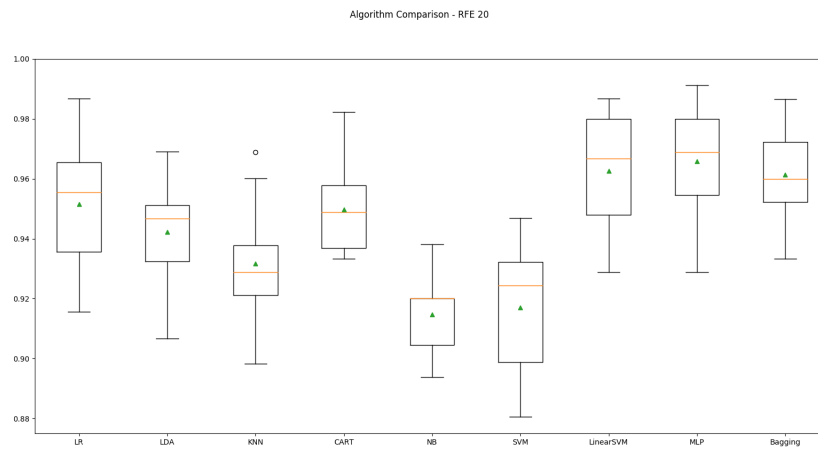
(a) RFE with 20 features


(b) RFE with 15 features

(c) ETC

Figure C.1: Classification's accuracy results using Recursive Feature Elimination method for *(a)*-20 top features, *(b)*- 15 top features, and using *(c)*- Extra Trees Classier method. Classifiers from *left* to *right*: Logistic Regression, Linear Discriminant Analysis, K-Nearest Neighbours, Decision Trees, Gaussian Naive Bayes, Support Vector Machine, Linear SVM, Multi-layer Perceptron Classifier and Bagging. The *vertical lines* represent non-outlier data points that extend to the most extreme (whiskers), the *circle* represents data that extend beyond the whiskers, the *green triangles* represent the mean value, and the *orange lines* represent the median of each box.
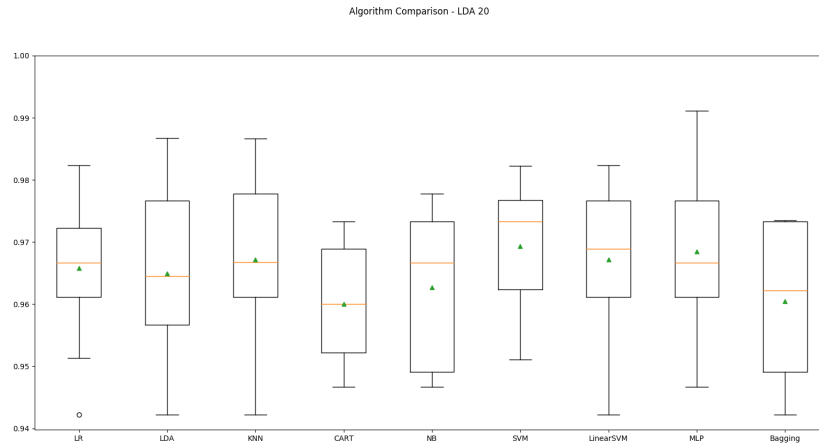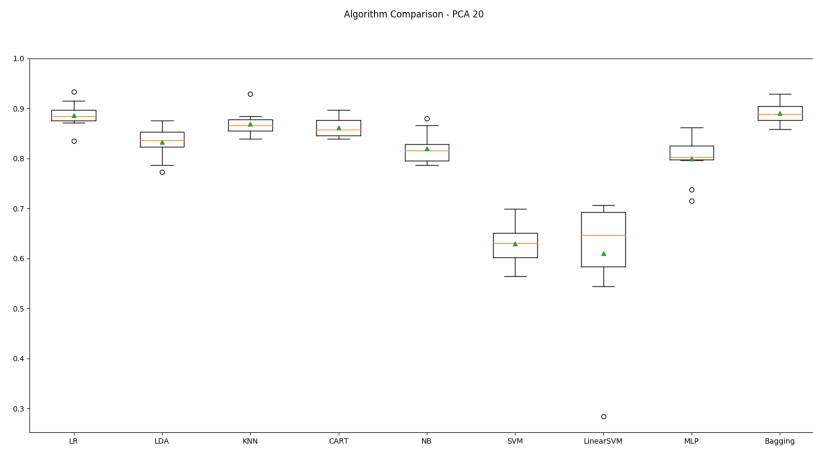
(a) LDA with 20 components
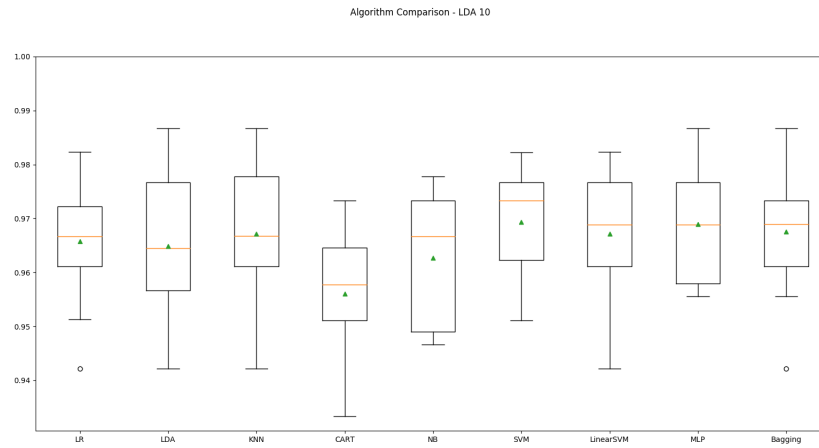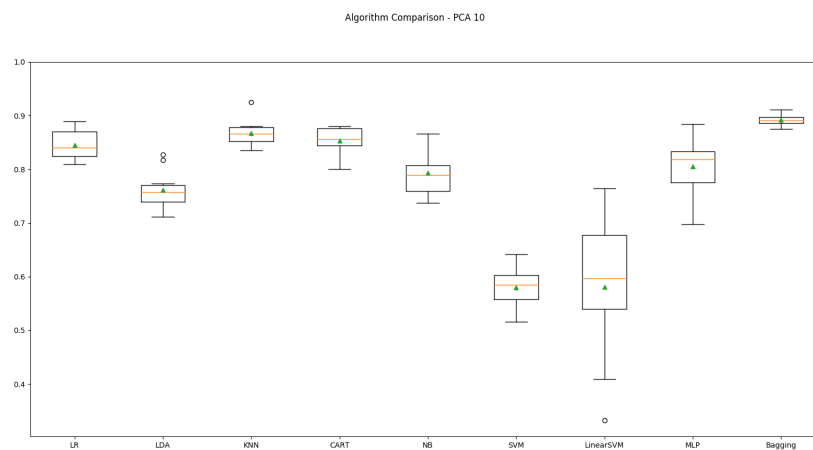

(b) LDA with 10 components
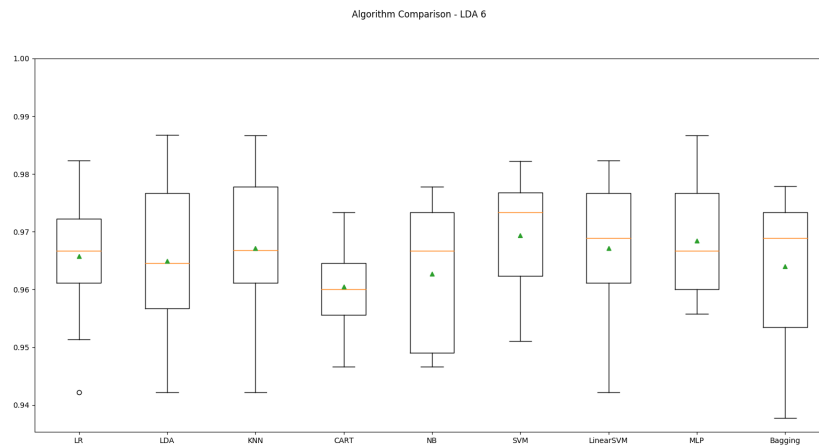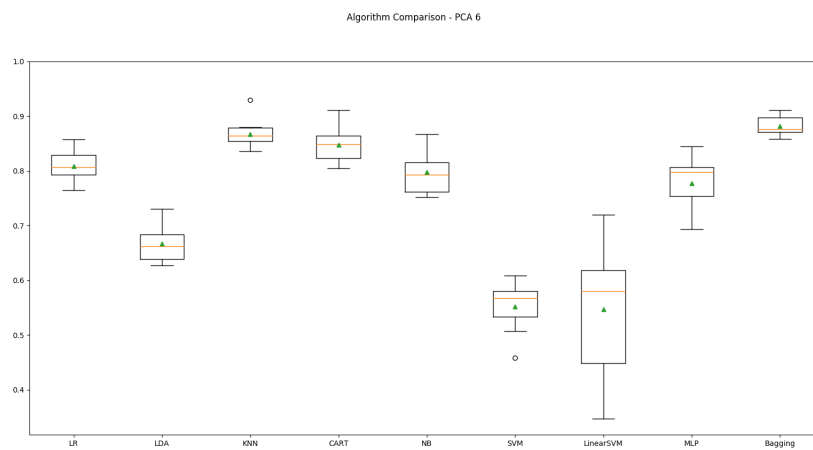

(c) LDA with 6 components

Figure C.2: Classification's accuracy results using Local Discriminant Analysis method with *(a)*-20 components, *(b)*- 10 components and *(c)*- 6 components. Classifiers from *left* to *right*: Logistic Regression, Linear Discriminant Analysis, K-Nearest Neighbours, Decision Trees, Gaussian Naive Bayes, Support Vector Machine, Linear SVM, Multi-layer Perceptron Classifier and Bagging. The *vertical lines* represent non-outlier data points that extend to the most extreme (whiskers), the *circle* represents data that extend beyond the whiskers, the *green triangles* represent the mean value, and the *orange lines* represent the median of each box.

(a) PCA with 20 components

(b) PCA with 10 components

(c) PCA with 6 components

Figure C.3: Classification's accuracy results using Principal Component Analysis method with *(a)*- 20 components, *(b)*- 10 components and *(c)*- 6 components. Classifiers from *left* to *right*: Logistic Regression, Linear Discriminant Analysis, K-Nearest Neighbours, Decision Trees, Gaussian Naive Bayes, Support Vector Machine, Linear SVM, Multi-layer Perceptron Classifier and Bagging. The *vertical lines* represent non-outlier data points that extend to the most extreme (whiskers), the *circle* represents data that extend beyond the whiskers, the *green triangles* represent the mean value, and the *orange lines* represent the median of each box.

Appendix D

Resting Heart Rate Tables

Tables D.1 and D.2 show resting heart rate evaluation considering gender and age [1].

Table D.1: Resting Heart Rate for men.

Age	18-25	26-35	36-45	46-55	56-65	65+
Athlete	49-55	49-54	50-56	50-57	51-56	50-55
Excellent	56-61	55-61	57-62	58-63	57-61	56-61
Good	62-65	62-65	63-66	64-67	62-67	62-65
Above Average	66-69	66-70	67-70	68-71	68-71	66-69
Average	70-73	71-74	71-75	72-76	72-75	70-73
Below Average	74-81	75-81	76-82	77-83	76-81	74-79
Poor	82+	82+	83+	84+	82+	80+

Table D.2: Resting Heart Rate for women.

Age	18-25	26-35	36-45	46-55	56-65	65+
Athlete	54-60	54-59	54-59	54-60	54-59	54-59
Excellent	61-65	60-64	60-64	61-65	60-64	60-64
Good	66-69	65-68	65-69	66-69	65-68	65-68
Above Average	70-73	69-72	70-73	70-73	69-73	69-72
Average	74-78	73-76	74-78	74-77	74-77	73-76
Below Average	79-84	77-82	79-84	78-83	78-83	77-84
Poor	85+	83+	85+	84+	84+	84+

---

[1]http://www.topendsports.com/testing/heart-rate-resting-chart.htm